Development and Splice Lengths for High-Strength Reinforcement

Volume II: Drift Capacity of Structural Walls with Lap Splices

CPF Research Grant No. 02-17

a Report to the Pankow Foundation

by W. Pollalis, and S. Pujol

April 2020

CHARLES PANKOW
FOUNDATION
Building Innovation through Research

Table of Contents

List of Figures

1. Abstract

Twelve large-scale RC specimens with lap splices in the longitudinal reinforcement were tested at Purdue University's Bowen Laboratory to produce data to evaluate the deformability of structural walls. Previous work on lap splices (e.g. Vol. I) has focused mainly on splice strength. But in consideration of demands requiring structural toughness (e.g. blast, earthquake, differential settlement), deformability is arguably more important than strength.

The configuration of tension reinforcement in structural walls often differs from configurations used in conventional bond tests. In walls, several potential planes of splitting resulting from bursting stresses caused by bond can occur. In a conventional test beam with a single layer of reinforcement splitting is mainly constrained to a single plane. To study the response of lap splices in conditions more representative of those occurring in structural walls and to obtain data on splice deformability, eight specimens were tested under four-point bending and four additional specimens were tested as cantilevers under constant axial force and cyclic reversals of lateral displacement.

Splice lengths ranged from 40 to 90 bar diameters. Clear bar cover was either 1.5 or 0.75 bar diameters, measured to the outer edge of transverse reinforcement. Clear bar spacing along the splice length was either 1 or 2.25 bar diameters. Measured bar yield stresses ranged from 60 to 93 ksi. Concrete strength varied from 5.2ksi to 6.2ksi (from specimen to specimen). In two (of four) of the cantilever walls, special confinement was provided by closed rectangular hoops placed around longitudinal boundary reinforcement at a spacing of 6 bar diameters. The aspect ratio of these test walls was nearly 5, to reflect the idea that lap splice failure is more likely to be critical in more slender structures and because projecting tests of squat walls to taller walls is not simple -especially if the loading rig used to test squat walls may affect their deformability.

All specimens failed abruptly by disintegration of the lap splice regardless of how the loading was controlled and what detailing was used. Abrupt losses of lateral strength in a dynamic scenario are, needless to say, undesirable. The experience or the profession with dynamic demands comes mostly from structures that can sustain large fractions of their lateral resistance through the applied displacement history.

In the tested beams with constant moment regions, mean surface strain near the end of the lap splice was observed to be approximately 1.5 times drift ratio (defined here as midspan deflection divided by half the clear span). In walls, as in previous tests, peak surface strain[1] near the splice end was also observed to be nearly 1.5 times drift ratio (or even more). And drifts at failure ranged between 1.3 and 3.3%. As a consequence, strains at failure exceeded by a large margin the strain at the elastic limit of all the bars used. Yet, the bar stresses inferred to have occurred at failure are close to what would have been expected based on the investigation reported in Vol I and similar investigations in which splice failure occurred –in most instances- without large plastic bar deformation. It follows that plastic strain was not critical to bond strength. It also follows that for a given estimate of splice strength and a given stress-strain relationship, drift at splice failure can be estimated as a factor times the strain expected at the stress causing bond failure. For the observations obtained, developing a relationship between lap splice properties and drift at splice failure is feasible. But given

[1] Inferred from measurements of deformation made along the edge of the wall along gage lengths of 12 and 24 bar diameters (and 1/7 to 2/7 of the wall length)

1) the limited number of observations available,
2) that in the field the conditions and tolerances are likely to be less favorable than in the tests described in this report, and
3) that it is unlikely that, in practice, a good representation of the relationship between stress-strain will be known ahead of time –especially for cyclic demands from wind or earthquake-

the following reasonable lower bounds to drift capacity are provided instead of an elaborate relationship between drift and splice properties.

For structural walls with lap splices comparable to those tested, the observations collected suggest that drift capacity can be as low as 0.5% for splices with minimum cover (0.75 in.), minimum transverse reinforcement with 90-deg hooks, and lap splice lengths selected to reach yielding in the spliced bars. That is, splice failure can occur as yield is reached or soon after. For lap splices 1.3 times longer, drift ratio at splice failure is projected to increase to approximately 0.75% or more. For cover twice as large and transverse reinforcement that is continuous around the lap splice, drift capacity is projected to increase to nearly 1% for splices designed to yield and 1.5% or more for lap splices 1.3 times longer.

Last, large numbers of loading cycles in the linear range of response did not seem to have an appreciable effect on splice deformability.

The evidence gathered suggests that lap splices with minimum cover and confined only by minimum transverse reinforcement with 90-deg hooks should not be used in applications requiring toughness in structural walls.

2. Object and Scope

The main object of this study was to produce data to quantify the deformation capacity of structural RC walls with reinforcement lap splices near their bases.

This study was conducted as the last phase of a multi-phase project. Previous results were reported by Fleet, Glucksman, and Frosch (2019) in Volume I of this report.

The configuration of the bars in the lap splice was of special interest. The specimens tested had lap splices in Grade-60 and Grade-80 #8 steel reinforcing deformed bars. The spliced bars were configured in groups of four and six bars with clear bar spacing in the splice of at least one bar diameter. Relative to the neutral axis occurring in bending about an axis perpendicular to the plane of the wall, the bars in tension in the wall boundary were placed in two or three layers, with two bars in each layer. In this configuration, bursting stresses caused along the lap splice by the bond between concrete and steel can cause splitting cracks in two directions. One of these directions is parallel to the length of the wall (longitudinal splitting), and the other is parallel to the thickness of the wall (transverse splitting - Figure 1).

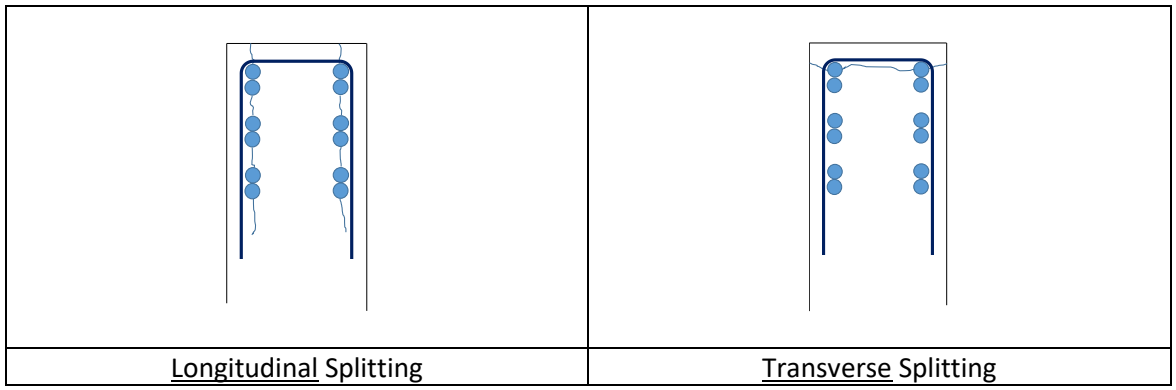

Figure 1 – Illustration of directions of splitting

In conventional tests (Volume I) to study bond, this condition that splitting can occur in two perpendicular directions seldom occurs, but in a structural wall it is common, and field observations indicate that either splitting direction can control (Figure 2). For the same reason, it is not clear how to use existing formulations to estimate required development length because they have been conceived –mostly- for cases in which spliced bars are placed in a single layer creating mainly one single obvious plane of potential (often transverse) splitting.

Figure 2 – Longitudinal splitting observed in Concepcion, Chile, Alto Rio Building, 2010 (Song, 2013).

Quantification of splice deformability was also of special interest. Most previous studies on bond focused on splice strength instead. This study addresses the question of how much lateral drift a wall can tolerate before splice failure occurs.

3. Introduction

Much of the past work on lap splices focused on quantification of the strength of the splice. From the classic study by D. Abrams (1913) to the first phase(s) of the project of which this study is part, researchers have reported test results and their idealizations in terms of bond strength (defined in this Volume as peak bar force divided by embedded bar surface area), peak bar stress, or embedment length required to yield the bar.

Less attention has been given to the problem of deformability: if a lap splice is sized so that the spliced bar can reach yield stress or exceed it by a given margin, how much deformation can the splice accommodate before failure? Deformability is as or more important than strength in RC. Deformability allows for redistribution of forces and controlled response to extreme demands (such as blast and earthquake).

This study focused on deformability of RC elements with lap splices. The study was supported by two series of tests:

-Monotonic tests of specimens with a constant moment region

-Cyclic tests of large-scale cantilevered RC walls with a moment gradient caused by a single concentrated and cyclic lateral force applied near the 'free' end of the wall.

In all cases the intent was to consider how lap splices may affect the drift capacity of RC structural walls. Until recently, lap splices were excluded from critical regions of other types of elements, but they were still allowed in critical regions of structural walls even in applications related to seismic demands. In part because of the observations produced by this study, the latest design recommendations by the American Concrete Institute now ban the use of lap splices in critical regions of RC structural walls classified as 'special.' But other walls not so classified can still include lap splices in critical regions. Those walls can be used in areas not perceived to have high seismic risk, but in most instances, it would be preferable for them to have ample toughness.

In this investigation special attention was given to Grade-80 reinforcement because, as suggested in Volume I, the splice length required to develop the yield stress is not proportional to said stress. Instead, required splice length increases faster than yield stress. Or said in a different way, peak bar stress increases at a decreasing rate with increases in splice length. This observation: 1) makes high-strength steel more critical, 2) is caused by concentration of bond stresses near the ends of the splice that make the mid segment of the splice less effective in providing bond (Kluge and Tuma, 1945).

4. Literature Review

There is abundant information on previous studies on bond strength. Summaries have been produced by Orangun (1977), Sozen and Moehle (1990), ACI 408 (2001, 2012), Canbay and Frosch (2005), and Fleet (Volume I, 2018), among others. In comparison, much less work has been done on the response of structural walls with lap splices in their longitudinal reinforcement. An exhaustive review of tests on RC structural walls with lap splices was published by Almeida et al. (2017) and Tarquini et al. (2015). Their review was motivated by reports of field evidence of problems with lap splices in structural walls. In their report the authors also summarize said field evidence. Among other cases, the evidence includes observations reported by Kilic and Sozen (2003), Kim and Shiohara (2012), and Song (2013), suggesting collapses of chimneys and a building were caused at least in part by failures of lap splices with lengths deemed to be sufficient today. Earlier evidence of splice failures may have been obscured by 1) signs of different types of failures, and 2) difficulties recognizing splitting cracks as the result of splice failure. But in 1964 (Kunze et al. 1965), the collapse of the Four Seasons Apartment Building in Anchorage Alaska was clearly traced back to problems in slab-wall and slab-column connections and failures of short lap splices at bases of structural walls.

Figure 3 – Four Seasons Apartment Building, Anchorage Alaska (Kunze et al. 1965).

Figure 4 – Failure of lap splices reported by Song (2013).

Table 1[2] provides a birds-eye view of experimental data summarized by Tarquini et al. (2015). Most of the reported tests (15 out of 17) had aspect ratios (ratio of shear span to wall length) of 3.0 or less. And in a number of these tests the nominal shear span was increased by application of moments at the top of the specimen. It is not clear to what extent the loading rigs used to control the applied moment may have affected the flexibility of the specimen-rig system.

Selected recent investigations related to structural walls are described next.

[2] available from public access at https://www.zenodo.org/record/2653488)

Table 1. Properties of test walls reported by Tarquini, https://www.zenodo.org/record/2653488)

Test Unit	Main Ref.	Ref. Unit	Geom.	Scale	l_s	d_{bl}	$n_{splices}$	c_{b0}	c_{s0}	c_{si}	s	d_{bt}	L_s	h	FS	SD	Comments
					(mm)	(mm)	(-)	(mm)			(mm)	(mm)	(mm)	(mm)	(-)	(-)	
W1	Paterson and Mitchell (2003)	[-]	Symm. Rectang.	1:1	900	25	2	63	40	60	350	11	3250	1200	N	Y	The specimen exhibited very poor ductility, failing soon after yielding at a lateral drift of 0.6%. There was a brittle failure of the lap splices at the tensile end of the wall that led to a significant drop in the wall capacity. A visible vertical side splitting crack along the entire length of the lap splice was visible prior to failure.
W2		[-]	Symm. Rectang.	1:1	900[a]	25	2	63	40	60	350	11	3750	1200	N	Y	The wall, which had a lap splice zone located 600 mm above the foundation, showed a ductile response until almost 2% drift. As inelasticity (and cracks) spread from the bottom and reached the height at which the splice started, a brittle tensile failure of the lap splices on one side of the specimen occurred, resulting in a large drop in the capacity of the wall.
CW2	Elnady (2008)	[-]	Symm. Rectang.	1:3	360	16	2	27	27	17	180[b]	6[b]	5000	1000	Y	Y	At the very first loading cycle at a low drift of 0.05%, flexural cracks developed at the bottom of the wall and spread to near midheight. Upon increasing the lateral load, the existing cracks started to open up and a new horizontal crack developed just at the top end of the lap splice zone. At a drift below 0.1% (far below the yielding point) the wall failed prematurely due bond slip of the lap splices.
CW3		[-]	Symm. Rectang.	1:3	360	16	2	27	27	17	180[b]	6[b]	2250	1000	N	Y	At 0.5% drift two diagonal cracks were observed at inclined ±45° direction. While loading, cracks opened up and extended from corner-to-corner of the wall in both directions. At a horizontal drift of approximately 1.5% the wall failed due to bond slip of the lap splice.
VK2	Bimschas (2010)	VK1	Symm. Rectang.	1:2	600	14	4	26	26	31	200	6	3300	1500	N	Y	The first side splitting cracks in the tensile edge of the wall appeared at 1.5% drift. At 2% drift, a large bond crack extended along the entire lap splice height. By the second cycle at this drift level the four reinforcement bars in the outmost layer of each tension zone of the cross section were essentially ineffective due to bond failure of the splices. With the increase of the lateral loading, more lap splices successively failed causing a subsequent progression of the cyclic strength degradation of the member.
VK4	Hannewald et al. (2013)	VK3	Symm. Rectang.	1:2	600	14	4	26	26	31	200	6	3300	1500	N	Y	At about 1% drift, while loading in one direction, compression cracks appeared at the wall edge. At the same drift level, upon reversal, splice failure occurred followed by a sensible drop of the wall strength. At the second peak at 1% drift, some splices at the tension side of the pier also failed. At 1.2% drift, all cover concrete along the splices sounded hollow. The wall had thus reached its residual capacity (25% of the peak force) and the force-displacement relationship remained rather flat even when higher displacement levels were imposed.
VK5		VK6	Symm. Rectang.	1:2	600	14	4	26	26	31	200	6	4500	1500	N	Y	At 1% drift, vertical side splitting cracks were clearly visible along the splice length in the tension wall side. Also noticeable was a horizontal crack above the splice level. During loading to 1.5% drift, splice failure occurred followed by a decrease of the wall lateral strength. As for VK4, at this point the specimen had reached its residual strength capacity (30% of the peak force) which remained rather constant with the increase of the displacement demand.
W1*	Layssi and Mitchell (2012)	[-]	Symm. Rectang.	1:1	600	20	2	36	50	6	250[c]	11[c]	3250	1200	Y	Y	The wall exhibited a non-ductile cyclic response due to brittle side splitting of the external lap splices prior to yielding. The specimen was able to withstand only 80% of the predicted flexural capacity.
W2*		[-]	Symm. Rectang.	1:1	600	20	2	36	50	6	250[c]	11[c]	3250	1200	Y	Y	Same behaviour as for wall W1 described above. However, specimen W2 was only able to carry 68% of its predicted flexural capacity
PW2	Birely (2012)	PW4	Symm. Rectang.	1:3	609	13	2	19	19	19	51[d] 152[e]	6[d] 6[e]	6710	3048	N	N	Cover spalling initiated above the splice region at 0.75% drift (determined from imposed top displacements at 3.66m). After 3 cycles at the same drift level the longitudinal reinforcement was exposed and longitudinal bars buckled in the boundary element above the splice region. At 1.05% drift concrete crushed where buckling had occurred and the damage extended to the web of the wall, propagating down towards the top of the of the web splices.

Table 1 (Continued).

RWS	Aaleti et al. (2013)	RWN	Unsymm. Rectang.	1:2	1140	19	2	25	18	21	51[d]	190[e]	6[d]	9[e]	6096	2286	N	Y	Noticeable strength degradation appeared at 1.2% drift with the fictitious flange in tension probably due to slipping occurring in the splice region. Main cracks were located approximatively above the lap region and in the wall base. Bond degradation progressed increasingly with the demand. In the end, as the crack at the wall-foundation interface became wide enough, the slip of the bars relative to one another led to initial local buckling of the longitudinal reinforcement in the boundary element with d_{bl}=19mm.
					1730	29	2	31	9	9	62[d]	190[e]	6[d]	9[e]					
W-60-C	Villalobos (2014)	W-MC-C	Symm. Rectang.	1:1	1520	25	2	30	19	56	64[d]	127[e]	6[d]	10[e]	3660	1520	N	Y	Splitting cracks were first observed at drift ratios ranging from 0.25% to 0.5%; the widest side splitting cracks occurred near the splice ends, being widest near the base. At the final imposed displacement neither continuous splitting cracks along the entire splice length nor fully-exposed splices were present. However, the loss in strength due to bond degradation in the splice regions is easily inferable from the global force displacement response of the specimen at 2% drift ratio.
W-40-C		W-MC-C	Symm. Rectang.	1:1	1020	25	2	30	19	56	64[d]	127[e]	6[d]	10[e]	3660	1520	N	Y	Similarly to the specimen W-60-C, tensile splitting cracks were observed at early stages of loading. For this particular wall, however, before reaching the target drift ratio of 2.5% a crack that ran the entire length of the boundary splices occurred. A drop in lateral load (10% and 4% of the peak lateral load respectively in each direction) occurred when this crack formed. With further displacement reversals the relative slip between splices on one face of the boundary elements led to further decrease of the wall strength until the boundary elements were fully exposed.
W-60-N		W-MC-N	Symm. Rectang.	1:1	1520	25	2	30	19	56	127[f]		10[f]		3660	1520	N	Y	The response of W-60-N was similar to the one described above for the specimen W-60-C. However, the smaller amount of confining reinforcement present in W-60-N led to an anticipated onset of strength degradation occurring at a value of drift of 1.5% (0.5% less than the one observed in W-60-N).
W-60-N2		W-MC-N	Symm. Rectang.	1:1	1520	25	2	30	19	56	127[g]		10[g]		3660	1520	N	Y	The cyclic behaviour of the specimen W-60-N2 was substantially identical to the one of W-60-N.
TW3	Almeida et al. (2015)	TW2	T-shaped	2:3	215	6	2	15	15	39	130[h]		6[h]		3150	2700	N	Y	When loading towards the wall end without flange, the test unit failed due to crushing of the wall base. When loading towards the flange, the wall exhibited a softened due to a progressive failure of the lap splices. It is noteworthy to pinpoint that almost all the deformations concentrated in a crack above and below the lap splice zone.

Legend: ***Ref. Unit***: reference unit with continuous reinforcement; l_s: length of the lap splice; d_{bl}: diameter of the longitudinal reinforcement; $n_{splices}$: number of splices potentially crossed by a splitting crack; c_{bo}: clear face cover of reinforcing bars; c_{so}: clear side cover of reinforcing bars; c_{si}: half of the clear spacing between splices in the plane of a splitting crack; ***s***: spacing of lateral or confining reinforcement (consisting in classical closed hoops or stirrups when not differently specified); d_{bt}: diameter of the horizontal reinforcement(consisting in classical closed hoops or stirrups when not differently specified)t; L_s: *shear span;* ***h***: wall length; ***FS***: lap splice failure before the wall has reached the flexural capacity ; ***SD***: specimen experiences strength degradation due to the presence of lap splices. ***NOTE***: all quantities aforementioned are associated to the outmost reinforcement layer perpendicular to the plane of bending.

*Used to differentiate the 2 test units from those of Paterson and Mitchell (2003) which are equally labelled. [a]Lap splice zone starts 600 mm above the foundation level. [b]Shear reinforcement consisting of 2 straight single leg rebars (no reinforcement preventing face splitting). [c]Single leg rebar located in between the longitudinal reinforcement. [d]Quantity referred to the confining hoops present in the boundary element. [e]Quantity referred to the shear reinforcement. [f]Shear reinforcement consisting of 2 single leg rebars with final 135° hook. [g]Shear reinforcement consisting of 2 single leg rebars with final 90° hook [h]Horizontal reinforcement placed inside the flexural reinforcement.

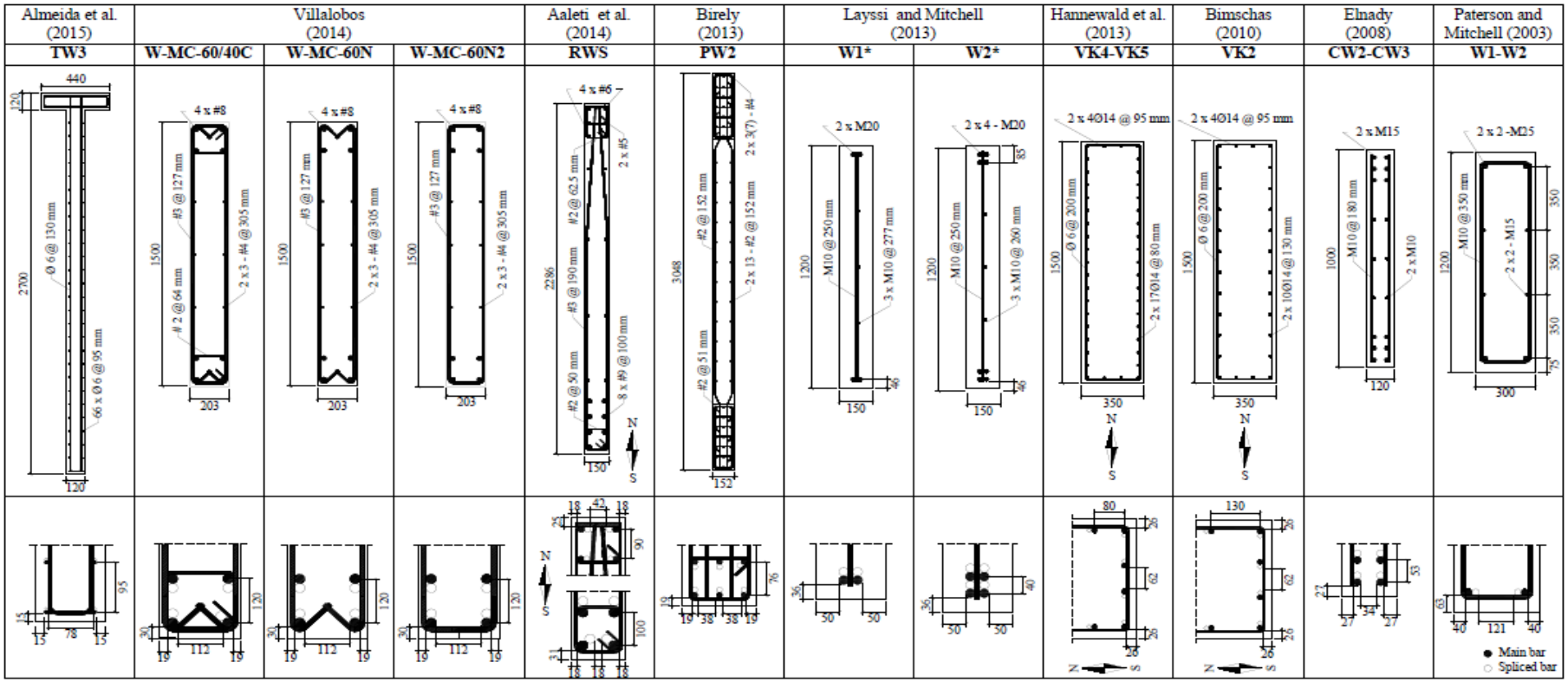

Almeida et al. (2015) – TW3

f'_c = 43.3 MPa
f_y = 465 MPa
f_u = 620 MPa
ε_{sh} = 2.5 ‰
ε_{su} = 80 ‰

Villalobos (2014) – W-MC-60C

f'_c = 31 MPa
f_y = 461 MPa
f_u = 655 MPa
ε_{sh} = 12
ε_{su} = 180 ‰

Villalobos (2014) – W-MC-60N

f'_c = 33.8 MPa
f_y = 461 MPa
f_u = 655 MPa
ε_{sh} = 12
ε_{su} = 180 ‰

Villalobos (2014) – W-MC-60N2

f'_c = 31.7 MPa
f_y = 468 MPa
f_u = 668 MPa
ε_{sh} = 2.5
ε_{su} = 190 ‰

Aaleti et al. (2014) – North

f'_c = 55.9 MPa
f_y = 465 MPa
f_u = 634 MPa
ε_{sh} = 9.6 ‰
ε_{su} = 100 ‰

Aaleti et al. (2014) – South

f'_c = 55.9 MPa
f_y = 491 MPa
f_u = 669 MPa
ε_{sh} = 9.6 ‰
ε_{su} = 100 ‰

Birely (2013) – PW2

f'_c = 40.3 MPa
f_y = 579 MPa
f_u = 694 MPa
ε_{sh} = N/A
ε_{su} = 91.2 ‰

Layssi and Mitchell (2013) – W1*

f'_c = 31.2 MPa
f_y = 460 MPa
f_u =637 MPa
ε_{sh} = N/A
ε_{su} = N/A

Layssi and Mitchell (2013) – W2*

f'_c = 31.2 MPa
f_y = 460 MPa
f_u =637 MPa
ε_{sh} =2.5 ‰
ε_{su} = N/A

Hannewald et al. (2013) – VK4

f'_c = 39.2 MPa
f_y = 521 MPa
f_u = 609 MPa
ε_{sh} = 28.6 ‰
ε_{su} = 110 ‰

Hannewald et al. (2013) – VK5

f'_c = 35.2 MPa
f_y = 521 MPa
f_u = 609 MPa
ε_{sh} = 28.6 ‰
ε_{su} = 110 ‰

Bimschas (2010) – VK2

f'_c =39.0 MPa
f_y =521 MPa
f_u =609 MPa
ε_{sh} =28.6 ‰
ε_{su} =110 ‰

Elnady (2008) – CW2

f'_c = 37.3 MPa
f_y = 450 MPa
f_u = 760 MPa
ε_{sh} = N/A
ε_{su} = N/A

Elnady (2008) – CW3

f'_c = 37.5 MPa
f_y = 450 MPa
f_u = 760 MPa
ε_{sh} = N/A
ε_{su} = N/A

Paterson and Mitchell (2003) – W1

f'_c = 25.9 MPa
f_y = 423 MPa
f_u = 667 MPa
ε_{sh} = N/A
ε_{su} = N/A

Paterson and Mitchell (2003) – W2

f'_c = 33.4 MPa
f_y = 423 MPa
f_u = 667 MPa
ε_{sh} = N/A
ε_{su} = N/A

Notes: (i) the mechanical properties of the steel are relative to the rebar(s) of the controlling boundary reinforcement (represented in the zoomed-in section details); (ii) N/A = not availabe; (ii) Ø, #, M : tag for European, US and Canadian rebar sizes respectively.

Figure 5 – Details reported by Tarquini https://www.zenodo.org/record/2653488.

4.1 Tests at Minnesota (Johnson)

Johnson et al. (2007, https://datacenterhub.org/resources/138, also Aaleti et al. 2013) tested three 6-in. wide, 7.5-ft long, 20-ft tall structural walls: one control specimen with continuous reinforcement, one test wall with mechanical splices, and one test wall with lap splices near its base. The length of the lap splices was 60 bar diameters. One end of the wall had #6 and #5 longitudinal bars with lap lengths of 45 and 38 in. The other end had #9 longitudinal bars with lap length of 68 in. Concrete cover was 3/4 in. Boundary elements were confined with rectangular hoops with reinforcement area ratio equal to 0.6% in the direction of the wall thickness. But not all spliced bars were placed within the confined concrete as shown in Figure 6 below.

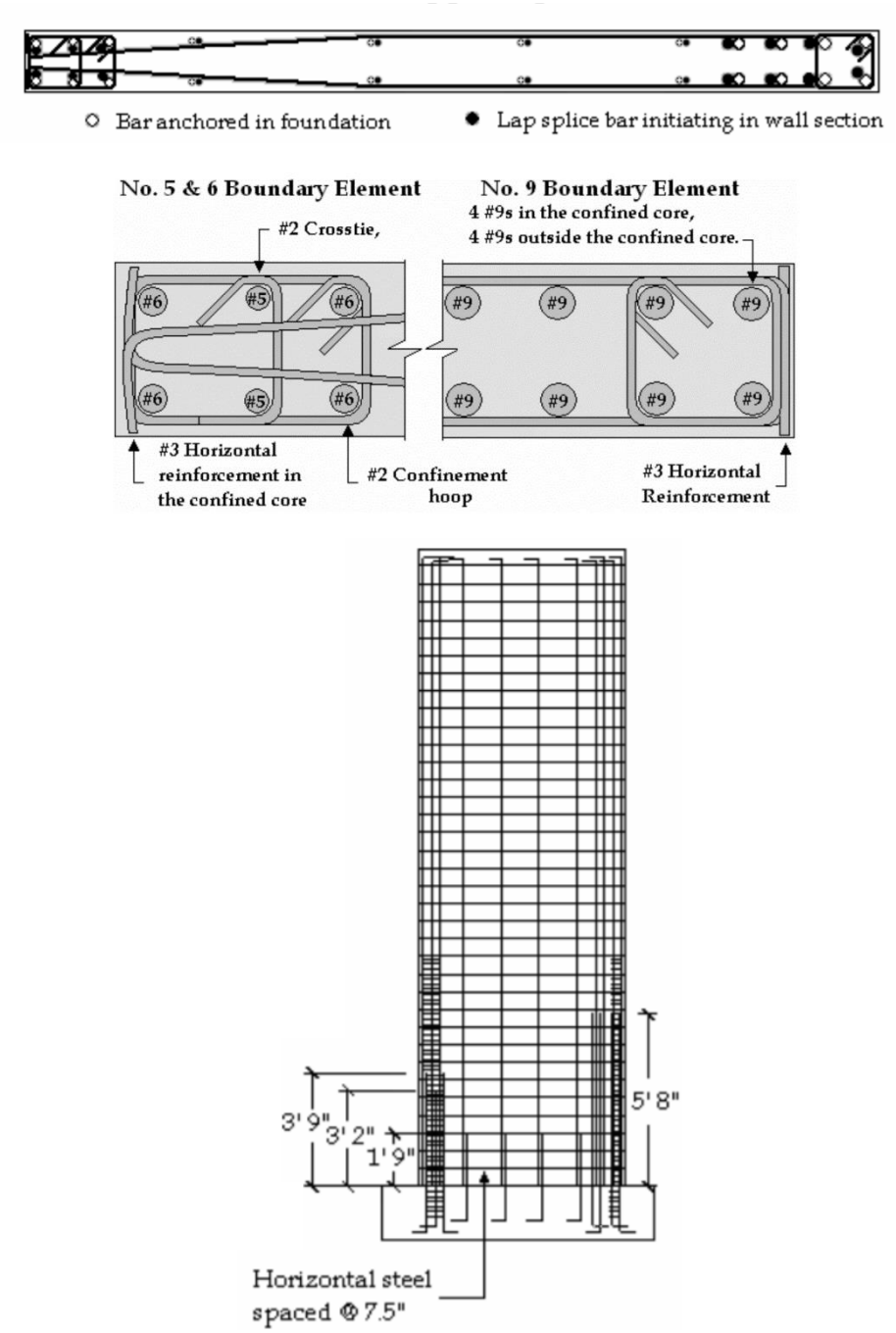

Figure 6 – Details of wall tested by Johnson et al. (2007) – https://datacenterhub.org/resources/138

The walls were tested as cantilevers with a single cyclic concentrated force near the top but no axial load. Splice failures were not observed. But lap splices were observed to cause strain concentration leading to bar fracture. While the comparison specimens reached drift ratios as large as 4%, the mentioned #6 and #5 bars with lap splices fractured at a drift ratio of 2%. The #9 bars, on the other hand were not subjected to large demands until the described fracture occurred. The force-drift relationship measured is illustrated in Figure 7 below. The 'asymmetry' in the applied displacement history makes the interpretation of the results challenging.

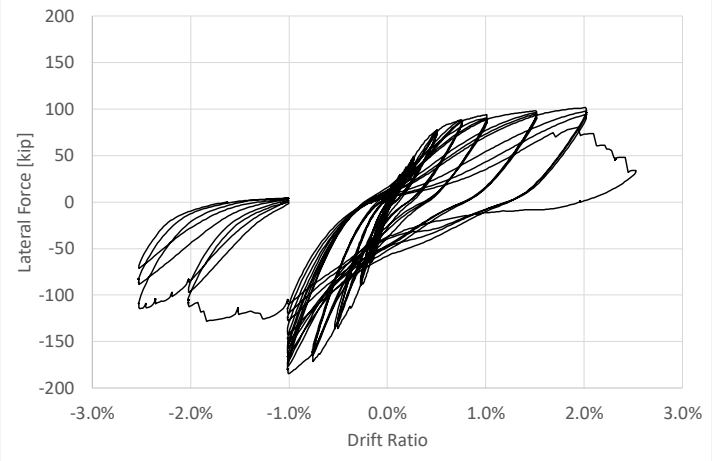

Figure 7 – Load-deflection relationship reported by Johnson (2007).

4.2 Tests at U of I by Birely et al.

Birely (2012) tested four cantilevered squat walls with lateral force and moment applied at their free ends in an elaborate setup depicted in Figure 8. In three out of four test walls, two additional lateral loads were applied at third points along the clear height of the specimen. The aspect ratio of the test wall was 1.2: wall length was 10 ft and clear height was 12 ft. Wall thickness was 6 in. Longitudinal boundary reinforcement was provided using #4 bars with yield stresses ranging from 51 to 84 ksi. Concrete strength varied between 4 and 5.5 ksi.

Three out of four walls had lap splices in all longitudinal reinforcement. Lap splice lengths were 24 or 36 bar diameters for #2 bars in the web and 48 bar diameters for #4 bars used in wall boundaries. Minimum cover measured to the centre of the spliced bar was 1 in. Spacing of boundary longitudinal reinforcement was 3 or 4.25 in. (Figure 9).

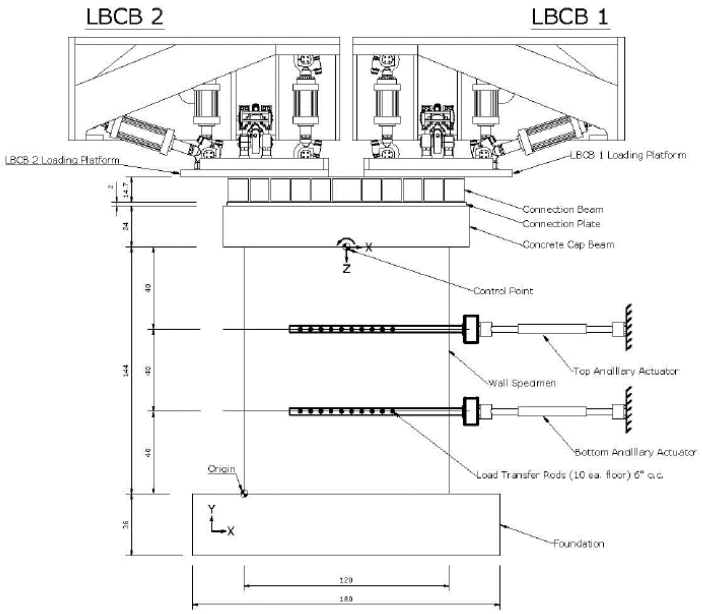

Figure 8 –Setup used by Birely (2012)

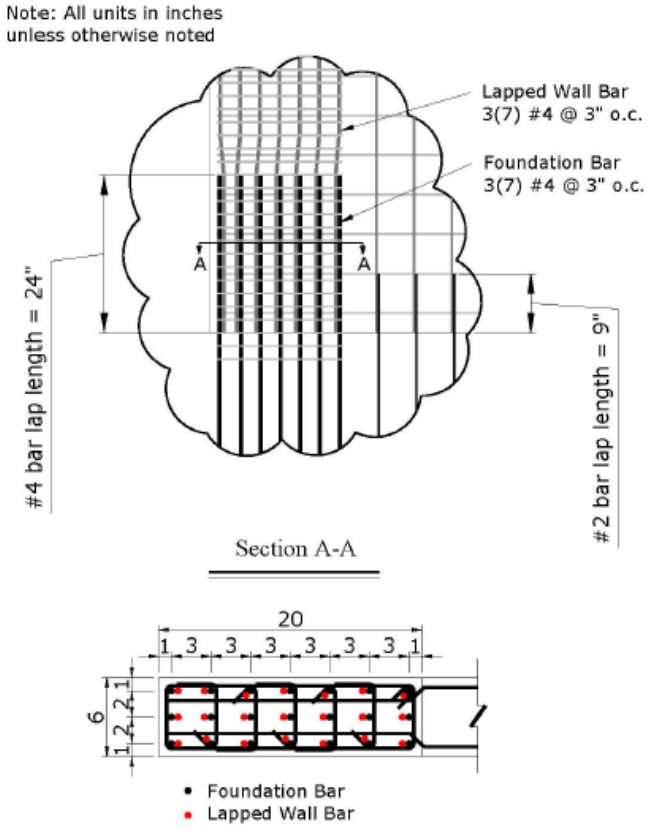

Figure 9 – Typical Splice in Specimens by Birely.

Specimen PW1 had lap splices and was reported to fail because of fracture of longitudinal bars at a drift ratio of 1.5%. Drift ratio was reported as top displacement divided by clear wall height. In

specimen PW1 there was concrete spalling along splitting cracks running the length of the lap splice near the edge of the wall (Figure 10). This spalling can be interpreted to suggest the occurrence of a splice failure in the outermost bars in tension. The plausible splice failure was not reported as such. Nevertheless, after removal of loose concrete at the end of the test, fractures were observed in "all of the bars on the front of the east boundary element, except the extreme bar" suggesting the latter may have slipped.

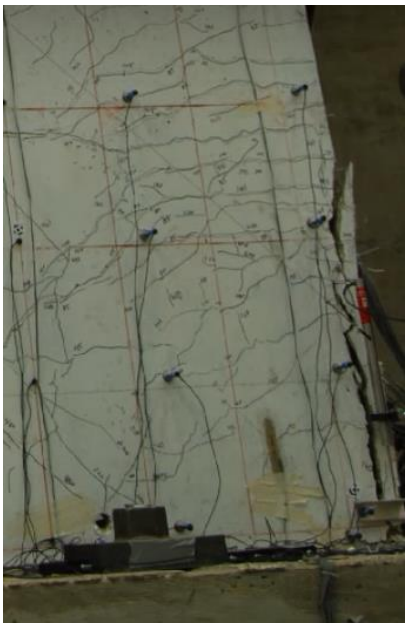

Figure 10 –Splitting cracks in lap splice in Specimen PW1 by Birely (2012).

The failures of the other two specimens with lap splices occurred at a drift ratio of 1% and were controlled by concrete crushing and bar buckling near the top of the lap splice. The ratio of axial load to product of concrete strength and gross cross-sectional area $P/(f'_c A_g)$ was close to 0.1. Given this, and given that moment demand was largest at the bottom of the splice, it is not clear why the failure occurred at the top instead. Strain concentration caused by the lap splices is a plausible explanation. Buckling of bars (anchored in the top of the specimen) at bends near the top of the splice may have contributed to the damage concentration in that location.

The drift ratios at failure reported in this investigation are rather small. That is in part a result of how drift ratio was reported (as the ratio of displacement at top of test wall to wall height). Nevertheless, because moment was applied at wall top to represent the interaction between the lower and upper segments of a hypothetical taller wall, it could be argued that the measured drift ratio should be projected to the top of said taller wall. The projection is not simple because it requires an assumption about curvature distribution. For the sake of argument, one could assume most deformations would occur in the tested segment while the rest of the wall simply rotates as a rigid object. If one also assumes the variation of curvature in the tested segment was linear, varying from a maximum at the foundation to zero at the top of the test wall, geometry requires the drift ratio for the hypothetical taller wall to be

$$\frac{3}{2} \times \left(1 - \frac{\beta}{3}\right) \times measured\ drift\ ratio$$

Where β is ratio of test height to total height. If the total height is equal to the test height, then β=1 and the product above is equal to the measured drift ratio. In the limit, for a wall of infinite height, β=0 and the roof drift ratio is 1.5 times the measured drift ratio.

If the curvature in the tested segment is assumed to be constant instead, the relationship above becomes:

$$2 \times \left(1 - \frac{\beta}{2}\right) \times measured\ drift\ ratio$$

For measured drift capacities of 1% and 1.5%, the described and crude projections imply roof drift ratios of 1.5% to 2% and 2.3% to 3% for tall walls. But to what extent are these projections reliable? And to what extent did the loading mechanism stiffen the test specimen? The tests reported here were designed to avoid similar questions and allow for more direct interpretation of measurements.

4.3 Tests at Purdue

4.3.1 Tests by Villalobos

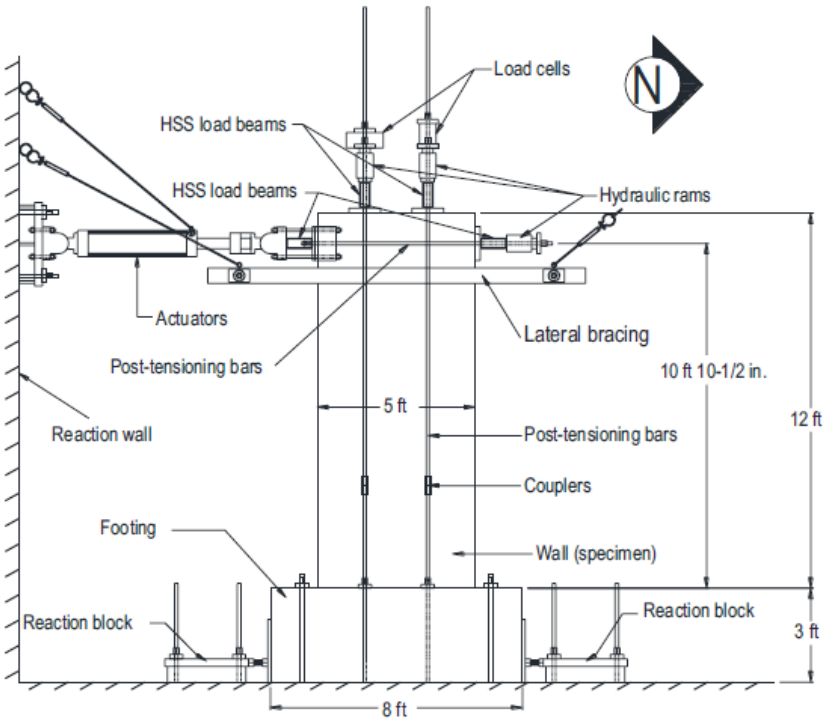

Figure 11 – Setup by Villalobos (2014, 2017).

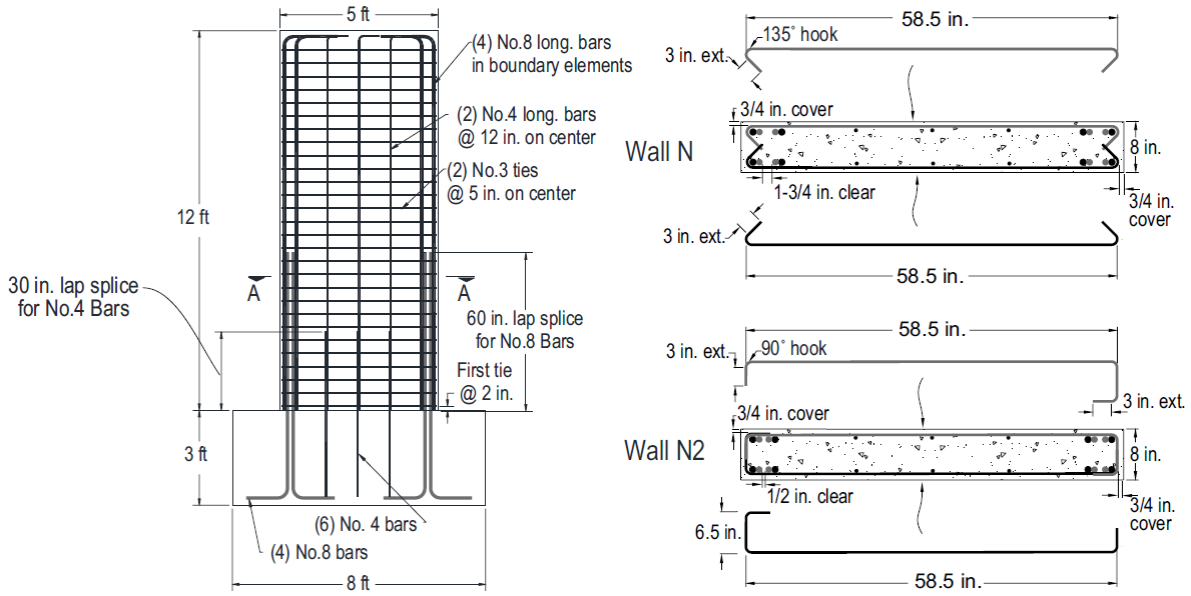

Figure 12 – Details of specimens tested by Villalobos (2014, 2017).

Villalobos tested small-scale structural walls (2014, 2017). These walls were tested as cantilevers with a single lateral load near their free ends. These walls had lap-spliced #8 Gr.-60 longitudinal bars in their boundaries. Lap splices were 60 bar diameters long in specimens without special boundary confinement provided by hoops. They extended from wall base to nearly mid-height. In the two specimens with lap splices in boundaries confined by hoops, lap splice lengths were 40 and 60 bar diameters.

In spite of observed damage in lap splices (Fig. 13), failure in all specimens was dominated by damage caused by compression instead of splice failure. It was concluded that the moment gradient reduced the demands on the splices that could have –otherwise– dominated wall response.

Figure 13 –Splitting in specimen by Villalobos (2014, 2017).

4.3.2 Tests by Richter and Hardisty

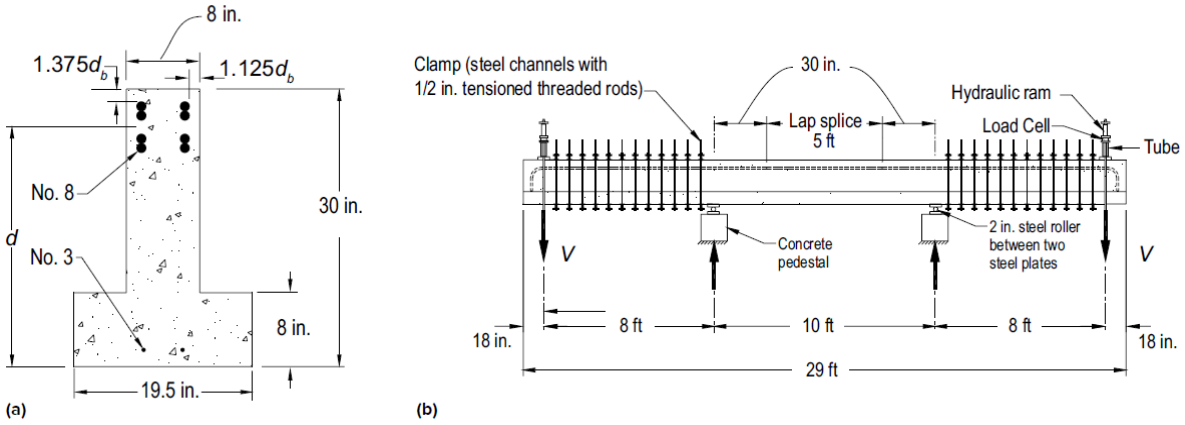

Figure 14 – Cross section and elevation, specimens by Richter and Hardisty (2012, 2015).

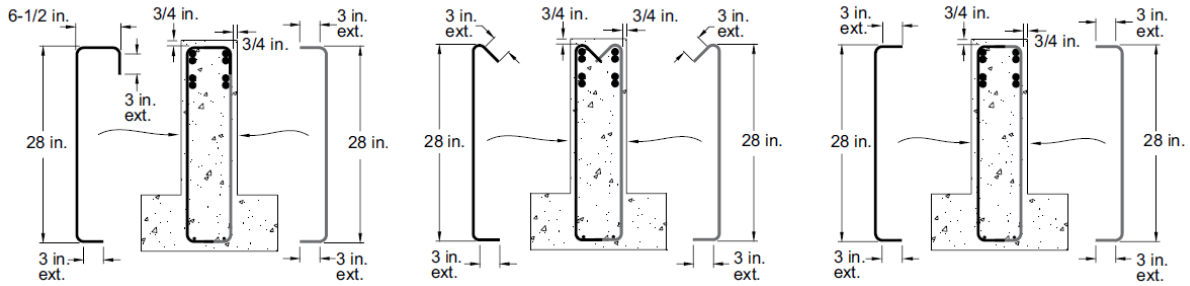

Label Assigned in This Study:

Type I	Type II	Type II
Specimens T-60-8-B and E	Specimen T-60-8-A	Specimens T-60-8-D and F

Figure 15 – Details of Specimens Tested by Richter and Hardisty (2012, 2015).

Richter and Hardisty (2012, 2015) tested beams with lap splices in constant moment regions. The details of the longitudinal reinforcement (bar size, bar spacing, cover) resisting tension caused by bending moment were similar to the details investigated by Villalobos (2014, 2017). In the tests by Richter and Hardisty, all specimens failed by abrupt disintegration of the lap splice caused by bursting stresses related to bond. Figure 16 illustrates how drift ratio at failure (maximum midspan deflection divided by half the length of the constant-moment region) varied with transverse reinforcement ratio. Notice the large difference between the drifts reached by specimens T-60-8-A and B. The difference can be attributed to a reduced clear distance between spliced bars. This difference in drift was not associated with a large difference in peak bar stress.

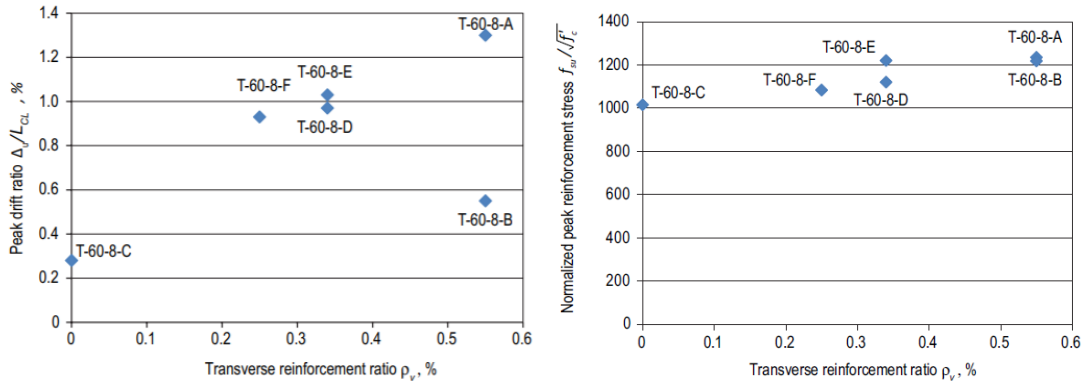

Figure 16 – Test Results by Hardisty et al. (2015).

It is likely that the differences between variations in maximum drifts and bar stresses observed in Figure 16 can be explained in reference to the stress strain curve of the steel used. Figure 17 shows how peak bar stress varied with normalized drift. The variation is superimposed on an idealized stress-strain curve matching measurements reported by Richter (2012). The comparison suggests that a small increase in peak stress after yield resulted in a large increase in strain after yield. In the case of an element with moment gradient, however, the yield plateau does not have as pronounced an effect as it does in an element under constant moment (Wight and Sozen, 1975). Therefore, it is not easy to project the results from conventional 'bond tests' of beams in 'four-point bending' to walls with moment gradients. Nevertheless, the data suggest that there may be a way to relate splice properties, peak bar stress, and drift capacity in elements controlled by splice strength.

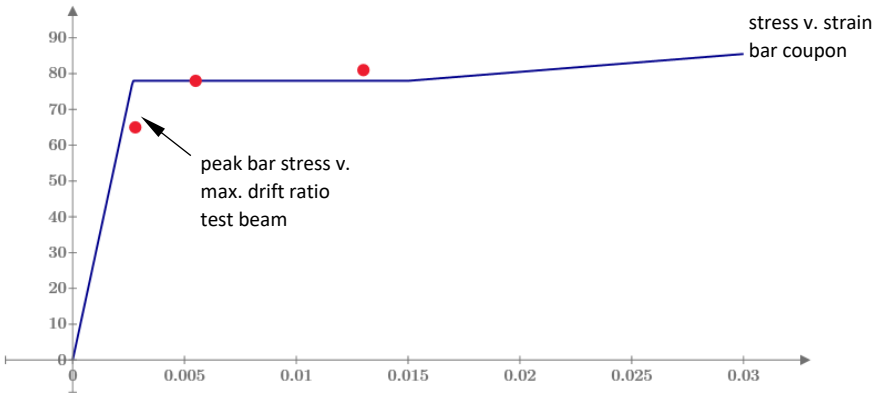

Figure 17 – Stress-Strain and Stress-Normalized Drift for specimens by Hardisty et al. (2015).

The comparison made also shows that strain is what produced drift, not bond strength (whether expressed as bond stress or as stress in the bar). Understanding that the capacity of a structural system to resist earthquake demands is often expressed better in terms of drift, the example above suggests that the data from bond tests need to be re-examined in terms of strain or some measure of deformability, not stress only.

4.3.3 Observations by Wang

Observations reported by Y. Wang (2014) are useful to understand strains that may occur in walls subjected to large lateral displacements. In a wide range of structural walls with strain gradients, Wang observed that, on average, drift ratio and maximum surface tensile strain near the end of the wall in tension are related as follows:

$$Surface\ Strain = C\ \times Drift\ Ratio$$

with C raging from 1.5 to 2.5. The expression suggested by Wang is illustrated against test data in Figure 18. The x axis represents strains measured on the concrete surface near the base of the wall for gage lengths ranging from 0.2 to 0.25 times wall length (7 to 12 bar diameters).

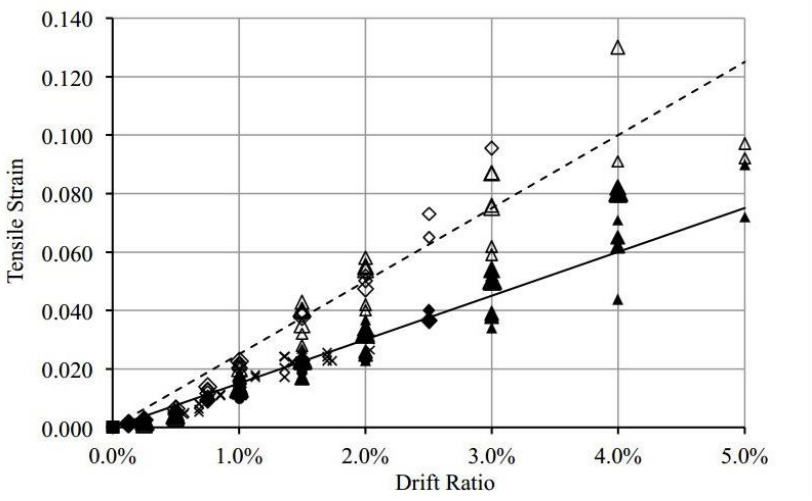

Figure 18 – Inferred strains reported by Wang (2014)

The observations by Wang suggest again a direct connection between strain and drift that follows directly from geometry. If an expression is produced to estimate peak bar stress for given lap-splice properties (such as the expression suggested in Volume I), then it follows that drift capacity can be quantified as a function of the parameters that control lap-splice strength and the stress-strain relationship for the spliced reinforcement. To explore this idea two series of tests were done: eight four-point bending tests of beams with lap splices in configurations resembling those encountered in structural walls, and four tests of full-scale cantilevered walls.

5. Methods

5.1 Elements with Constant-Moment Regions (Test Beams)

As observed by Villalobos (2017), moment gradient affects lap-splice strength. In the presence of pronounced gradients, lap splice strength tends to be larger. The same was observed by Ferguson et al. (1969, 1971). At the same time, it is difficult to scale lap splices because the bond strength of small bars tends to be larger than the bond strength of large bars. For these reasons, it is preferable to test lap splices in the configuration and at the scale in which they are to be used. But that is not always simple. A compromise to address the problem caused by moment gradient is to test a large beam under four-point bending to subject the lap splice to constant moment in the center span.

5.1.1 Setup and Specimen Description

Eight large beams were tested in four-point bending. Figure 19 shows the setup used to test splices in constant moment regions.

Figure 19 – Four-Point Bending Test Setup – Lap Splice Visible at the Top of the Beam at Midspan.

Supports were provided by 2-in. thick steel plates resting on 2.5-in. diameter steel rollers. The plates were 8-in. long in the longitudinal direction of the test beam, and the rollers were 14 ft apart from one another. Near the free end of each overhang, downward concentrated force was applied 10 ft from the closest roller and 1 ft from the free end of the overhang. These forces were transferred to the test beam through 1.5-in. thick steel plates with a length of 6 in. in the longitudinal direction of the test beam.

Figure 20 illustrates the cross sections investigated. All cross-sections were rectangular with dimensions of 10 in. (width) by 48 in. (total depth). Transverse reinforcement Type II had 90-degree hooks to terminate reinforcement.[3] Transverse reinforcement Type III had a spliced u-shape 'staple' surrounding the longitudinal bars. Longitudinal reinforcement consisted of four #8 bars with lap splices in the constant moment region and arranged in two layers of two spliced bars each.

[3] Refer to Figure 15 for labels assigned to details tested by Richter and Hardisty (2015, 2012). Label 'Type II' includes one specimen (T-60-8-A) with 135-deg. hooks and two specimens (T-60-8-D and F) with 90-deg hooks.

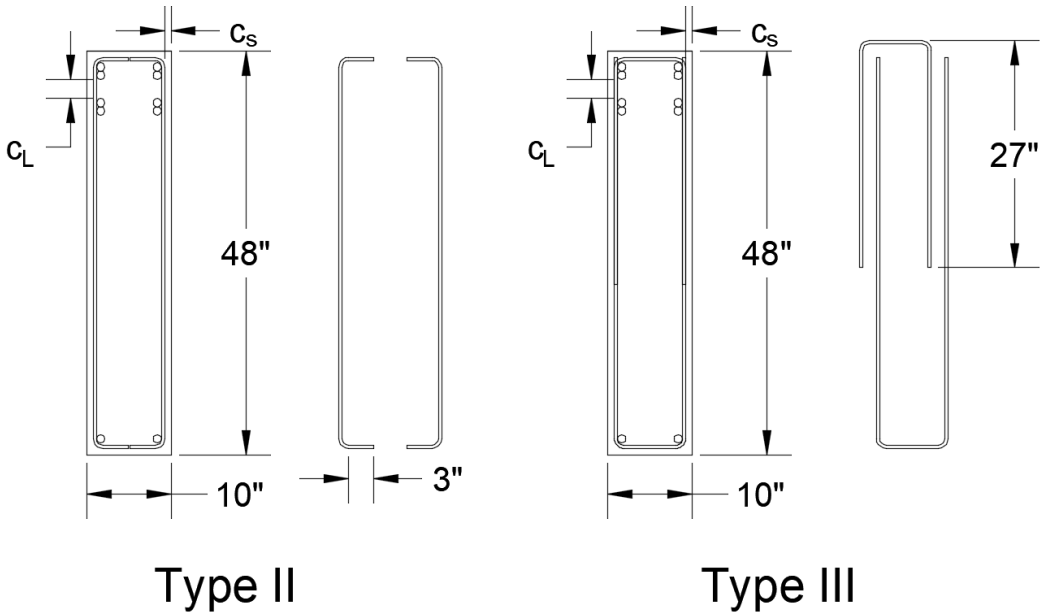

Figure 20 – Typical beam cross sections and Transverse Reinforcement Detailing. See Table 2 for Descriptions and Values for c_L and c_s.

Lap splices were configured in test beams in two ways. Lap splice configurations and specimen elevations are shown in Figures 21 and 22.

Configuration A

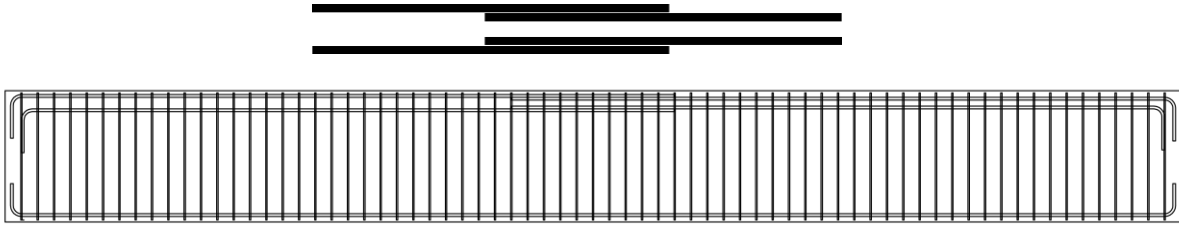

Figure 21 – Lap splice Configuration A and Beam elevation.

Configuration B

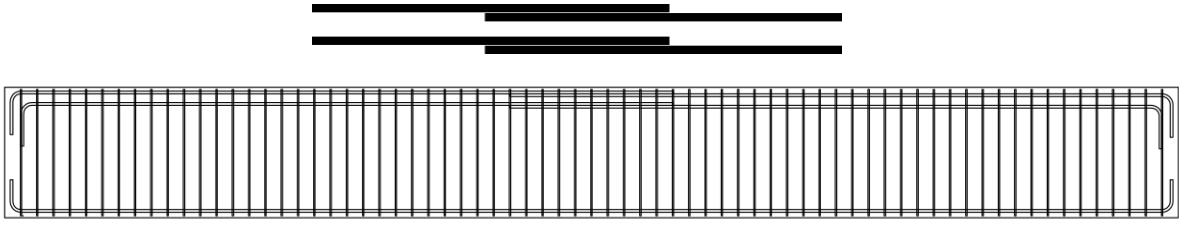

Figure 22 – Lap Splice Configuration B and Typical Beam elevation.

Test beam WB60U3 was fabricated with configuration A. All other test beams had configuration B. Reported values of effective depth refer to the centroid of the reinforcement along the splice. That is to say, the reported effective depths are the averages of the effective depths on either side of the lap splice.

The geometry of the cross section was chosen with the following ideas in mind:

- In a boundary element of a structural wall, splitting caused by bursting stresses related to bond can occur on planes both perpendicular and parallel to the plane of the wall (Figure 1).
- The strain gradient along the length of the wall (parallel to the long direction of the cross section) causes differences in bar stresses at different distances from the neutral axis. These differences in bar stresses can affect the performance of the lap splice.
- Splitting stresses are sensitive to bar and cover size.

Tables 2 and 3 list key parameters for all test beams. Specimen IDs start with 'WB' for all specimens tested in four-point bending. The numbers 60 and 80 denote the nominal steel grade of the longitudinal reinforcement (in ksi). The letter U was added for consistency with the IDs used for cantilevered walls and refers to boundary reinforcement not enclosed by closed hoops.

Table 2. Parameters related to concrete and longitudinal reinforcement used in test beams

Specimen ID	Effective Depth [in.]	Measured Concrete Strength [psi]	Nominal Long. Bar Grade [ksi]	Long. Bar Diameter [in.]	Total Number of Spliced Bars	Bars on potential splitting plane	Long. Bar Yield Stress [ksi]	Long. Bar Strength [ksi]	Splice Length [in.]	Min. Clear Cover, c_s [in.] †	Min. Clear Bar Spacing, c_L [in.]
WB60U0	43.75	5.4	60	1	4	2	60	94	60	.75	2.25
WB60U1	43	5.8	60	1	4	2	71	103	50	1.5	2.25
WB60U2	43.63	6	60	1	4	2	71	103	60	1.5	1
WB60U3	43.63	6.2	60	1	4	2	71	103	60	1.5	1
WB60U4	44.38	5.6	60	1	4	2	71	103	60	.75	1
WB60U5	44.38	5.8	60	1	4	2	71	103	60	.75	1
WB80U1	44.38	5.3	80	1	4	2	93	119	80	.75	1
WB80U2	43.5	5.2	80	1	4	2	93	119	80	1.5	1

†labeled as c_s in figure 20, Min. Clear Cover is measured from the concrete surface to the outer face of transverse reinforcement
††labeled as c_L in figure 20

Table 3. Parameters related to transverse reinforcement used in test beams

Specimen ID	Nominal Trans. Bar Grade [ksi]	Trans. Bar Measured Yield Stress [ksi]	Trans. Bar Diameter [in.]	Number of bars† (legs) crossing potential transverse splitting plane*	Total Area of bars crossing potential transverse splitting plane* Atr [in.^2]	Tie or Stirrup Spacing [in.]	Transverse Reinf. Ratio %	Transverse Reinf. Type (shown in Fig. 20).
WB60U0	60	70	3/8	2	0.22††	6	0.37%	II
WB60U1	60	69	3/8	2	0.22	6	0.37%	III
WB60U2	60	69	3/8	2	0.22	6	0.37%	III
WB60U3	60	69	3/8	2	0.22	6	0.37%	III
WB60U4	60	69	3/8	2	0.22	6	0.37%	III
WB60U5	60	69	3/8	2	0.22††	6	0.37%	II
WB80U1	80	89	1/2	2	0.4	12	0.33%	III
WB80U2	80	89	1/2	2	0.4	12	0.33%	III

†effectively anchored
*parallel to short direction of cross section
††assuming 90-deg hook sufficed as anchorage

5.1.2 Loading Method

Loads were applied near cantilever ends by using center-hole hydraulic jacks pressurized using pumps operated by hand and threaded rods fastened to the laboratory floor. Applied loads were measured using two load-cells, one per cantilever. Load increments were applied to reach either force targets (at the beginning of the test) or displacement targets (after yielding). Beams were tested in up to 18 load steps. Between load steps, cracks were marked and mapped, and photos and notes were taken. Total test duration varied from 3.5 to 5.5 hours. Test beams were loaded and unloaded to reset the stroke of jacks and to allow application of additional deflections except for WB60U0, where load was maintained while jack stroke was reset.

The hydraulic equipment used does not allow exact control of force or displacement. But at each loading stop the load would tend to decrease (because of creep and/or relaxation) and the displacement would tend to remain nearly constant because the volume of oil in the jacks tended to remain constant as well. It has been said that earthquake demands should be simulated by controlling displacement instead of force. That is certainly the case in systems in which one can expect a gradual decay in resistance with increasing displacement. In the case of splice failure, resistance does not decay gradually. Splice failure is perhaps the most abrupt failure there is in RC. Once failure occurs, the fraction of the strength attributable to the bar(s) affected by the failure disappears. Even bar fracture can be less abrupt because fracture often affects one bar at a time while splice failure can affect all the bars in the boundary element at once. It was therefore deemed unnecessary to conduct the four-point bending tests described here with special controls. The walls described next, on the other hand, were tested using displacement control.

The weight of the equipment used to apply forces near each cantilever free end was 350lbf. The unit weight of the (plain) concrete used was measured to be nearly 146 pcf. The average unit weight of the specimens was estimated to be 150 pcf.

5.2 Elements with Moment Gradients (Test Walls)

5.2.1 Setup and Specimen Description

Four large-scale walls were tested as cantilevers with a single lateral cyclic force concentrated near the free end. The total height of each specimen (including foundation) was 40 ft (Figure 23) and was limited by the clearance of the overhead cranes at Bowen Laboratory.

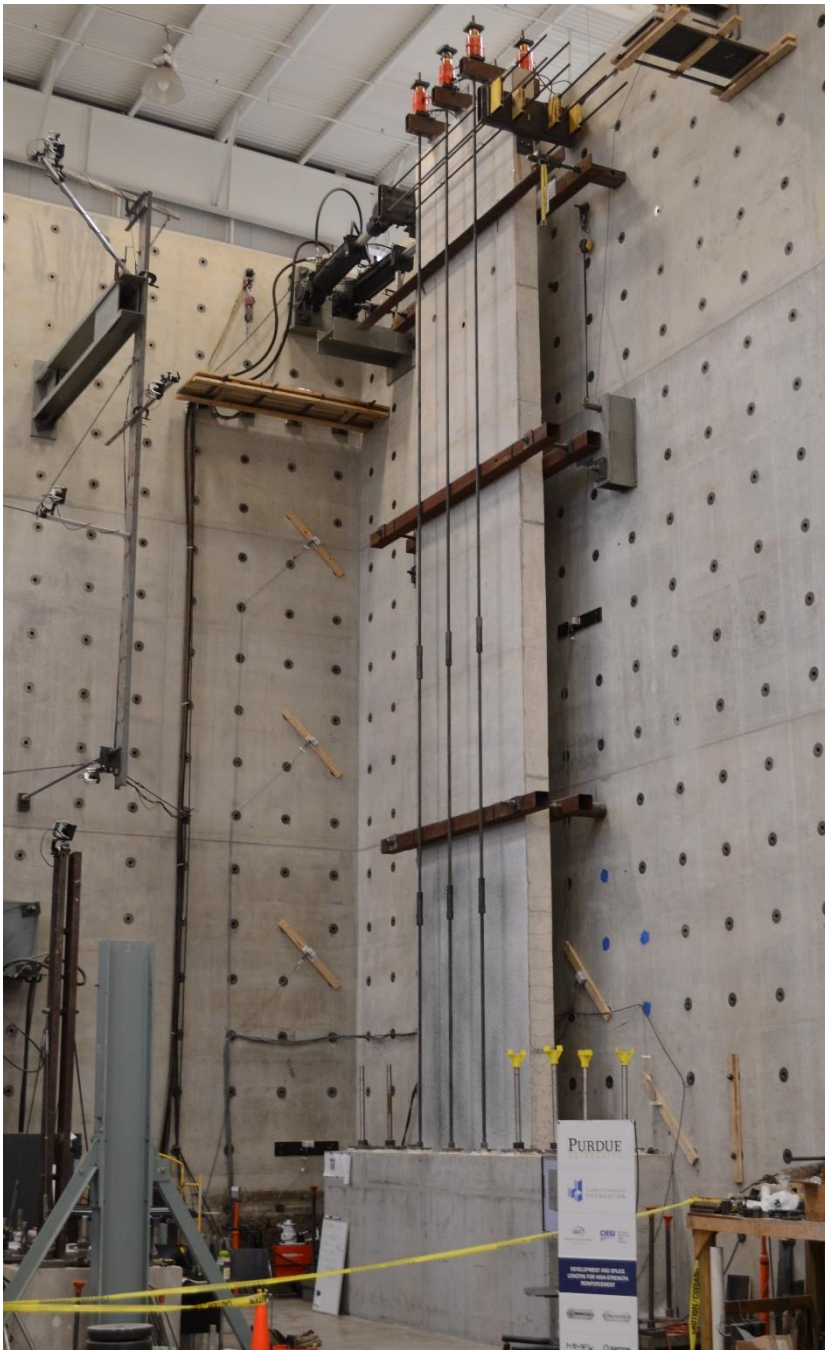

a) Overall Photo

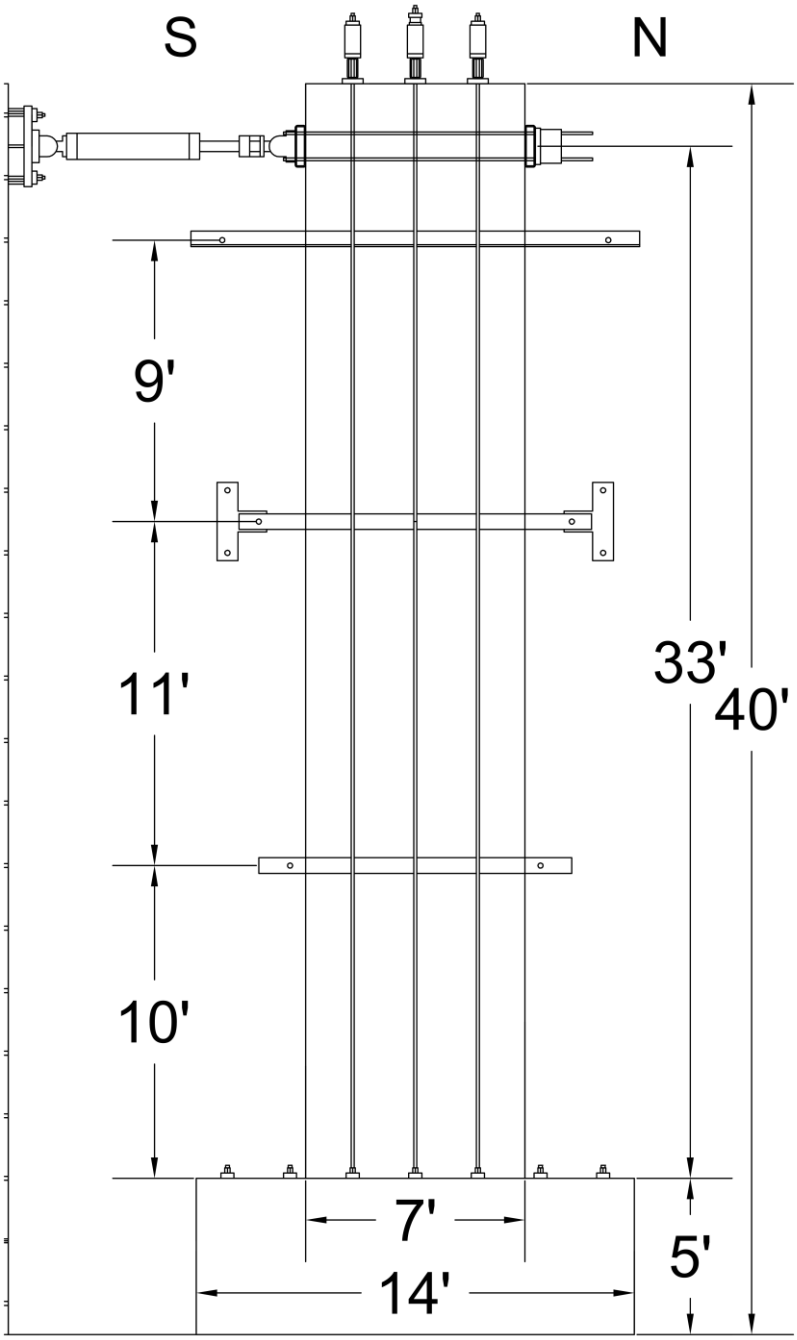

b) East Elevation

Figure 23 – Setup for Test Walls.

All test-wall cross-sections were rectangular, with a length of 7 ft and a thickness of 10 in. (Fig. 24). Wall height (from top of foundation to line of action of lateral force) was 33 ft, for an aspect ratio of 4.7 (Fig. 23). The foundation was 5-ft deep, 14-ft long, and 4-ft wide, and it was clamped down to the laboratory floor with a total vertical force of 2500 kip. This force was reached by post-tensioning eight 2-in. diameter threaded rods (four near each end of the foundation) to 240 kip each, and six 1.25-in. additional threaded rods flanking the web of the test wall in two lines of three rods each. These smaller threaded rods were post-tensioned to 100 kip each, and they were coupled with additional rods that extended to the top of the test wall to allow for application of axial force (Figure 23).

Stops were provided at each end of the foundation to prevent sliding. These stops had a clamping force of 600 kip each and they were installed to allow bearing between the anchor rods used to clamp them and access holes in the reaction floor. No perceptible motion was measured to occur in the foundation in any of the four tests conducted (in which lateral forces as large as 156 kip were reached).

To test walls with a large aspect ratio (4.7) was deemed important for two reasons:

a. It is not simple to project results from tests of cantilevered test walls with small aspect ratios in which both moment and lateral force are applied at the top of the cantilever. In these instances, it is unclear to what extent the loading rig required to apply and control both moment and lateral force can stiffen the test specimen and affect results. In addition, in these tests, a wall segment not included in the test specimen is assumed to select the ratio of applied moment to applied shear. For the purposes of projecting measured drifts, the variation of curvature that needs to be assumed to occur in this hypothetical wall segment is not obvious.
b. Lap splice failure is more likely to be critical in more slender walls because it may lead to their overturning more easily than in a squat wall.

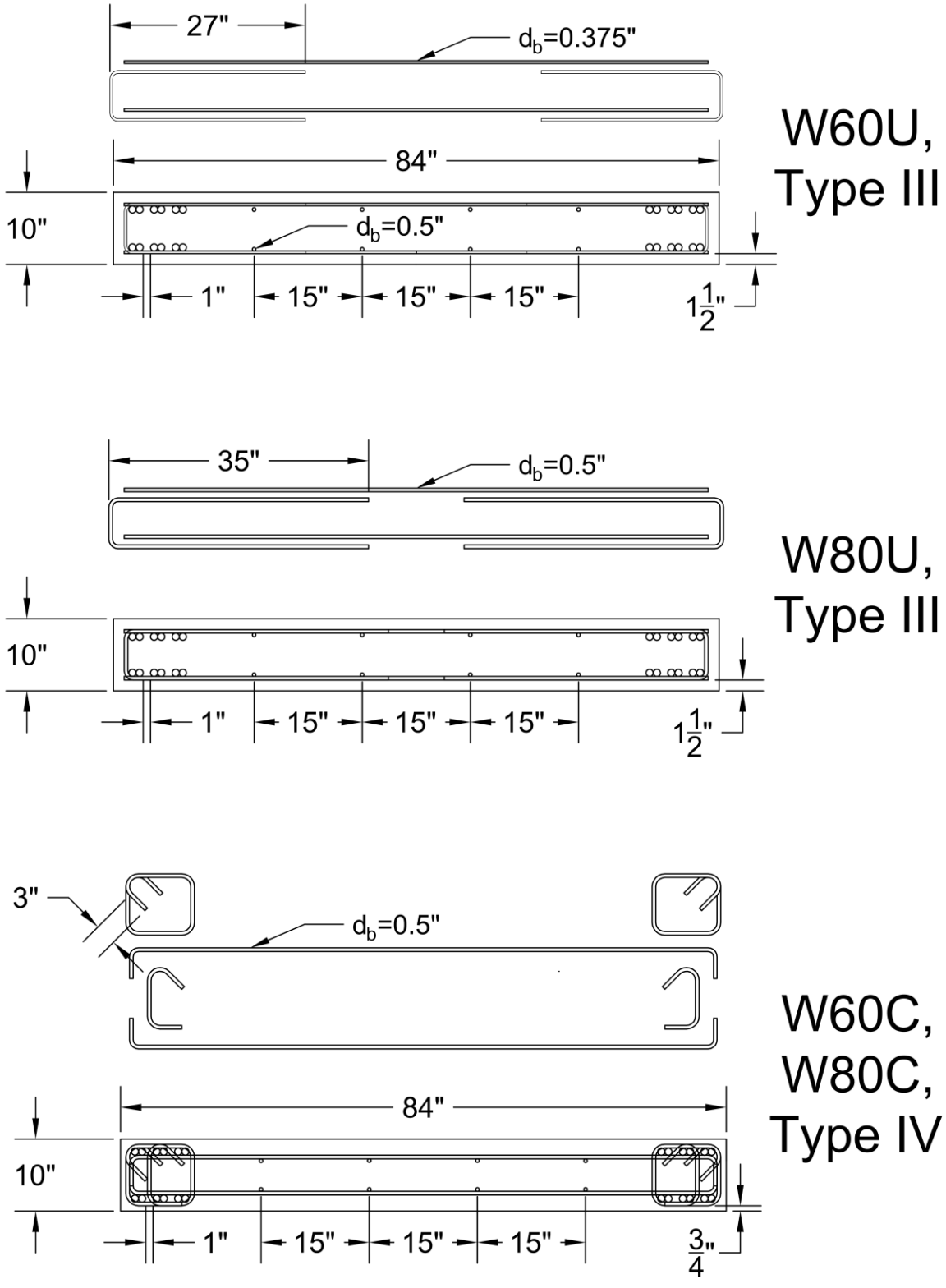

Figure 24 – Wall Cross Sections and Type III and Type IV Transverse Reinforcement Details.

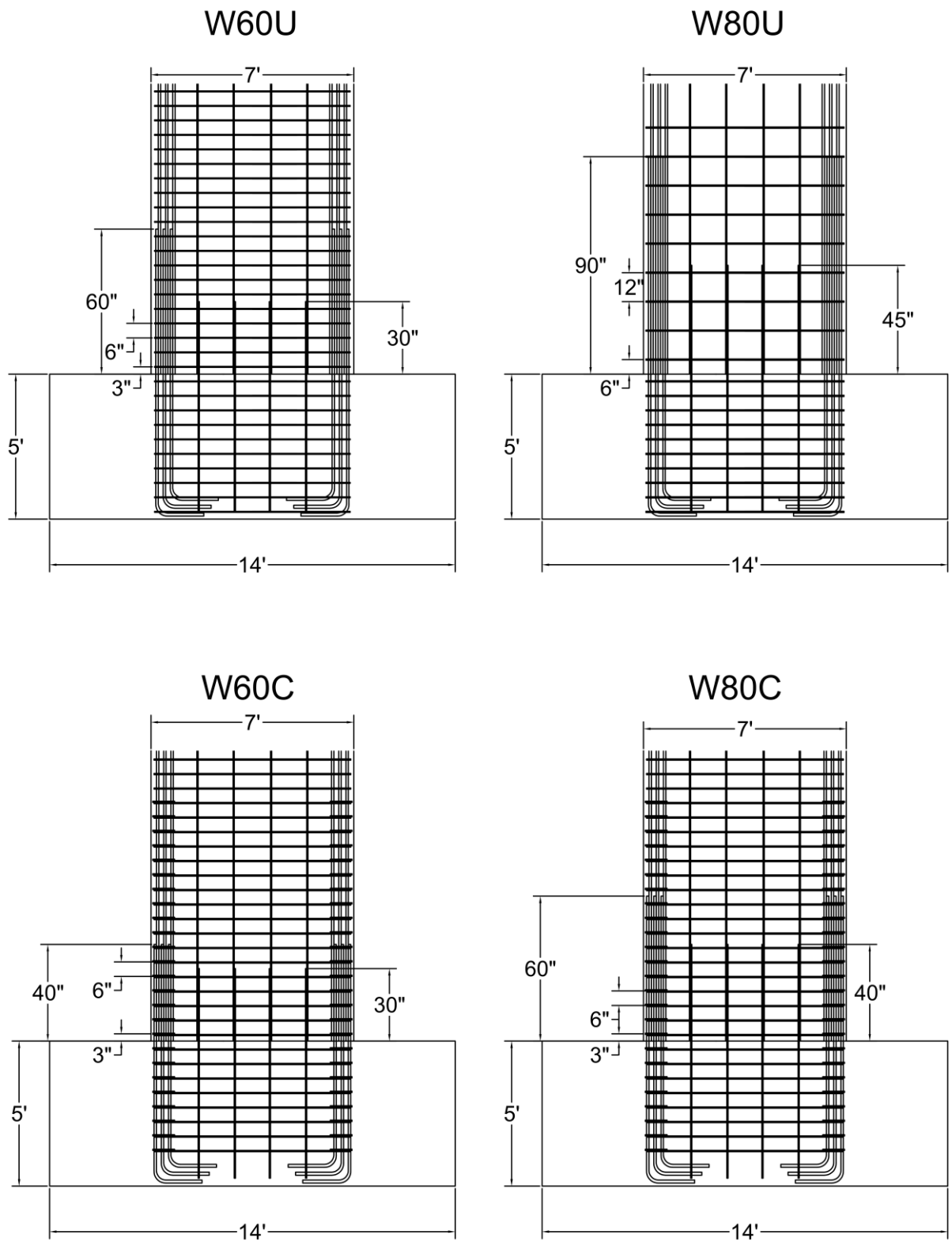

Figure 25 – Test Wall Partial Elevations

Lap splices were configured so that the outer bars anchored in the foundation were closer to the outer edge of the cross section than the bars terminated at top of foundation and extending towards top of wall. No 'dog legs' or kinks were used to align bars away from the lap splice because such detail can cause bar buckling (Section 4.2).

Tables 4 and 5 list key parameters for all test walls. Specimen IDs start with the letter 'W' for all walls tested as cantilevers. As for four-point bending tests, the numbers 60 and 80 denote the nominal steel grade of the longitudinal reinforcement. The letter U refers to boundary reinforcement not enclosed by closed hoops and the letter C identifies elements with closed hoops in boundaries.

Longitudinal reinforcement was #8 Grade-60 (W60U and C) and Grade-80 (W80U and C) bars organized in three layers of two bars each (relative to the neutral axis occuring for moment perpendicular to the plane of the wall) in the boundaries of the cross section (Figure 24). Web longitudinal reinforcement was #4 bars organized in four layers of 2 bars each. Boundary longitudinal bars had lap splices extending from the top of the foundation and towards the top of the wall with lengths of 40 (W60C), 60 (W60U and W80C), and 90 (W80U) bar diameters (Table 4). Web longitudinal bars had 60 (W60U and W60C), 80 (W80C) and 90 (W80U) bar diameter lap splices. Transverse reinforcement was made with #3 (W60U) and #4 (W60C, W80U, W80C) bars of the same grade as the vertical bars. The spacing of transverse bars was 6 in. (W60U and C, W80C) and 12 in. (W80 U). Transverse reinforcement types indicating the detailing used in each specimen are listed in Table 5 and refer to Figure 24. Clear cover (to the outer edge of ties) was 0.75 in. in W60U and W80U and 1.5 in. in W60C and W80C.

Reinforcement in the foundation consisted of 16 #8 longitudinal bars running along the length of the foundation, top and bottom, arranged as shown in Figure 26. These bars had 90-deg hooks at either end with extensions up to 30 bar diameters long. These hooks were confined with u-shaped ties parallel to the length of the foundation as illustrated in Figure 27. Transverse reinforcement consisted of hoops and cross ties cut from #4 bar resulting in a transverse reinforcement ratio of 0.63% (in the vertical direction). Additional reinforcement was provided in the horizontal direction perpendicular to the length of the foundation by means of #4 bars, distributed as shown in Figure 28. Stronger self-consolidating concrete was used to cast the foundation. Two different batches of concrete were needed to cast each foundation.

Measured material properties are described in Section 6.

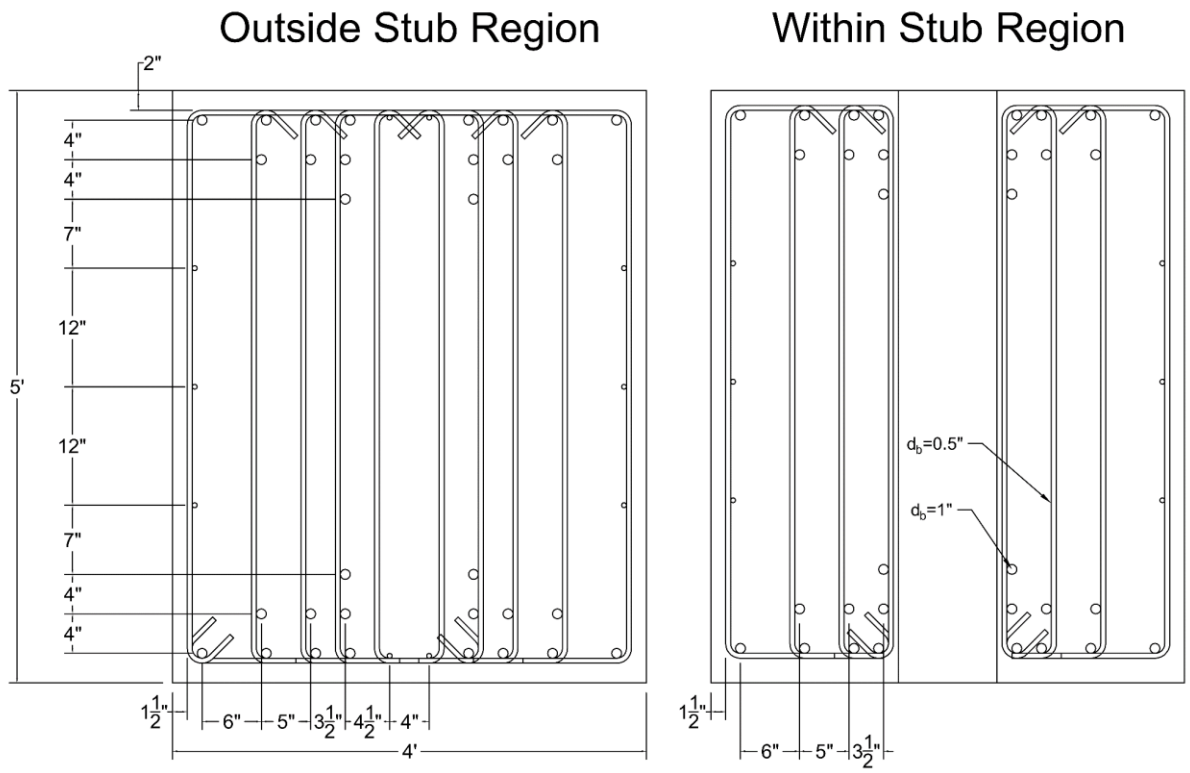

Figure 26 – Cross Sections of Test Wall Foundation.

Figure 27 – Reinforcement in Wall Foundation – Confinement of End Hooks.

Figure 28 – Reinforcement in Wall Foundation – Side View.

Table 4. Parameters related to concrete and longitudinal reinforcement

Specimen ID	Effective Depth [in.]	Measured Concrete Strength [psi]	Nominal Long. Bar Grade [ksi]	Long. Bar Diameter in Boundaries [in.]	Total No. of Spliced Bars	Bars on potential splitting plane	Mea. Long. Bar Yield Stress [ksi]	Long. Bar Strength [ksi]	Splice Length [in.]	Min. Clear Cover [in.] †	Min. Clear Bar Spacing [in.]
W60U	78.13	5.4	60	1	6	2	70	97	60	1.5	1
W60C	78.75	5.6	60	1	6	2	70	97	40	0.75	1
W80U	78.	6.1	80	1	6	2	93	119	90	1.5	1
W80C	78.75	6.0	80	1	6	2	93	119	60	0.75	1

† Measured to outer edge of transverse reinforcement

Table 5. Parameters related to transverse reinforcement

Specimen ID	Nominal Trans. Bar Grade [ksi]	Trans. Bar Diameter [in.]	Number of bars† (legs) assumed crossing potential transverse splitting plane*	Total Area of bars crossing potential transverse splitting plane* Atr [in.^2]	Tie or Stirrup Spacing [in.]	Transverse Reinf. Ratio %	Type (in reference to Fig. 24).
W60U	60	3/8	2	0.22	6	0.37%	III
W60C	60	1/2	2††	0.4	6	0.67%	IV
W80U	80	1/2	2	0.4	12	0.33%	III
W80C	80	1/2	2††	0.4	6	0.67%	IV

†effectively anchored

*parallel to short direction of cross section

††assuming ties anchored within the core of the boundary did not cross splitting planes parallel to either the length or the width of the cross section

5.2.2 Loading Method

Lateral load was applied at 33ft from the top of the foundation using two separate 110-kip Shore Western actuators with swivels at each of their ends and operating in displacement control. The actuators were synchronized to move equal displacement increments using an MTS FlexTest controller. When extending towards the test wall, the actuators reacted against a transfer beam bearing against the closest face of the test wall. To transfer forces in the opposite direction, the actuators were connected by eight 1-in. diameter high-strength threaded rods fastened to a second transfer beam reacting against the opposite face of the specimen. Figure 29 depicts the loading rig used.

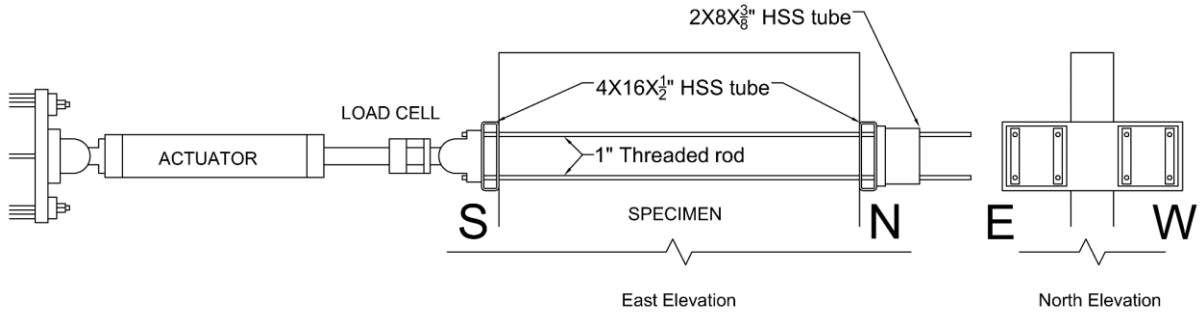

Figure 29 – Lateral Loading Rig

Axial load was applied using six external post-tensioning rods and three transfer beams placed atop the specimen as illustrated in Figure 30. These rods were coupled with the six central rods anchoring the foundation down to the strong floor. They were stressed using six hollow jacks connected to a common hydraulic pump controlled manually to keep the total axial load within +-20 kips from the target load of 400 kips. Careful control of the axial load was needed because longitudinal axis of the wall elongates as the wall deflects laterally. Figure 31 shows a typical axial load record. Equipment weight and self-weight account for an additional 34 kip of axial load. The total axial load was 10.3% of the product of nominal concrete strength and gross cross-sectional area.

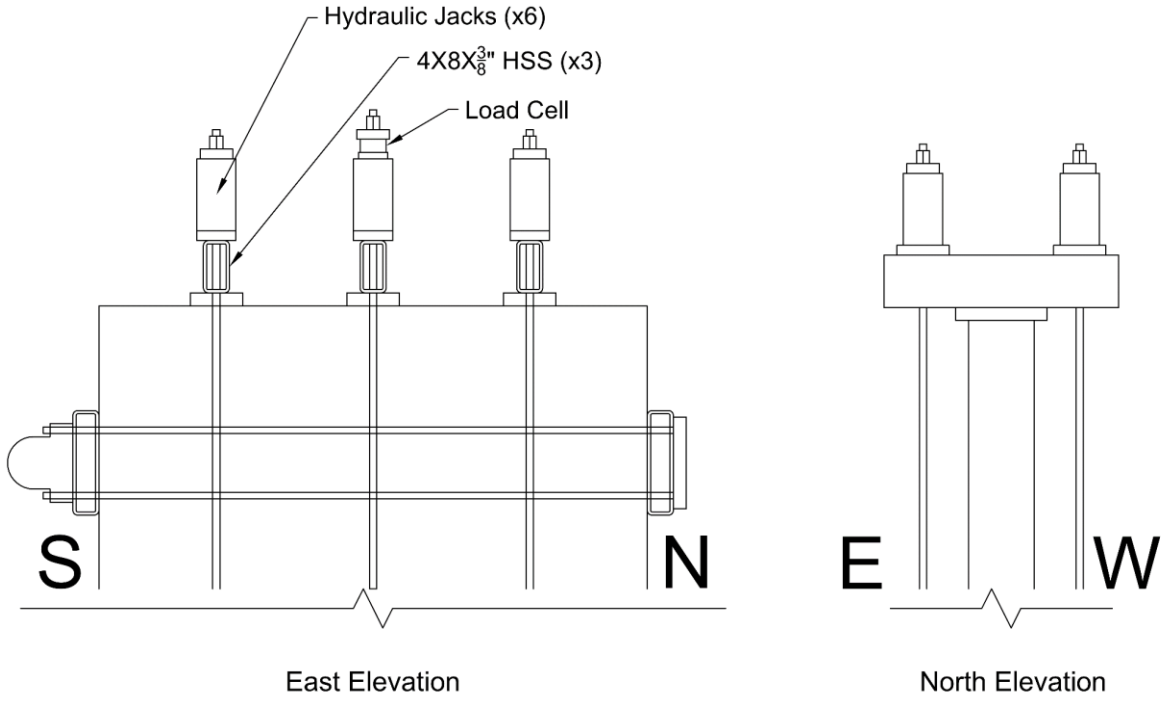

Figure 30 – Axial Loading Rig.

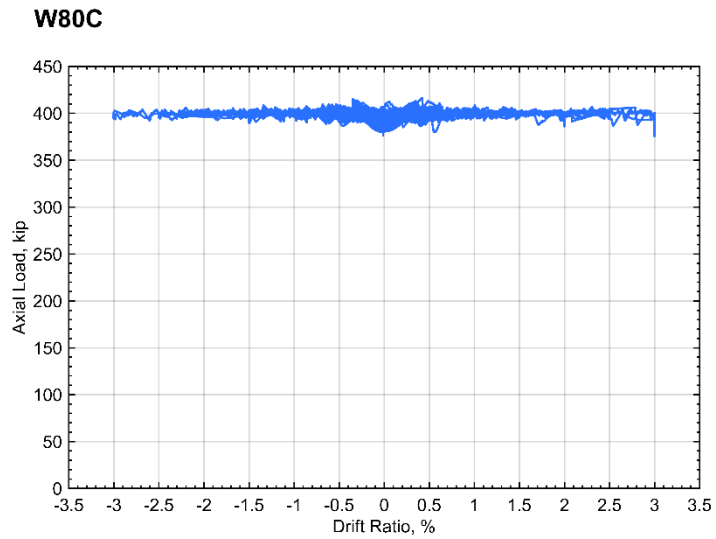

Figure 31 – Typical Axial Load Record.

Two different loading schemes or 'protocols' were used for lateral loads. The first scheme was adapted from the recommendations by FEMA 461. It is illustrated in Figure 32. The scheme is not the result of an attempt to try to reproduce a 'realistic' displacement history produced by an earthquake. It is instead a compromise representing a demanding set of cycles that can be used to compare alternatives (in this case to size and confine lap splices).

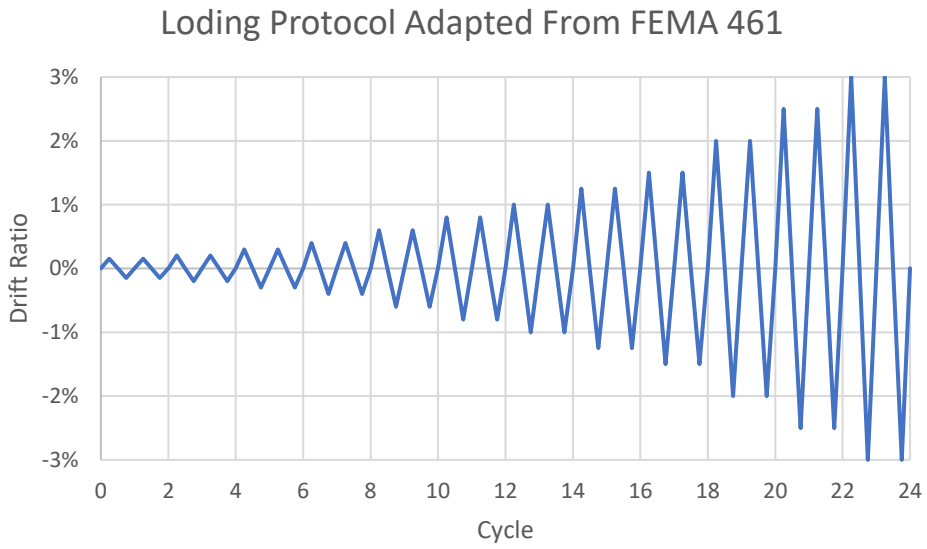

Figure 32 – Loading Protocol A.

In the second scheme, the initial cycles in the first scheme were replaced with an intense sequence of hundreds of cycles of relatively small amplitude as illustrated in Figure 33. In relation to this figure, the yield deflection δ_y was selected as 0.7% of the wall height for test wall W60C and 0.85% of the wall height for test wall W80C. After the sequence of cycles, the protocol resumed with the next loading step adapted from FEMA 461 beyond $1.5\delta_y$.

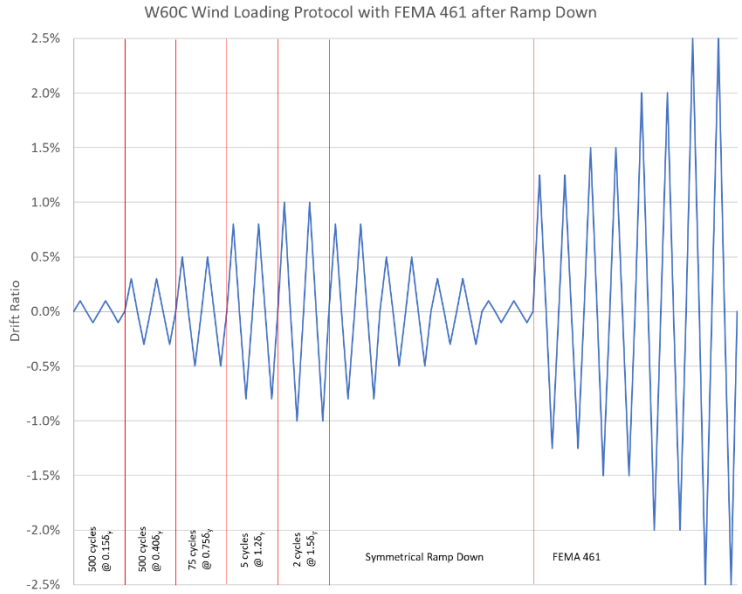

a) Specimen W60C

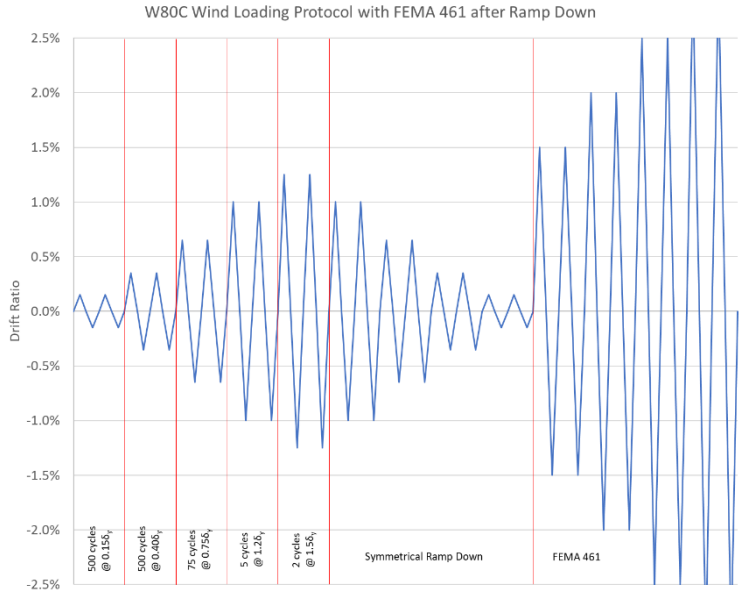

b) Specimen W80C

Figure 33 – Loading Protocol B.

Despite introducing an additional variation making a direct comparison between the results obtained with Scheme A and B more difficult, the additional small-amplitude cycles were introduced because:

-They may be deemed to represent conditions resembling what may occur in a slender structure under prolonged exposure to strong winds.

- They constitute a more demanding test of the lap splices that were expected to produce the best results (i.e. lap splices confined with tightly spaced closed hoops).

Target Drift Ratios for each loading protocol are available in the Appendix to this document.

6. Materials

6.1 Concrete

Concrete was obtained from a local ready-mix provider (IMI Inc.) in Lafayette, Indiana, who procures aggregates from US Aggregates in Battleground and Delphi, IN. All specimens were cast with concrete mixed using the same nominal proportions listed next.

Type I Portland Cement	460 lb
Sand	1500 lb
#8 Crushed Stone (max. particle size of ¾ in.)	1800 lb
Water	250 lb
Water / Cement Ratio	0.54

Concrete for Wall Foundations used the nominal proportions listed next:

Type I Portland Cement	580 lb
Class F Ash	145 lb
Sand	1350 lb
#8 Crushed Stone (max. particle size of ¾ in.)	950 lb
3/8” Pea Gravel 1800 lb	500
Water	279 lb
Water / Cement Ratio	0.38

Mix proportions reported on the day of casting by the ready-mix provider are listed in the Appendix to this document.

The measured compressive strengths of concrete cylinders cast and cured with the test specimens are listed in Table 6. The listed strengths are the average of at least three standard 6x12 in. cylinders tested within one day of specimen failure. In the case of the foundation the listed values come from two separate batches. The table also includes measured values of modulus of elasticity, modulus of rupture, and split-cylinder strength. Cylinders were tested using a 600-kip Forney Testing Machine.

Table 6. Measured Mechanical Properties of Concrete

Specimen ID	Cylinder Compressive Strength [psi]	Modulus of Elasticity* [ksi]	Split Cylinder Strength [psi]	Modulus of Rupture [psi]
WB60U0	5410	--	590	--
WB60U1	5750	--	560	630
WB60U2	6020	--	560	720
WB60U3	6180	--	580	570
WB60U4	5610	--	525	610
WB60U5	5820	--	550	600
WB80U1	5290	--	510	600
WB80U2	5240	--	480	580
W60U	5370	5000	510	750
Foundation	7720	5200	560	760
W60C	5590	4800	510	750
Foundation	7980	5500	610	590
W80U	6060	4600	620	620
Foundation	7440	5100	645	580
W80C	5960	5100	565	820
Foundation	8560	5300	650	870

*Slope of secant to stress-strain curve drawn at a stress of 0.45f'c

6.2 Steel

In all test specimens reported here (Vol. II) longitudinal reinforcement was fabricated using 1-in. diameter (No.-8) reinforcing bars. All specimens marked with the number 60 had longitudinal reinforcement with a nominal grade of 60 ksi, and all specimens marked with the number 80 had Grade-80 bars. Transverse reinforcement was produced using No.-3 bars in all Grade-60 specimens tested in four-point bending (marked by the letters 'WB') as well as specimen W60U, and No.-4 bars in specimens WB80U1, WB80U2, W60C, W80U, and W80C.

All bars from a given grade and diameter came from a single production heat except for No.-8 Grade-60 bars which came from three different heats: one for specimen WB60U0, one for specimen WB60U1 to 5, and one for test walls W60U and W60C. Three 3-ft long coupons were tested for each heat. Key measured properties are listed in Table 7.

Table 7. Measured Mechanical Properties of Steel Reinforcing Bars.

Heat ID	Nominal Grade [ksi]	Bar Diameter [in]	Specimens Fabricated with Bars form Listed Heat	Orientation in Specimen	Yield Stress [ksi]	Peak Stress: Strength [ksi]	Strain at Onset of Strain Hardening	Strain at Peak Stress	Fracture Strain†
0††	60	3/8	WB60U0	Trans.	70	103			.16
1	60	3/8	WB60U1 WB60U2 WB60U3 WB60U4 WB60U5 W60U	Trans.	69	98	N/A	.108	.153
2	60	1/2	W60U W60C	Long. - Web	69	97	N/A	.103	.156
			W60C	Trans.					
3	80	1/2	W80U W80C	Long. - Web	89	112	.016	.097	.145
			W80U W80C	Trans.					
			WB80U1 WB80U2	Trans.					
4†††	60	1	WB60U0	Long. - Boundary	60	94	N/A	.130	.195
5	60	1	WB60U1 WB60U2 WB60U3 WB60U4 WB60U5	Long. - Boundary	71	103	N/A	.103	.187
6	60	1	W60U W60C	Long. - Boundary	70	97	0.014	.117	.205
7	80	1	WB80U1 WB80U2 W80U W80UC	Long. - Boundary	93	119	.012	.095	.161

†Measured with calliper after test completion –by butting both ends of fractured specimen– using four reference punch marks placed on the bar surface at a spacing of 2 in.

††Heat 0 was not tested. Reported values were obtained from Mill Certification Sheets provided by the fabricator.

††† Only 2 bars were tested from Heat 4

Tensile stress-strain curves measured for the mentioned 3-ft long coupons are plotted in Figures 34 and 35. They were produced from measurements obtained using a 120-kip Baldwin universal testing machine and an Epsilon extensometer with a gage length of 2 in. Clear distance between the grips of the testing machine was 2ft. In reading these curves consider that gage length can affect the descending part of the curve. For this reason and to protect the instrument, the extensometer was removed after it was judged that the peak stress was reached during each coupon test. Figures 34 through 36 focus on strains smaller than 8% because strains inferred to have occurred during the tests of walls and beams did not exceed this value. Refer to Table 7 for information of peak stress and the associated strain.

No. 3 (3/8 in) Heat 0	N/A
No. 3 (3/8 in) Heat 1	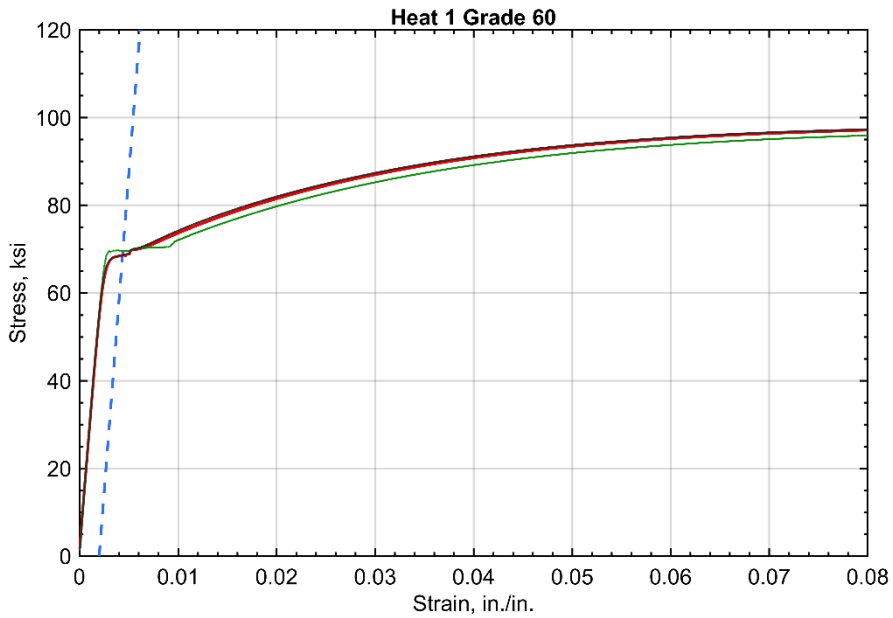

No. 4 (1/2 in) Heat 2	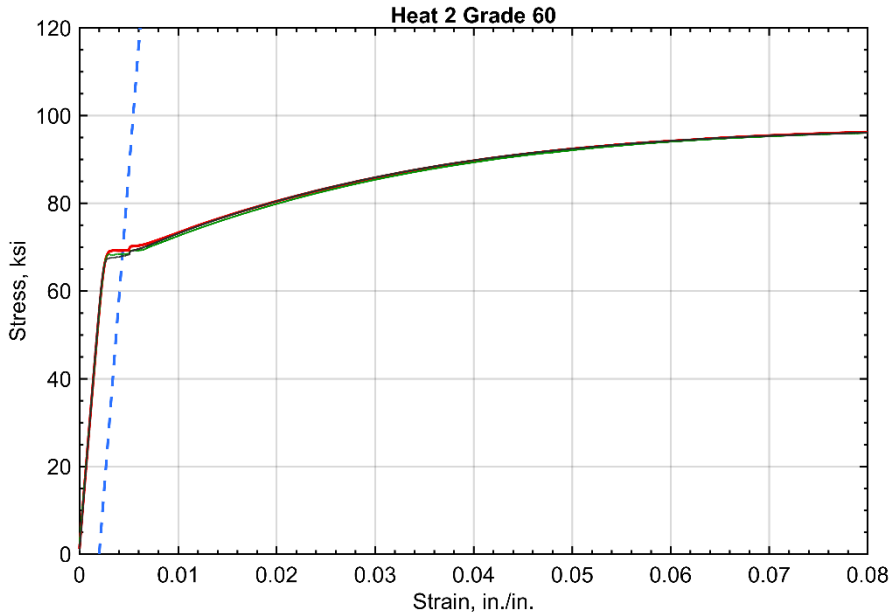
No. 8 (1 in) Heat 4	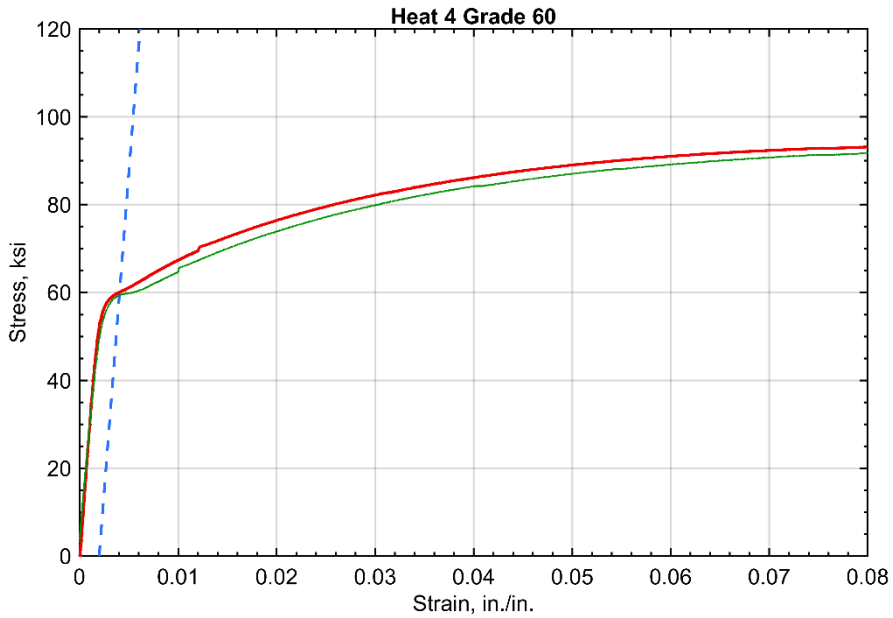

No. 8 (1 in) Heat 5	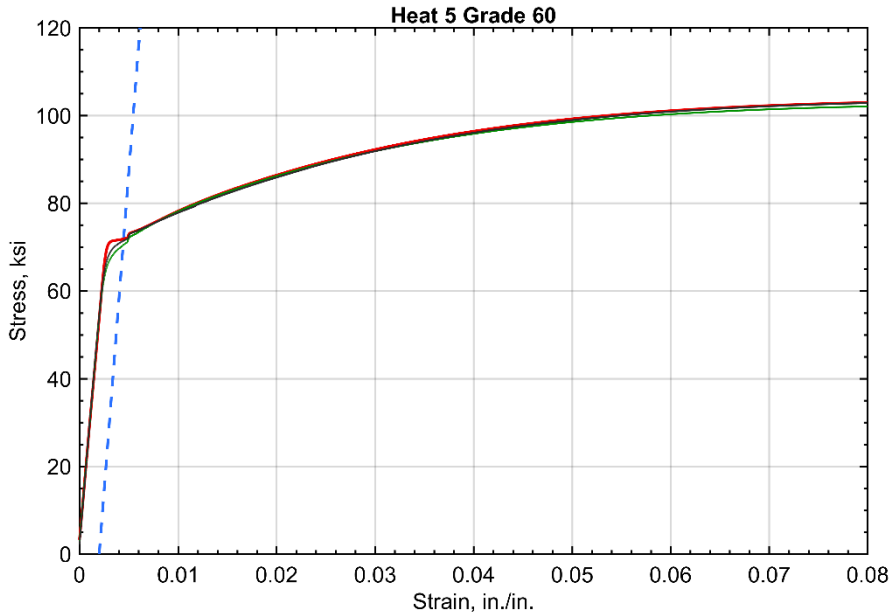
No. 8 (1 in) Heat 6	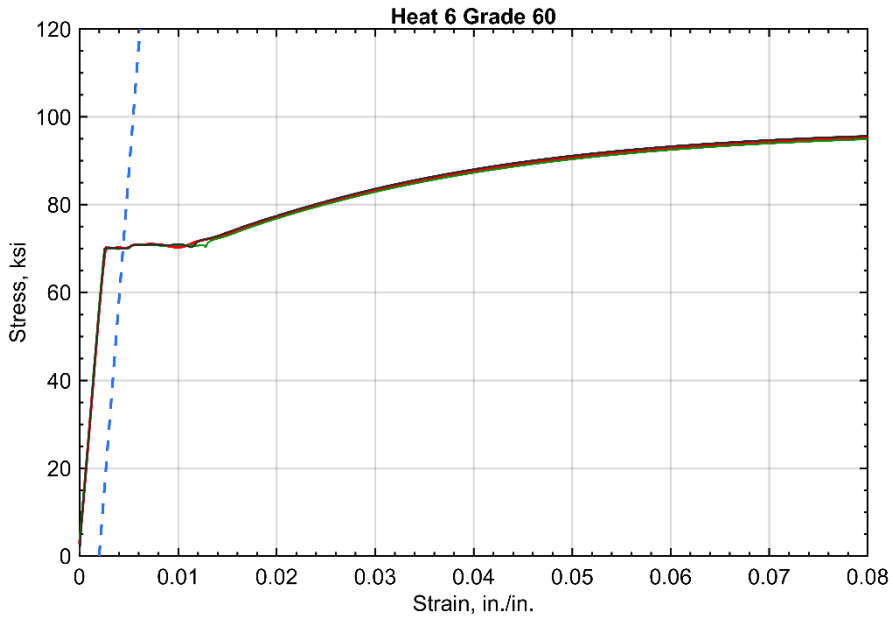

Figure 34 – Stress-Strain Curves Measured in Grade-60 Bars.

No. 4 (1/2 in) Heat 3	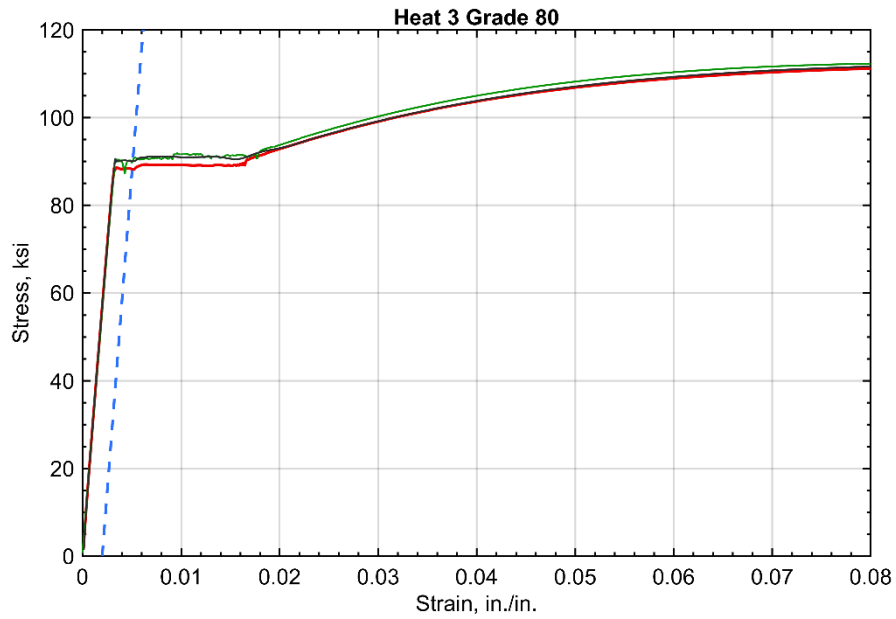
No. 8 (1 in) Heat 7	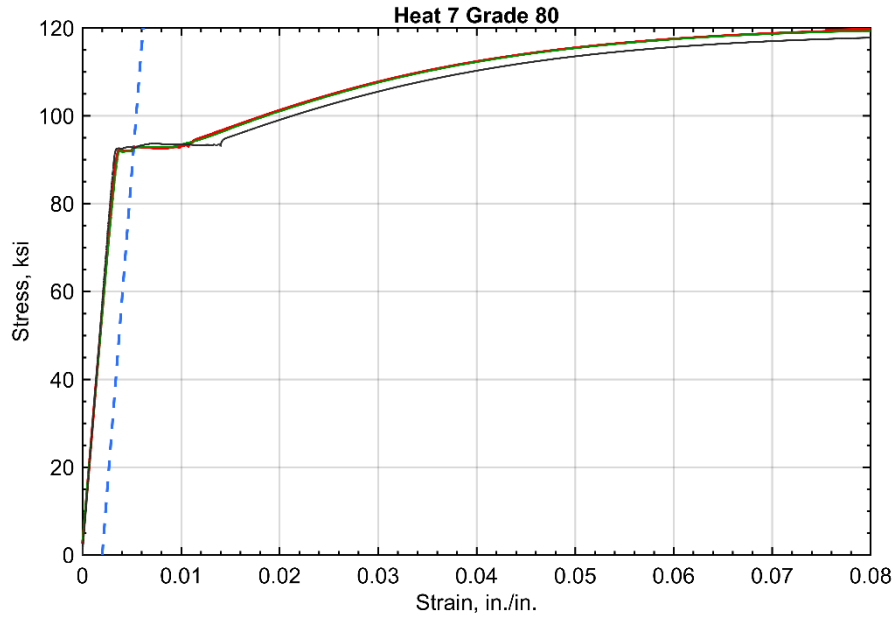

Figure 35 – Stress-Strain Curves Measured in Grade-80 Bars.

Figure 36 shows a comparison between the stress-strain curve obtained from the No.-8 Grade-80 bars used in this investigation and curves from samples obtained by Wiss Janney and Elstner (WJE) Inc[4]. in a separate investigation of representative properties of steel reinforcing bars in the USA. The comparison shows that the used bars represent a plausible upper bound in terms of yield stress and strength.

[4] Conrad Paulson, Personal Communication.

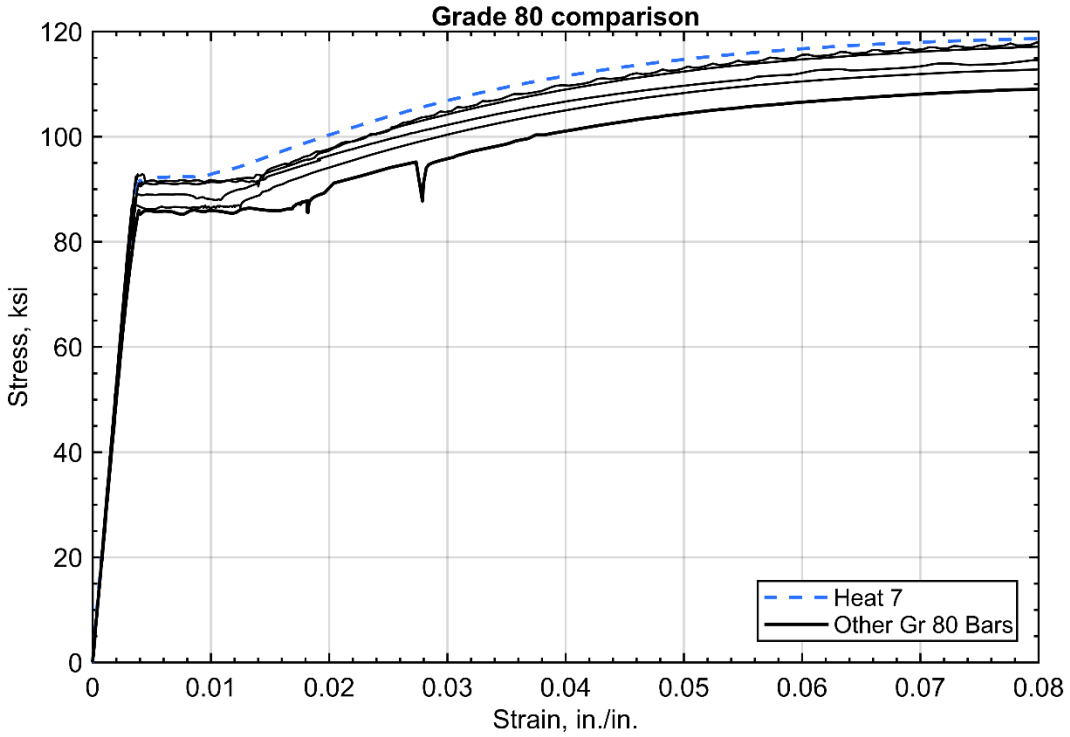

Figure 36 – Comparison of stress-strain curves of Grade-80 reinforcement used as longitudinal reinforcement used in this investigation and other bars obtained in the USA in a separate study by WJE Inc.

Figure 37 compares the stress-strain curves obtained for the bars used as longitudinal reinforcement in this study. All No.-8 bars used as longitudinal reinforcement in boundaries of test walls had a yield plateau. In contrast, the Grade-60 No.-8 bars used as longitudinal reinforcement in four-point bending tests of beams did not have a yield plateau. Wight and Sozen (1975) have shown that a yield plateau tends not to affect the force-deformation response of an element resisting demands causing a moment gradient. In other words: cantilevered elements respond as if their reinforcement had no plateau even if it does have one. In that sense it is convenient that the plateau did not occur in Grade-60 bars used to fabricate the test beams, which had no moment gradient along their test spans and are expected to be sensitive to the effects of the plateau.

All stress strain curves are representative of the monotonic response of the reinforcing steel and, as mentioned by Aktan (1973), will not accurately reflect stress-strain response of steel subjected to cyclic loading where steel is subjected to both tension and compression forces (i.e. in Wall tests). That being said, compressive steel strains are likely to be low in the boundary of a wall under loading reversals (at least up until concrete spalling and bar buckling), so the effects of cycling on the stress strain response is expected to be smaller than in cases in which compressive strains are as large as tensile strains.

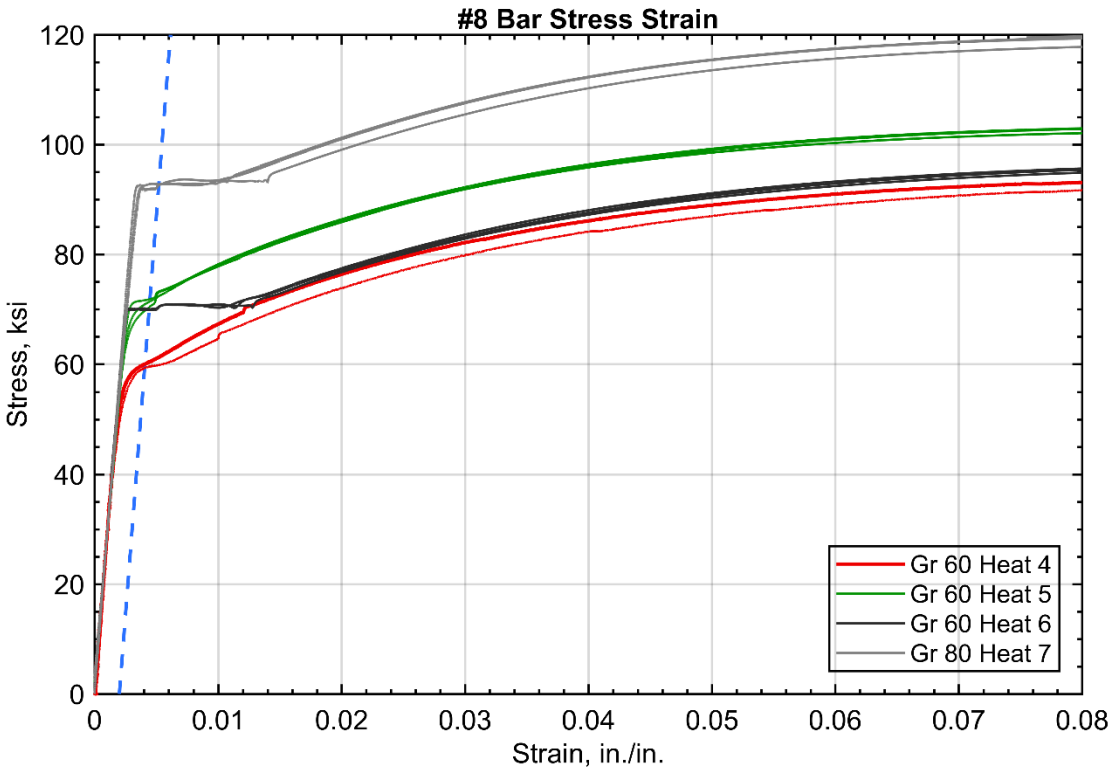

Figure 37 – Comparison of stress-strain curves of longitudinal reinforcement used in this investigation.

7. Fabrication Process

7.1 Casting

Test beams (tested in four-point bending) were cast on their sides and later tilted up for transportation and testing. Each beam was cast in a single 10 in. lift with concrete from a single batch. All formwork was made with coated plywood. As-built dimensions for test beams are available in the Appendix to this document. Beams were tilted up and transported to the testing setup using four clevises installed in the lifting inserts shown in Figure 39 and were attached in pairs to two 20-ft long straps and two separate 30-tn overhead cranes operating nearly in sync. Lifting inserts did not coincide with the lap splices. During testing, beams were restrained in their lateral direction by the braces shown in Figure 41.

Figure 38 – Casting of Test Beam.

Figure 39 – Lifting Inserts used in Test Beams.

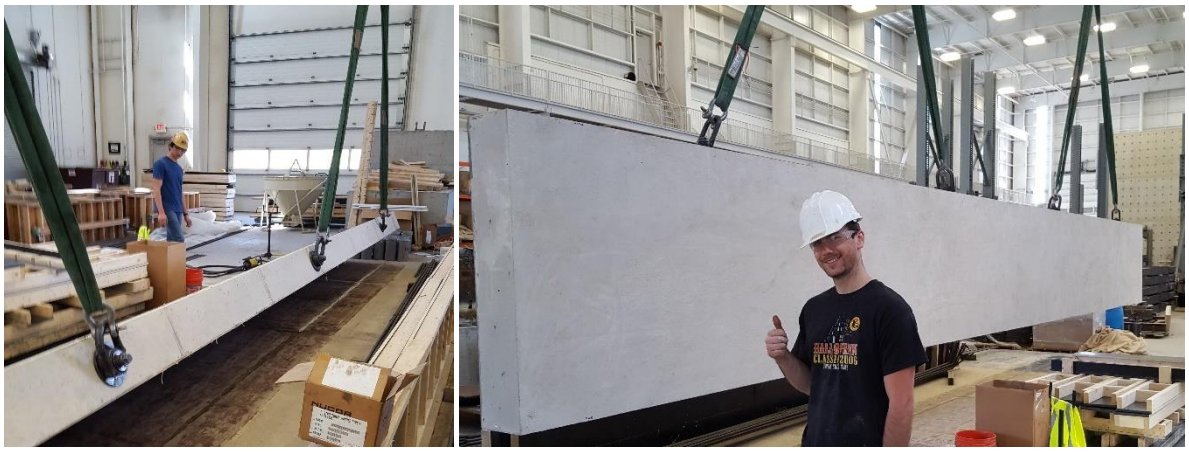

Figure 40 – Tilt-up and transportation of test beam.

Figure 41 – Bracing used in Four-Point Bending Tests of Beams.

Test walls were cast in a two-stage process. First, the segment of test walls extending beyond the foundation was cast on its side in similar fashion to how test beams were cast (Figure 42).

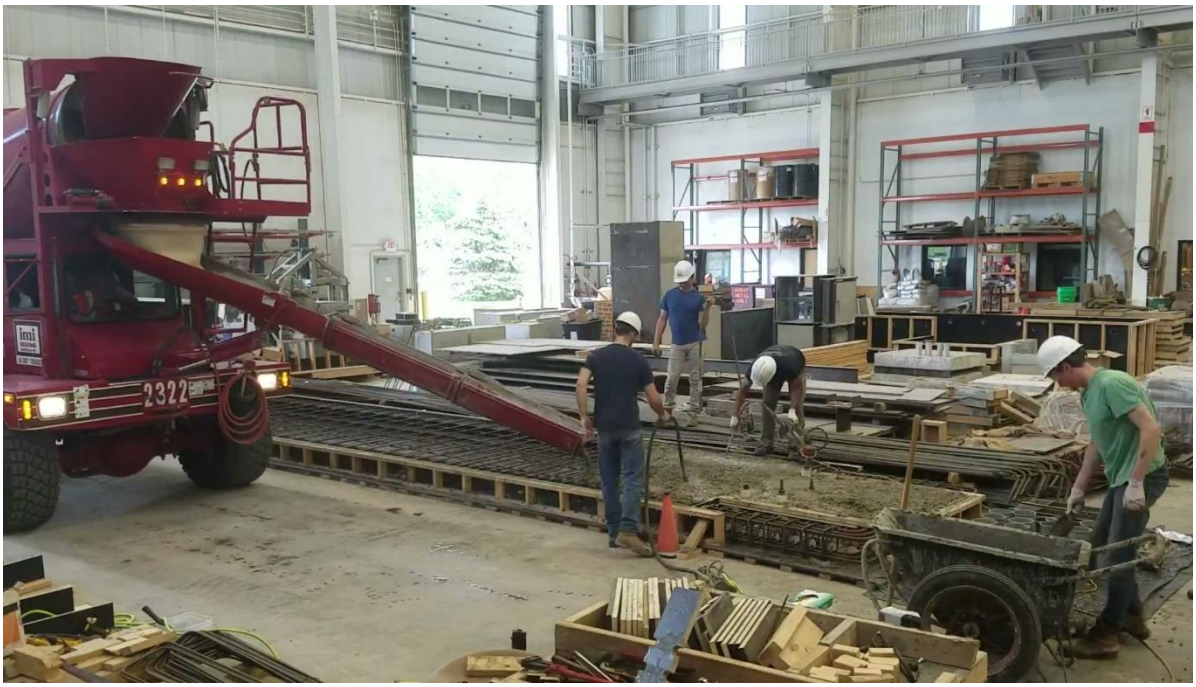

Figure 42 – First Stage of Casting of Test Wall.

In test walls, lap splices were cast in the first casting stage, with bar segments required for anchorage into the foundation protruding out of the formwork. The projection of the wall web into the foundation was also cast during the first casting stage to create a stub to support the wall during the second stage (in which the foundation was cast around this stub, embedding the lower ends of lap splices in the foundation concrete). The support stub was provided with shear keys on each face as illustrated in Figure 44. These faces were also roughened prior to casting of the foundation. The shear keys were 1-in. deep and had triangular cross sections with a 2-in. wide projection on the concrete surface. Sleeves were cast into the support stub to pass foundation reinforcement through them later as illustrated in Figure 45, improving the connectivity between stub and foundation. As-Built dimensions for test walls are available in the Appendix to this document.

Figure 43 – Photographs of formwork built around spliced reinforcement near base of test wall.

Figure 44 – Shear keys, steel bushing, and openings in supporting stub of test walls.

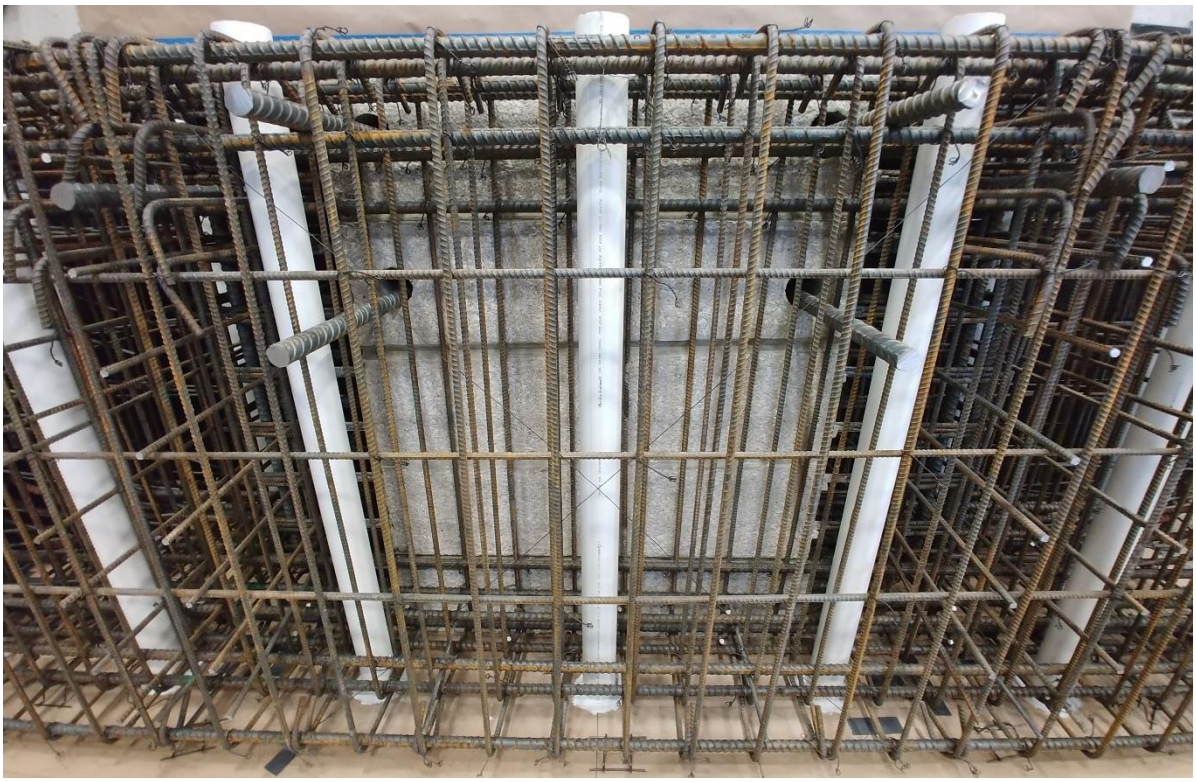

Figure 45 – Connectivity Reinforcement Passing Through Support Stub in Foundation of Test Walls.

Before the foundation was cast:

1) Each test wall was tilted up, rotating it 90 degrees along its longitudinal axis. In this operation the four clevises installed in the lifting inserts indicated in Figure 46 were used along the length of the wall and were attached in pairs to two 20-ft long straps and two separate 30-tn overhead cranes operating nearly in sync.
2) Once upright, the wall was then transported –with its longitudinal axis being horizontal- to a temporary steel frame (Figure 47).
3) While the wall was still attached to the two overhead cranes via lifting inserts, a 2 in. steel pin was inserted into a steel bushing cast in the concrete stub 18 in. from the line where the top surface of the foundation would meet the wall (Figure 46). The wall was then lowered from the cranes, resting the mentioned pin on the temporary steel frame on one end of the wall. The other end of the wall rested on a 2'x2'x2' concrete block.
4) Once the wall was resting on the frame and the concrete block, the clevises were removed from the wall and a pin was passed through a bushing cast along the longitudinal axis of the wall, 8 feet from the top of the wall. A single 20-ft strap and two clevises were used to fasten this pin to a single overhead crane.
5) Once the wall was supported by the temporary steel frame and the overhead crane, it was tilted up once more by lifting the pin near the top end of the wall. In this operation the specimen rotated 90 degrees about the axis of the pin passing through the stub that served as a pivot.
6) The wall was transported to the test setup where it rested against the laboratory floor through the support stub.
7) The wall was temporarily tied to the Strong Wall using 1.25in. Dywidag Bars passing through openings cast 7 feet from the top of the wall and 26in. from either side of the wall centerline.
8) The reinforcing cage for the foundation was assembled around the supporting stub.
9) Formwork was built around the foundation reinforcing cage.

Foundation concrete was cast using a 1-yard bucket that was lifted by a 30-tn overhead crane. Each foundation used approximately 12 buckets of concrete. Construction paper was used to prevent the concrete from adhering to the reaction floor of the laboratory, and polyethylene sheet was used to prevent concrete from adhering to the Strong Wall of the laboratory.

Lateral bracing was installed along the height of the wall to prevent out of plane buckling.

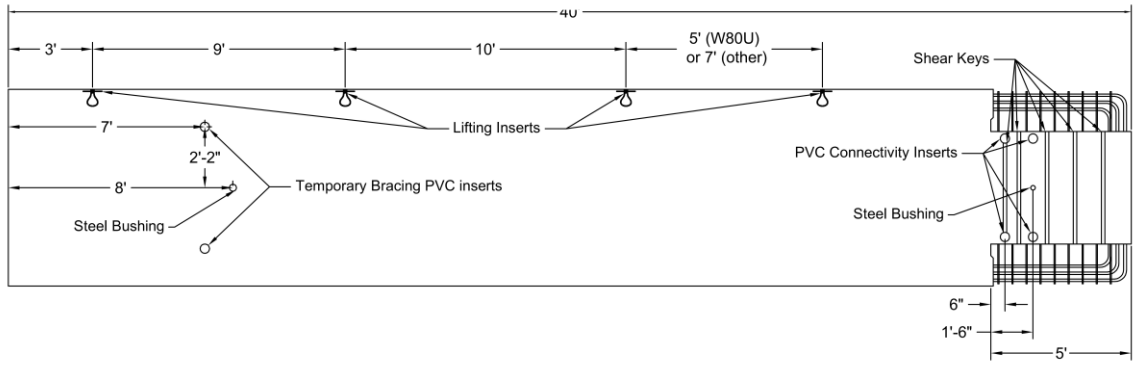

Figure 46 – Lifting Inserts and Openings in Test Walls.

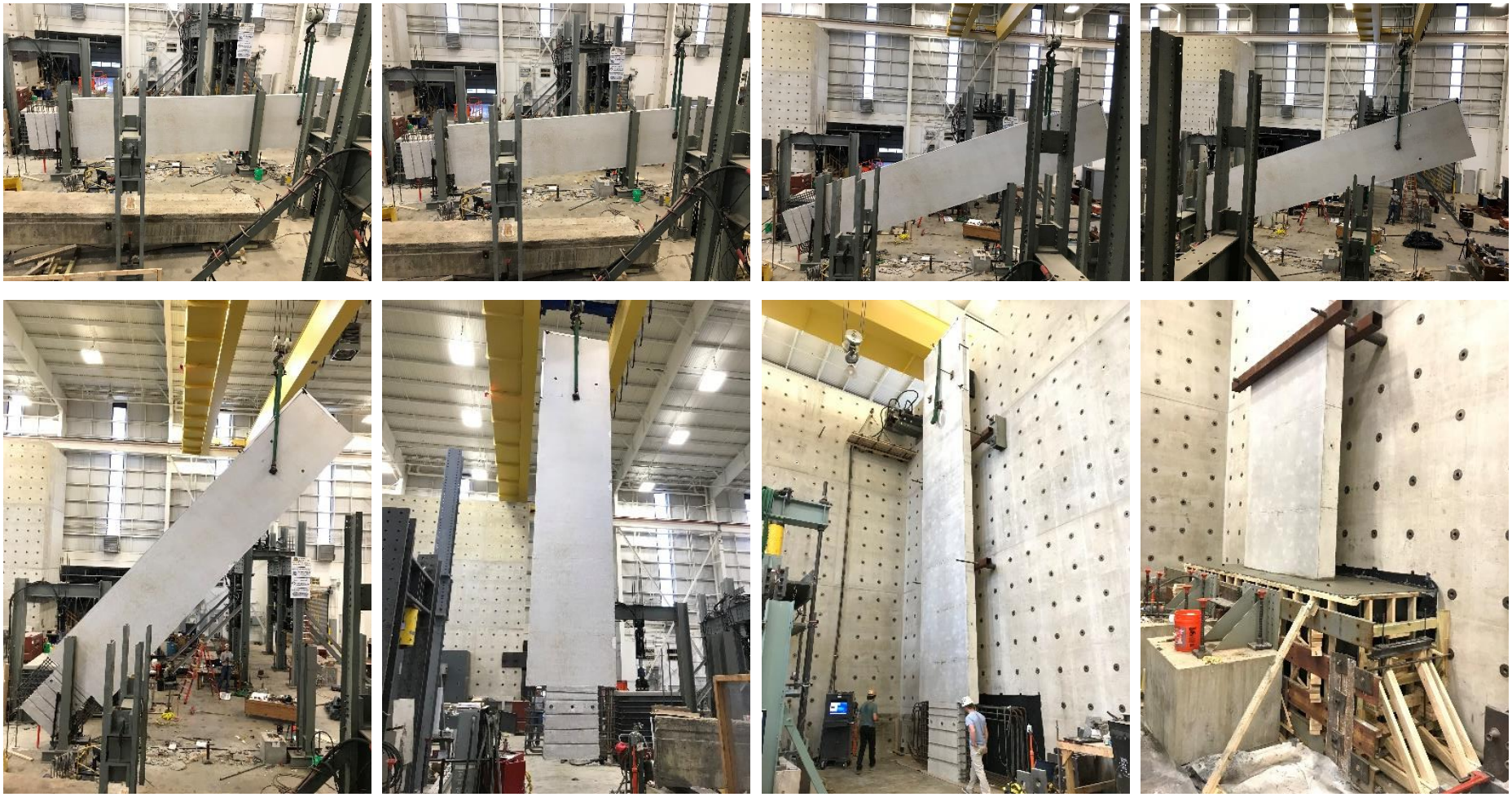

Figure 47 – Wall tilting process and foundation fabrication.

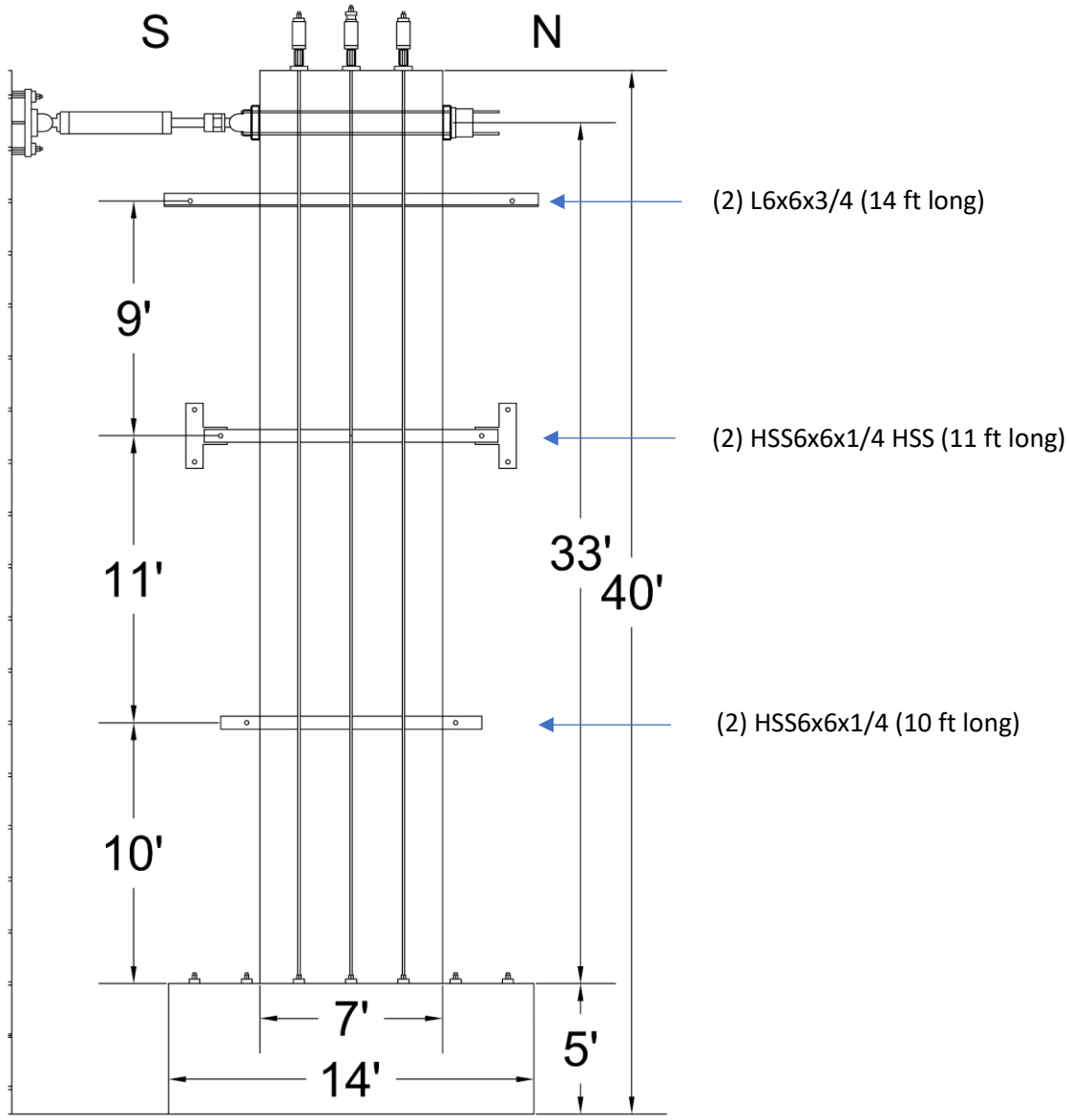

Figure 48 – Details of Bracing used for Test Walls.

7.2 Curing

All specimens, including test cylinders, were cured for 3 to 7 days under wet burlap and polyethylene sheets. Forms were stripped 3 days after casting. Specimens were stored in laboratory conditions (with temperatures varying between approximately 50 and 80 degrees) after curing. Foundations were cured in a similar manner as specimens were. Shrinkage cracks were not observed in test walls or beams. Wall foundations had narrow cracks[5] throughout, as shown in Figure 49.

[5] Cracks were no wider than 0.015 inches, with most cracks not exceeding 0.005 inches

Figure 49 – Shrinkage Cracks observed and marked on the foundation of Test Wall W80C.

7.3 Instrumentation

Four main types of sensors were used to measure forces and deformations in beam and wall tests: LVDTs, Encoders, Load Cells, and Pressure Transducers. All sensors were calibrated prior to testing. The resulting sensitivities convert voltage signals (or counts, in the case of the encoders) to equivalent physical values measured in the specimens. A list of the calibration constants and accuracies of each sensor used is given in Table 8 and Table 9. In addition to the aforementioned sensors, two optical target tracking systems were used to measure surface deformations of beams and walls. The OptoTrak system produced by Northern Digital, Inc. was used for beam tests, and the Optitrack system produced by NaturalPoint, Inc. was used for wall tests. The former uses infrared cameras to track wired LEDs. The latter also uses infrared cameras but tracks wireless reflective targets instead.

The beam sensor layout and optical target locations are depicted in Figure 50. Encoders were used to measure displacements in beams beneath points of load application, at midspan of the central length, and 40” on either side of midspan. LVDTs were used to measure relative motion at beam support plates. All displacement sensors were connected to steel brackets that were attached to the surface of the specimen with epoxy adhesive. A single center-hole load cell was used to measure the load in a hydraulic jack at each overhang, and then the measured force in the load cell was doubled to approximate the total load applied at its respective overhang. The total load reported is the average of the loads applied at both overhangs.

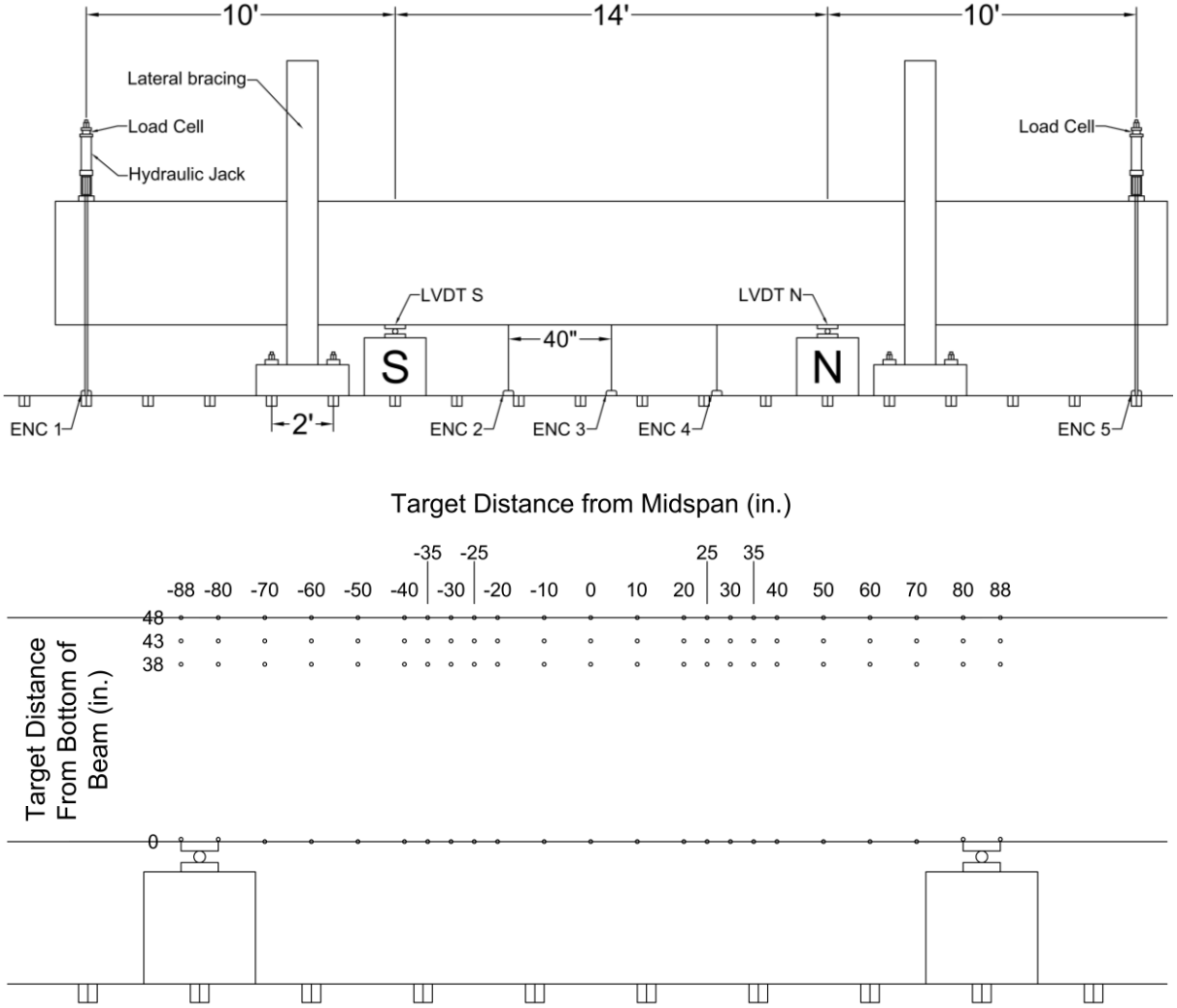

Figure 50 – Layout of Sensors used in Test Beams.

Notes: ENC stands for optical encoder (used to measure displacement), LVDT stands for linear variable differential transformer (used to measure displacement), Load Cells are force transducers.

The Wall sensor layout and target locations are depicted in Figure 51. Encoders were used to measure lateral displacements at 1in., 7ft, 15ft, 23ft, and 33ft along the height of the wall. LVDTs were used to measure foundation slip and uplift and were attached to the foundation 6 inches from the NW and SW corners of the top of the foundation, as well as the center of the north face of the foundation 2 feet below the top of the foundation. Axial load was measured from a pressure transducer placed in parallel to the manifold supplying pressure to all 6 of the hydraulic jacks applying axial load to the wall. A load cell located above the center East hydraulic jack was also used to monitor axial load. The average of the values obtained from the Pressure transducer and the Load cell was reported as the total axial load applied to the wall. Lateral load applied to the wall was measured by load cells integrated into the two Shore Western actuators used to control the lateral displacement of the wall.

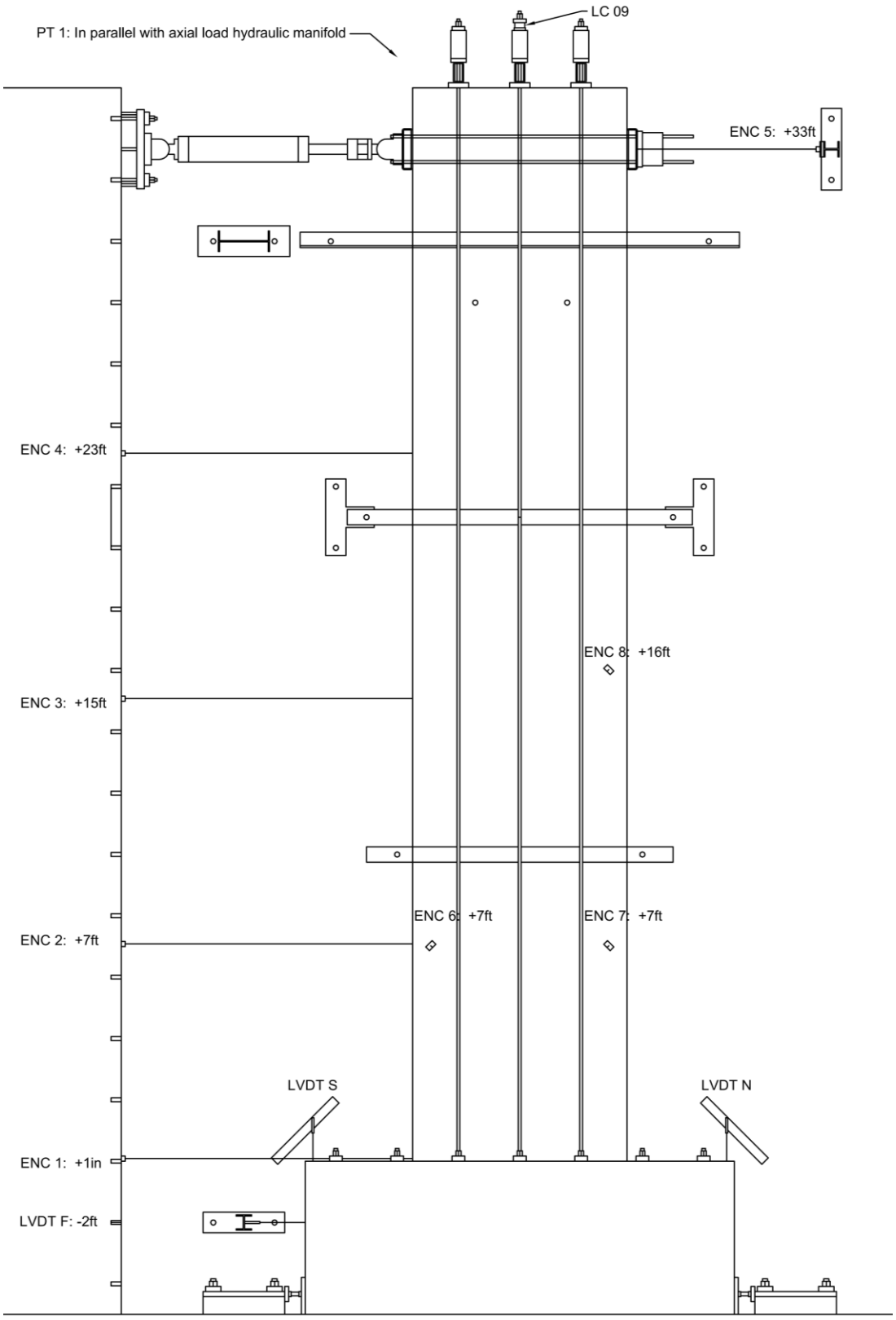

Notes: ENC stands for optical encoder (used to measure displacement), LVDT stands for linear variable differential transformer (used to measure displacement), LC stands for load cell (force transducer), and PT stands for pressure transducer. Both actuators were equipped with a load cell and an LVDT each.

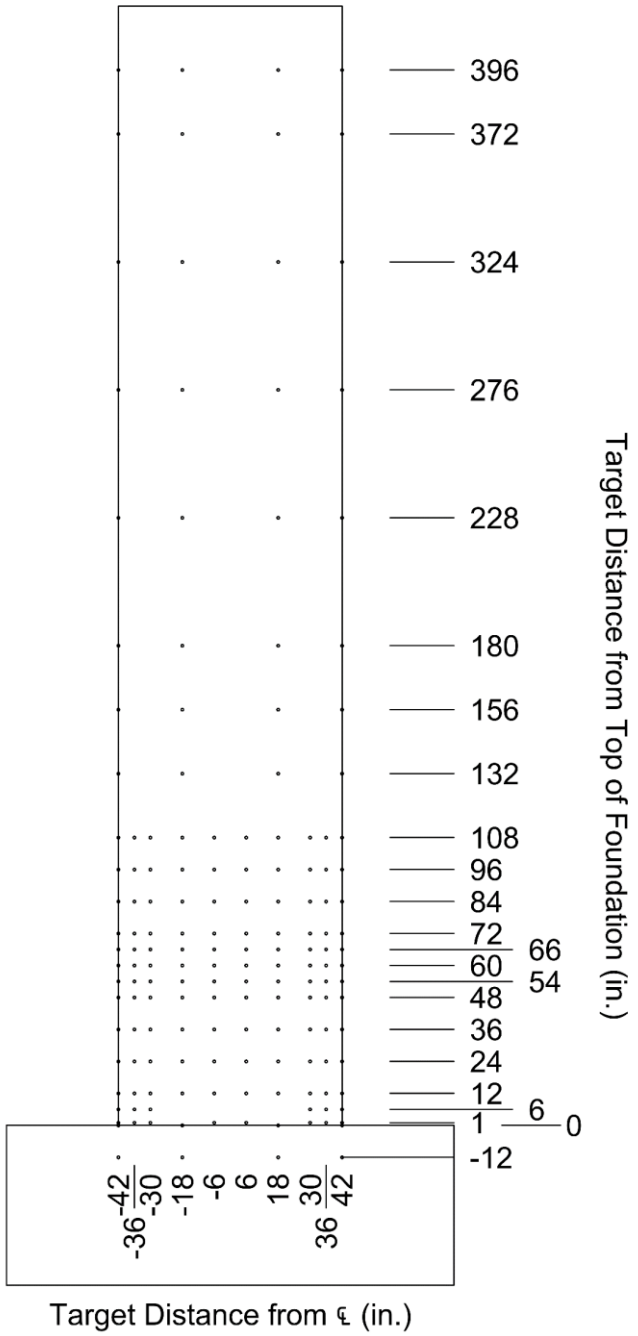

Figure 51 – Layout of Sensors used in Test Walls.

Table 8. Properties of Sensors Used in Tests of Beams.

LOCATION	SENSOR	BRAND	MODEL	FSV	Accuracy	Vex	SENSITIVITY	UNITS
S overhang 10 ft from support	ENC 1	UNIMEASURE	EP-50-DS-H5	50 IN	0.004IN	NA	0.004	IN/CNT
40 in S of MS	ENC 2	UNIMEASURE	EP-50-DS-H5	50 IN	0.004IN	NA	0.004	IN/CNT
Midspan	ENC 3	UNIMEASURE	EP-50-DS-H5	50 IN	0.004IN	NA	0.004	IN/CNT
40 in N of MS	ENC 4	UNIMEASURE	EP-50-DS-H5	50 IN	0.004IN	NA	0.004	IN/CNT
N overhang 10 ft from support	ENC 5	UNIMEASURE	EP-50-DS-H5	50 IN	0.004 IN	NA	0.004	IN/CNT
S Support	LVDT S	SCHAEVITZ	DC-EC-1000	+/- 1.0 IN	0.003 IN	30	0.10084	IN/V
N Support	LVDT N	SCHAEVITZ	DC-EC-1000	+/- 1.0 IN	0.002 IN	30	0.10229	IN/V
S overhang 10 ft from support	LC 09	HONEYWELL	3632-100K	100 KIP	0.98 KIP	10	-4610	KIP/V
N overhang 10 ft from support	LC 08†	HONEYWELL	3632-100K	100 KIP	0.69 KIP	10	-4509	KIP/V
	LC 03††	LEBOW	3175-50K	50 KIP	0.18 KIP	10	-2543	KIP/V
	LC 02†††	HONEYWELL	3632-100K	100 KIP	0.82 KIP	10	-4521	KIP/V

†LC 08 was used for test WB60U0 through U3 but was sent in for servicing and recalibration before WB60U4 was tested.

††LC 03 was used for WB60U4 and U5 during the time LC 8 was being serviced.

†††LC 02 was used for WB80U1 and U2 after receiving a replacement load cell form Honeywell. LC 03 did not have sufficient capacity to test Gr 80 Beams

Table 9. Properties of Sensors Used in Tests of Walls.

LOCATION	SENSOR	BRAND	MODEL	FSV	Accuracy	Vex	SENSITIVITY	UNITS
1.0 IN	ENC 1	UNIMEASURE	EP-50-DS-H5	50 IN	0.004 IN	NA	0.004	IN/CNT
7 FT	ENC 2	UNIMEASURE	EP-50-DS-H5	50 IN	0.004 IN	NA	0.004	IN/CNT
15 FT	ENC 3	UNIMEASURE	EP-50-DS-H5	50 IN	0.004 IN	NA	0.004	IN/CNT
23 FT	ENC 4	UNIMEASURE	EP-50-DS-H5	50 IN	0.004 IN	NA	0.004	IN/CNT
33 FT	ENC 5	UNIMEASURE	EP-50-DS-H5	50 IN	0.004 IN	NA	0.004	IN/CNT
5 FT - 7.5" from SW edge - OOP	ENC 6	UNIMEASURE	EP-50-DS-H5	50 IN	0.004 IN	NA	0.004	IN/CNT
5 FT - 7.5" from NW edge - OOP	ENC 7	UNIMEASURE	EP-50-DS-H5	50 IN	0.004 IN	NA	0.004	IN/CNT
16 FT - 7.5" from NW edge - OOP	ENC 8	UNIMEASURE	EP-50-DS-H5	50 IN	0.004 IN	NA	0.004	IN/CNT
BASE - 6.5 FT N OF CENTER - VERTICAL	LVDT N	SCHAEVITZ	DC-EC-1000	+/- 1.0 IN	0.003 IN	30	0.10229	IN/V
BASE - 6.5 FT S OF CENTER - VERTICAL	LVDT S	SCHAEVITZ	DC-EC-1000	+/- 1.0 IN	0.002 IN	30	0.10084	IN/V
-2 FT – S FACE OF FOUNDATION	LVDT F	SCHAEVITZ	DC-EC-1000	+/- 1.0 IN	0.003 IN	30	0.1006	IN/V
Axial Hydraulic Manifold	PT 1	OMEGA	PX302	10 KSI	0.05 KSI	10	103.2	KSI/V
East Center Axial Jack	LC 09	HONEYWELL	3632-100K	100 KIP	0.15KIP	10	-4622	KIP/V
33 FT – East Actuator	Load Cell	INTERFACE	1232ACK-100K-B	+/- 100 KIP	0.09 KIP	NA	10	KIP/V
33 FT – West Actuator	Load Cell	INTERFACE	1232ACK-100K-B	+/- 100 KIP	0.11 KIP	NA	10	KIP/V

Displacement sensors were calibrated using a Fowler Trimos height gage (Model V1004+) with an accuracy of 0.00025 in. Load cells used in beam tests were calibrated using a 120-kip Baldwin universal testing machine that was equipped with an Instron data acquisition system. The accuracy of the equipment used to calibrate these load cells was 600 lbf. The load cell used to measure axial load in wall tests was calibrated using in interface 50-kip load cell and readout, with an accuracy of 50 lbf. The load cells integral to the actuators were calibrated using a 200-kip Interface load cell and readout, with an accuracy of 200 lbf. The pressure transducer used in the wall tests was calibrated using an Omega digital pressure gage with an accuracy of 10 psi. The OptoTrak system has an accuracy of 0.002 in. and the Optitrack system has an accuracy of 0.01 in.

8. Test Results

8.1 Test Beams

The observations reported here focus on what occurred along the constant-moment test span.

All test beams failed abruptly by explosive disintegration of the lap splice. Figure 52 shows photographs of the test beams after failure. Observe the destruction that occurred along lap splices.

Test Beam	Photo of Failure
WB60U0	
WB60U1	

WB60U2	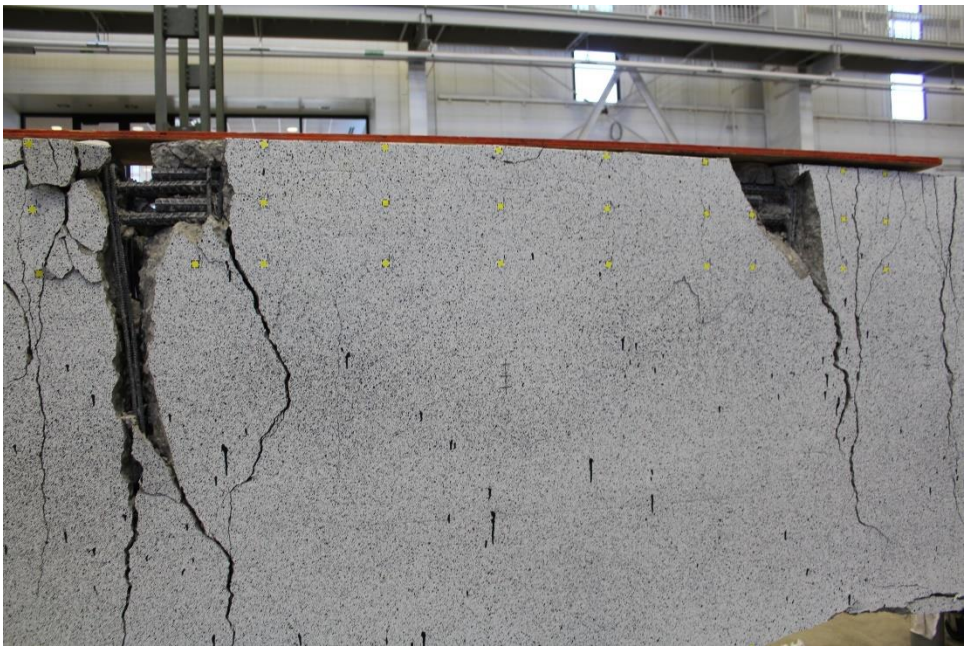
WB60U3	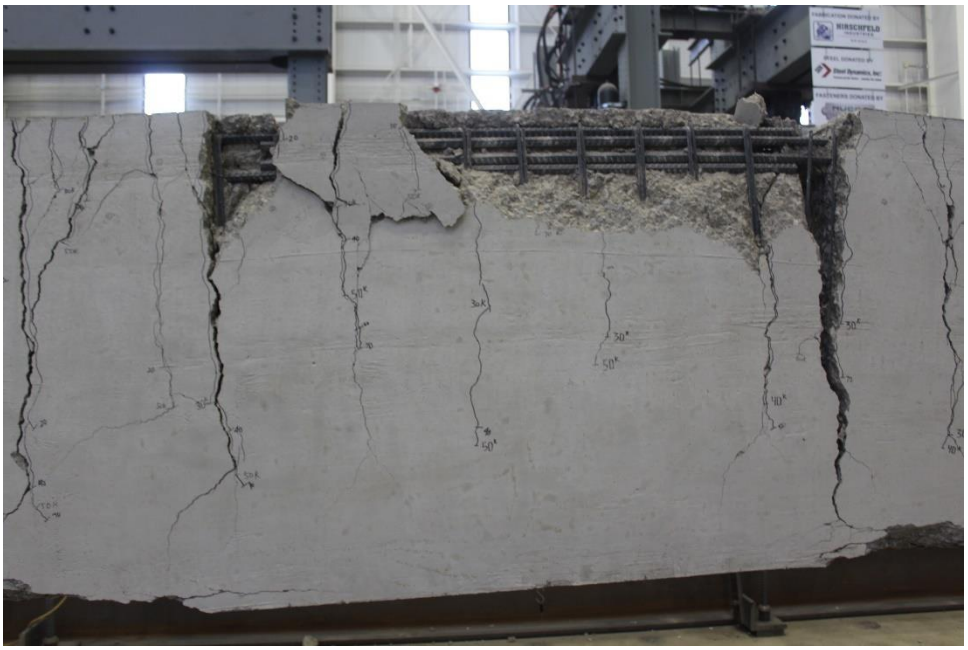

WB60U4	
WB60U5	

WB80U1	
WB80U2	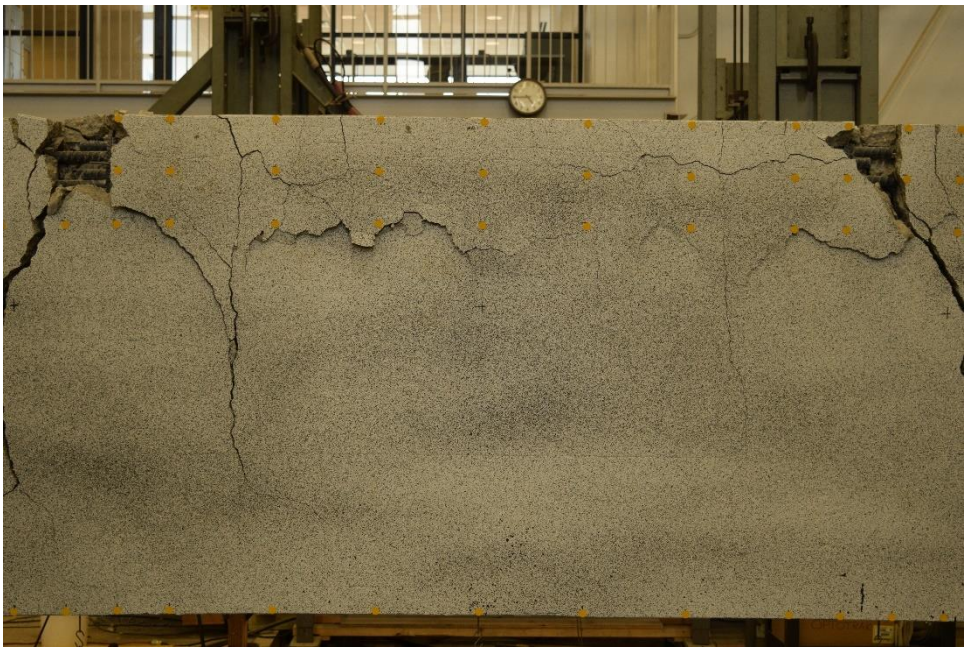

Figure 52 – Photographs Taken after Failures of Test Beams.

Beam failure was the direct result of the bursting stresses caused by the bond that occurs along the lap splice. Initial cracking was caused by tension induced by bending moments and occurred at loads close to 15 kip (applied on each overhang) plus self-weight (0.5kip/ft) and weight of loading equipment (0.35 kip at each end). These cracks were nearly perpendicular to the axis of the test beam. Flexural cracks were longer outside the splice length. In the splice length, the flexural cracks were shorter and narrower indicating a) a deeper compression zone and b) the initial effectiveness of the splice. The widest flexural cracks occurred at splice ends. This observation suggests that bar stress was larger at splice ends and decreased along the splice. Starting with Kluge and Tuma (1945, Richter, 2012) the distribution of bar stress along a splice has been observed to vary as illustrated in Figure 53. Notice that the illustrated distribution not only suggests higher stresses at splice ends but

it also suggests that towards the middle of the lap splice the bar stress tends to become nearly constant along the bar indicating no or small bond occurring there. In contrast the gradient of bar stresses indicates high bond stresses at both ends of the lap splices.

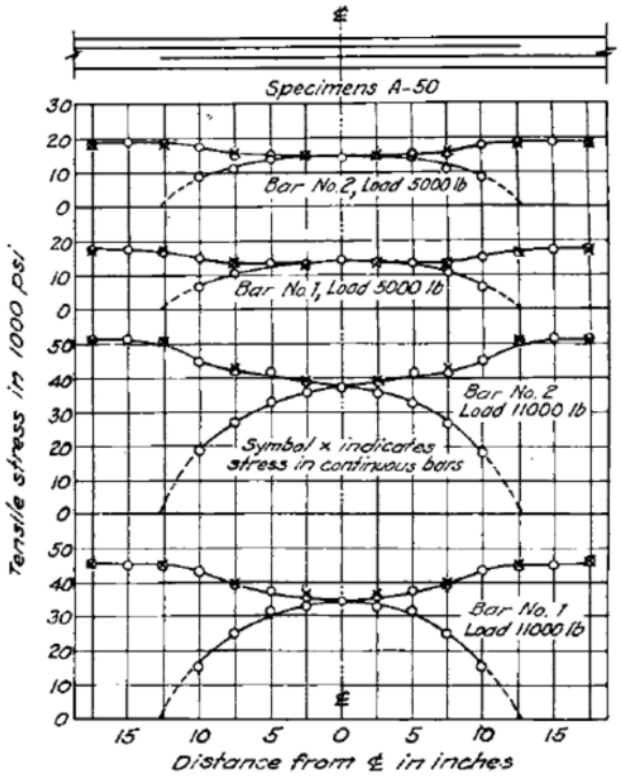

Figure 53 – Variations in Bar Stress along Lap Splices (after Kluge and Tuma, (1945).

The bar stress variation in Figure 53 suggests larger bond stresses occur near splice ends both in the terminated bar and its counterpart. As a consequence, splitting commenced at splice ends.

8.1.1. Crack Maps

Figure 54 illustrates cracking observed in test beams.

Specimen ID	Crack Map	Notes Load Step/Color/Max. Crack Width/ Max. Splitting Crack Width
WB60U0	N/A	
WB60U1	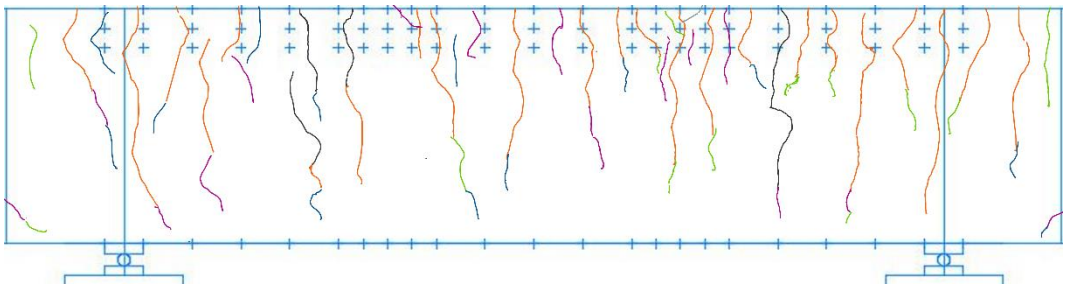	10 kips No Cracks 20 kips Black 5mil 30 kips Orange 10mil 40 kips Purple 10mil 50 kips Green 20mil 60 kips Blue 20mil
WB60U2	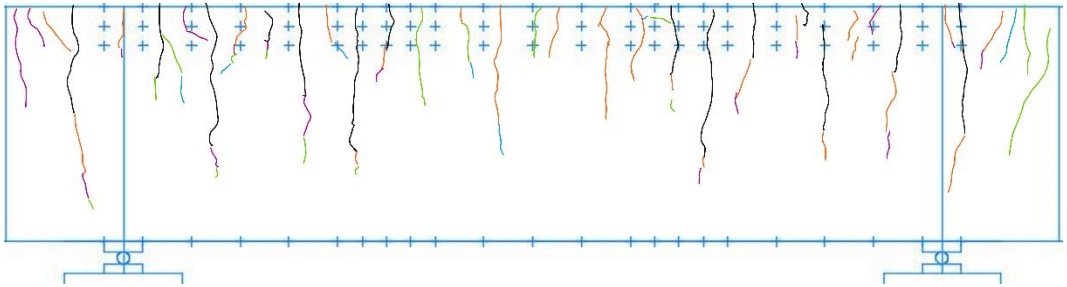	10 kips No Cracks 20 kips Black 5mil 30 kips Orange 10mil 40 kips Purple 15mil 50 kips Green 25mil 10mil splitting 60 kips Blue 25mil 20mil splitting
WB60U3	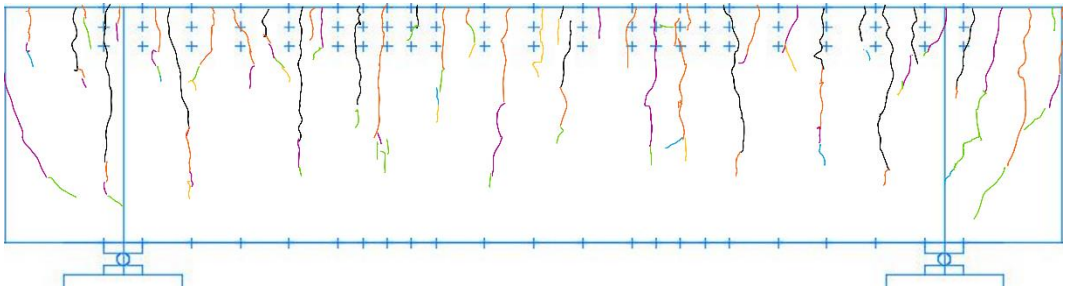	10 kips No Cracks 20 kips Black 5mil 30 kips Orange 10mil 40 kips Purple 15mil 50 kips Green 20mil 60 kips Blue 25mil 20mil splitting 70 kips Yellow 30mil 30mil splitting 75 kips N/M 45mil 40mil splitting 0.5in N/M >100mil 50mil splitting 0.75in N/M >100mil 100mil splitting 1.0in N/M >100mil >100mil splitting

WB60U4	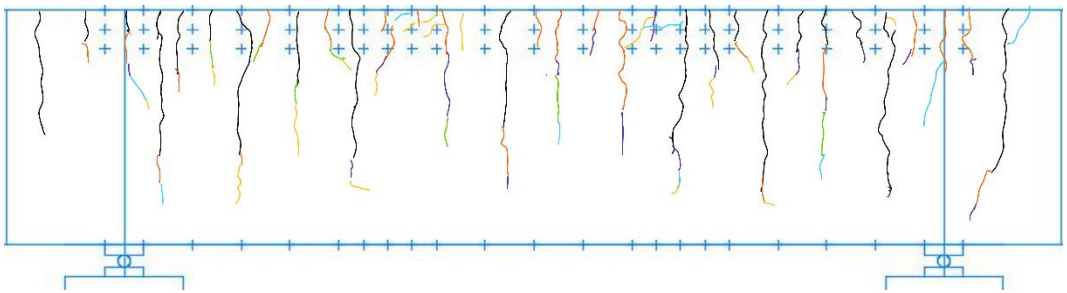	10 kips No Cracks 20 kips Black 5mil 30 kips Orange 10mil 40 kips Purple 10mil 50 kips Green 10mil 60 kips Blue 25mil 10mil splitting 70 kips Yellow 40mil 15mil splitting 75 kips N/M 75mil 25mil splitting 0.5in N/M >100mil 40mil splitting 0.75in N/M >100mil 50mil splitting 1.0in N/M >100mil >100mil splitting 1.25in N/M >100mil >100mil splitting
WB60U5	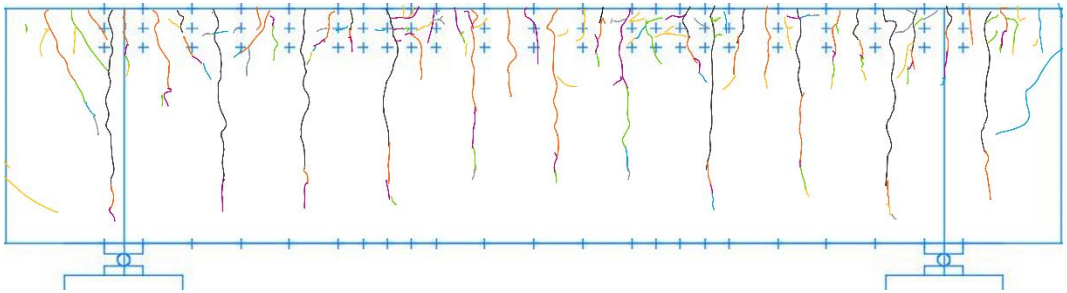	10 kips No Cracks 20 kips Black 5mil 30 kips Orange 15mil 40 kips Purple 20mil <5mil splitting 50 kips Green 25mil 5mil splitting 60 kips Blue 35mil 15mil splitting 70 kips Yellow 50mil 30mil splitting 75 kips Gray 75mil 40mil splitting 0.5in N/M >100mil 50mil splitting 0.75in N/M >100mil 75mil splitting 1.0in N/M >100mil >100mil splitting
WB80U1	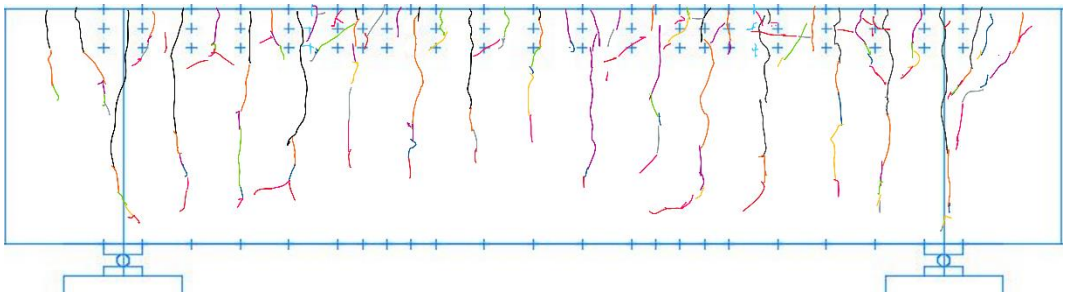	10 kips No Cracks 20 kips Black 5mil 30 kips Orange 10mil 40 kips Purple 15mil 50 kips Green 20mil 60 kips Blue 30mil 70 kips Yellow 35mil <5mil 80 kips Gray 50 mil 10mil 90 kips Pink 75mil 15mil 0.5in Red >100mil 20mil 0.75in N/M >100mil 30mil 1.0in N/M >100mil 50mil 1.25in N/M >100mil 75mil

WB80U2	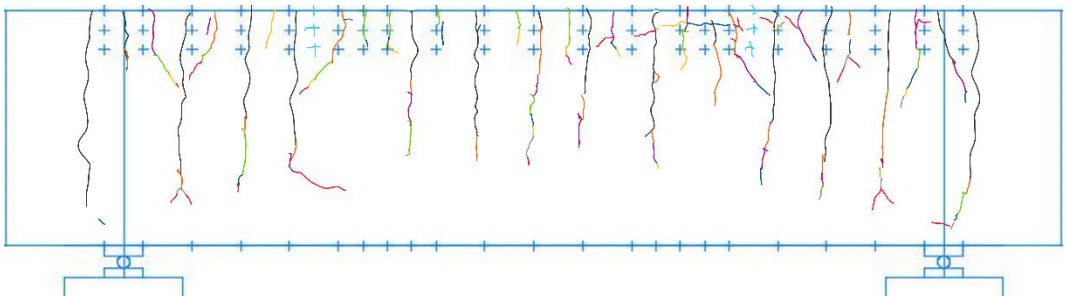				
		10 kips	No Cracks		
		20 kips	Black	5mil	
		30 kips	Orange	10mil	
		40 kips	Purple	15mil	
		50 kips	Green	20mil	
		60 kips	Blue	30mil	10mil
		70 kips	Yellow	35mil	15mil
		80 kips	Gray	50 mil	25mil
		90 kips	Pink	75mil	30mil
		0.5in	Red	>100mil	40mil
		0.75in	N/M	>100mil	50mil
		1.0in	N/M	>100mil	75mil

Figure 54 – Cracking in Test Beams.

Notes: 'mil' stands for 1/1000 in. N/M stands for 'Not Marked'

8.1.2 Force-Deformation Curves

Figure 55 shows measured load-deformation curves. Load-unload segments were the result of pauses in the test used to reset the stroke in the loading jacks in a safe manner. The most salient feature of the load-deflection curves is the failure point that indicates a sudden loss in strength resulting from the brittle failure of the lap splice. Lap splice failure in deformed bars does not result in bar slip in absence of a dramatic loss in strength as it occurs in plain bars. Lap splice failure results in nearly total and nearly instantaneous loss of strength. It is also interesting to see that the shapes of the measured load-deformation curves resemble the shapes of the stress-strain curves of the longitudinal reinforcement. While the curves for WB60U0 to 5 show no indication of a yield plateau, the curves for WB80U1 and 2 do show such an indication. The resemblance suggests that the shape of the stress-strain curve of the reinforcement plays a key role in the deformability of a lap splice.

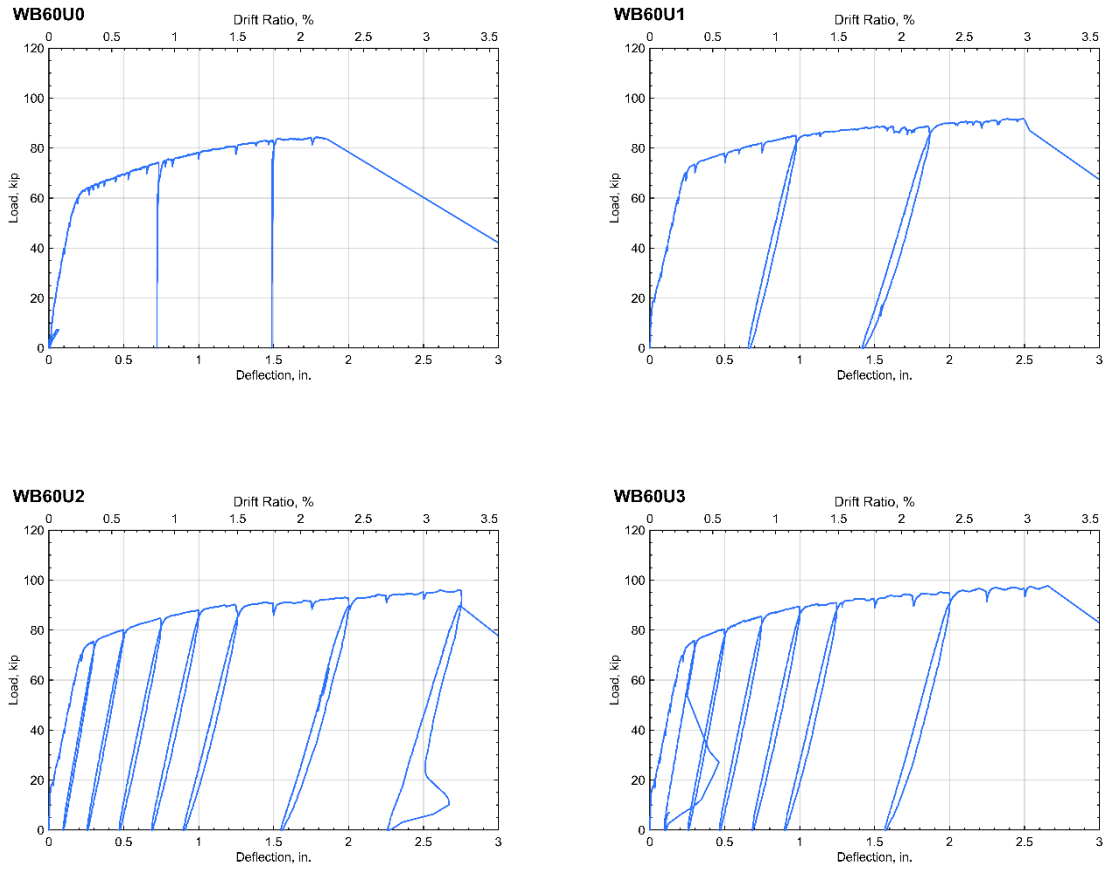

Figure 55 – Load-Deflection Relationships Measured in Test Beams.

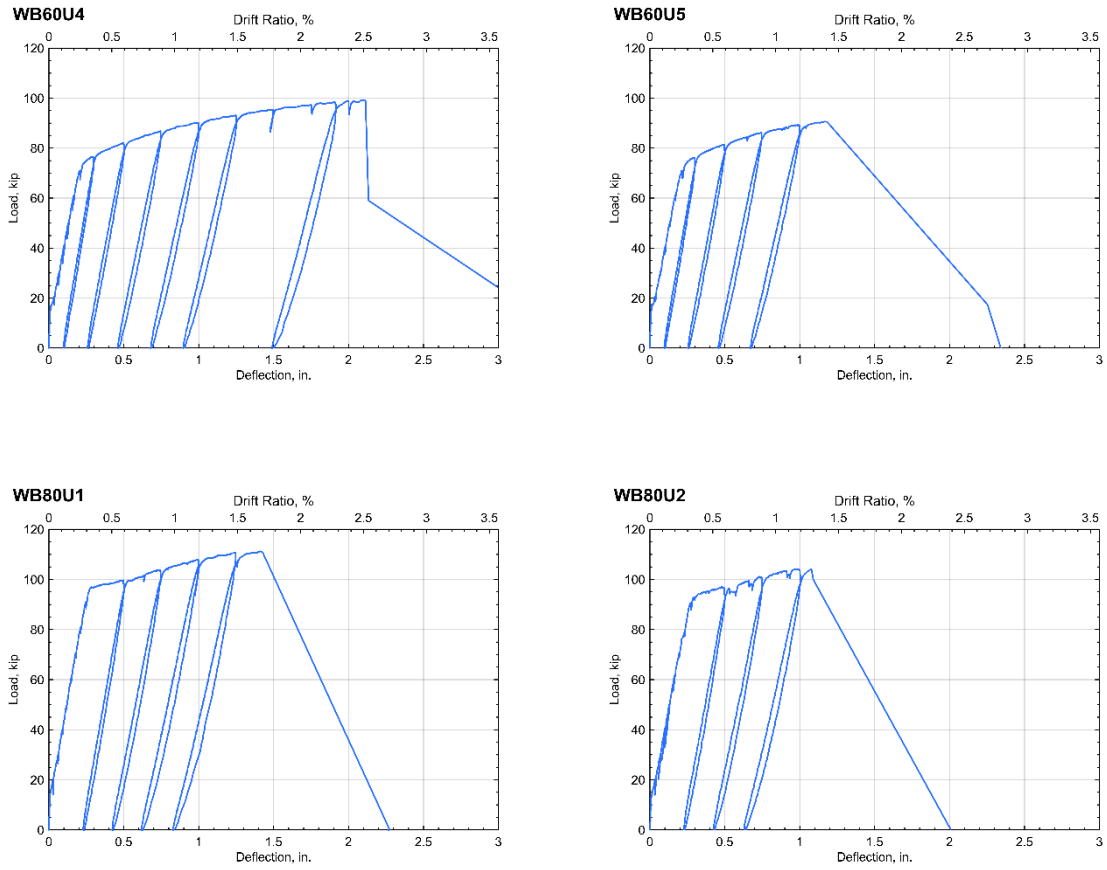

Figure 55 (Continued) – Load-Deflection Relationships Measured in Test Beams.

8.1.3 Stresses, Strains and Drift Ratios

Three measures of lap-splice performance are used here to organize the test results: mean peak bar stress, mean bond strength, and drift at failure. Mean peak bar stress and bond strength (interpreted as stress on surface of the bar) were estimated as follows:

1) Estimate moment at splice end attributable to self-weight and equipment weight ($0.35kip$):

$$w\frac{(11ft)^2}{2} - w\frac{14ft}{2}x + w\frac{x^2}{2} + 0.35kip \times 10ft = 23\ to\ 24kip \times ft$$

where $11ft$ is the total length of the overhang,
$14\ ft$ is the constant-moment (center) span,
x is distance from support to splice end
$3.7ft$ for an 80-in.splice, $4.5ft$ for a 60-in.splice, and $4.9ft$ for a 50-in. splice,
$10\ ft$ is the moment arm,
and w is self weight ($0.5kip/ft$).

2) Add the moment from 1) to the product of peak applied force (estimated as the mean of the values measured for each loading rig near each beam end) and moment arm ($10\ ft$).

3) Divide the obtained moment from 2) by an effective internal arm estimated as $0.93d$ (based on average measured material properties), where d is effective depth measured to centroid of reinforcement in tension.
4) Divide the force obtained from 3) by the area of the spliced bars (4 #8 bars totalling $3.16\ in^2$) to obtain peak bar stress.
5) Divide the force obtained from 3) by the surface area of the spliced bars (4 times π times bar diameter times splice length) to obtain peak mean bond stress (or bond strength).

Step 5) results in a measure of mean bond stress. As suggested by Figure 53, local bond stresses are likely to be larger near splice ends, while the middle of the splice length appears to contribute less to splice strength. Because the concrete working in tension around the bars is brittle, the lap splice has limited ability to redistribute forces once the ends of the splice start to fail. For this reason, as suggested by the formulation recommended in Vol. I, increases in splice length do not result in proportional increases in splice strength.

Maximum mean bond stresses ranged between 4.3 and $5.9\sqrt{f_c' \times psi}$, while drift ratios at failure varied from 1.3% to 3.3% (Table 10). Drift ratio is defined here as midspan deflection divided by half the constant moment span. The largest estimate of mean bond stress was 1.4 times the smallest estimate. In contrast, the maximum limiting drift ratio was 2.5 times the minimum. Relatively small variations in bond strength resulted in disproportionately larger variations in drift at failure. A plausible explanation is provided by Figure 56a. This figure superimposes the inferred values of peak bar stress and 1.5 times failure drift ratio on the stress-strain curves for the reinforcement used in specimens WB60U0-5 and WB80U1-2. The reason drift ratio is amplified using the factor 1.5 is explained next and reflects the observation that the relationship between drift ratio and strain is a function of the geometry of the specimen and the distribution of deformations occurring along its length. In that light, the superposition in Figure 56a suggests that the drift reached at a given bar stress was a direct consequence of the shape of the stress strain curve of the spliced steel. Test beams with Grade-80 reinforcing bars reached larger bar stresses at failure, they had stronger lap splices, but that did not translate into more deformable splices because the increase in stress did not produce as large an increase in strain as it would have produced in Grade 60 bars. And this observation follows from the direct geometric relationship that exists between strain and drift.

The approximation implied by Figure 56a –that strain was nearly 1.5 times drift ratio- can be visualized as follows. Two extremes are considered for illustration. In one extreme, the curvature distribution along the constant-moment span is assumed uniform. In this case midspan deflection δ (the moment of the area under the curvature diagram relative to the support) is:

$$\delta = \varphi \times \frac{(7ft)^2}{2}$$

Here φ is curvature along constant moment span (of length = 2 x 7ft).

As defined here, drift ratio DR is therefore:

$$DR = \frac{\delta}{7ft} = \varphi \times \frac{7ft}{2}$$

Assuming the neutral axis depth at failure is close to 15% of effective depth d:

$$DR = \frac{\varepsilon}{0.85d} \times \frac{7ft}{2}$$

For an average value of d of nearly 44 in.:

$$DR = \frac{\varepsilon}{0.85 \times 44in} \times \frac{7 \times 12in}{2} = 1.1\varepsilon$$

That is one of the mentioned extremes. It is an extreme because the distribution of curvature and deformation along the moment span is unlikely to have been uniform considering that the splice length was stiffer than the rest of the moment span. As a second extreme, consider the curvature along the constant-moment span to be uniformly distributed again but only outside the splice. Along the splice assume it was negligible. With these conditions midspan deflection δ (again the moment of the area under the curvature diagram relative to the support) would be:

$$\delta = \varphi \times \frac{(7ft - 2.5ft)^2}{2}$$

Here φ is curvature outside the lap splice. The length 2.5 ft is half the splice length (assumed rigid).

As defined here, drift ratio DR is therefore:

$$DR = \frac{\delta}{7ft} = \varphi \times \frac{(7ft - 2.5ft)^2}{2 \times 7ft}$$

Assuming the neutral axis depth at failure is again close to 15% of effective depth d:

$$DR = \frac{\varepsilon}{0.85d} \times \frac{(7ft - 2.5ft)^2}{2 \times 7ft}$$

For an average value of d of nearly 44 in.:

$$DR = \frac{\varepsilon}{0.85 \times 44in} \times \frac{(7ft - 2.5ft)^2}{2 \times 7ft} = \frac{\varepsilon}{2}$$

The two extremes considered bracket the strain in the test beam between nearly 1 and 2 times the drift ratio. Figure 56b shows surface strains measured with optical targets along the upper edge of the moment span of specimen WB60U2. The plot was produced for gage lengths of 10 in. except above supports where a shorter 8-in. gage length was used. The figure confirms that within the inner 40 bar diameters of the lap splice surface strain was much smaller than outside the splice. After yield, strain seems to have concentrated in the more flexible areas near splice ends and outside the splice. Large variations in strain occur because cracks were not uniformly spaced along the specimen. The observation that the inner 40 bar diameters (in a 60-bar diameter splice) remain relatively 'inactive' is consistent with observations by Richter (2012). It is also interesting that assuming that curvature was negligible in that length and uniform elsewhere in the moment span leads to

$$DR = \frac{\varepsilon}{0.85 \times 44in} \times \frac{(7ft - 20in)^2}{2 \times 7ft} = \sim \frac{2\varepsilon}{3}$$

or strain being nearly equal to 1.5 times drift ratio. For more information on the use of optical targets to infer strains, refer to work by Puranam (2018).

Figure 56c illustrates mean surface strain measured with the mentioned optical targets from above the support to a target placed 10 bar diameters inside the end of the splice. The total gage length considered to produce this average was 68 in. Mean strain was estimated adding deformations occurring between consecutive optical targets and dividing the result by this total gage length. The figure confirms that it is plausible to assume that, in the test beams WB60U0-5 and WB80U1-2, strain was close to 1.5 times drift ratio (defined as ratio of midspan displacement to half the constant-moment span). Considering the range of splice lengths in test beams (from 50 to 80 in.) leads to ratios of strain to drift ratio ranging from 4/3 to 2 (Figure 56d). Implications of variations in this ratio are discussed in Section 8.2.5.

The inferred relationship between strain and drift is imperfect, but it helps understand Figure 56a that suggests why elements with stronger bars reached smaller drifts at failure. The figure implies that lap splices may be more critical in reinforcing bars with higher strength. It also implies that more pronounced strain hardening (often measured using the ratio of bar strength to bar yield stress called T/Y ratio) may result in smaller deformation capacity in elements with lap splices.

But perhaps the most important implication of Figure 56a is that it suggests that drift capacity is affected by how 'far' beyond yield the reinforcement can 'go.' If the stress reached at bond failure is equal to yield, then drift at failure is likely to be quite small. Otherwise, if the stress at failure is larger than yield, plastic deformation can occur, producing drift. It is not enough to design a splice simply to develop the yield stress on the bar.

A final note about Figure 56a: the three points marked 90, 92, and 94 (ksi) at strains inferred (as 1.5 times drift ratio) between 4.5 and 5% correspond to test beams that failed in bond after some crushing of the concrete in compression had taken place near supports. It is plausible that the crushing affected the assumed internal lever arm helping explain why these points fall below their corresponding steel stress-strain curve.

For more on the reasons for and implications of the use of surface strains refer to Section 8.2.3.

Table 10. Key Results from Test Beams.

Specimen ID	Peak Applied Force [kip]†	Estimated Peak Reinforcement Stress [ksi]	Estimated Peak Mean Bond Stress [psi]	Midspan Disp. at Failure [in.]	Drift Ratio* at Failure %	Ratio of Provided Splice Length to Length Obtained using ACI 318-19 Recommendations (Assuming Transverse Splitting, See Sec. 8.1.4)	Inferred Mean Bond Strength $\sqrt{f_c' \times psi}$
WB60U0	84	81	339	1.86	2.2%	1.78	4.6
WB60U1	92	89	449	2.53	3.0%	1.53	5.9
WB60U2	96	92	386	2.74	3.3%	1.38	5.0
WB60U3	98	94	392	2.67	3.2%	1.40	5.0
WB60U4	100	94	396	2.11	2.5%	1.33	5.3
WB60U5	92	86	362	1.18	1.4%	1.36	4.7
WB80U1	111	105	330	1.42	1.7%	1.08	4.5
WB80U2	104	100	315	1.09	1.3%	1.08	4.3

Notes:

*Ratio of midspan lateral (vertical) deflection to half constant-moment span

† Mean of two values (one per cantilever)

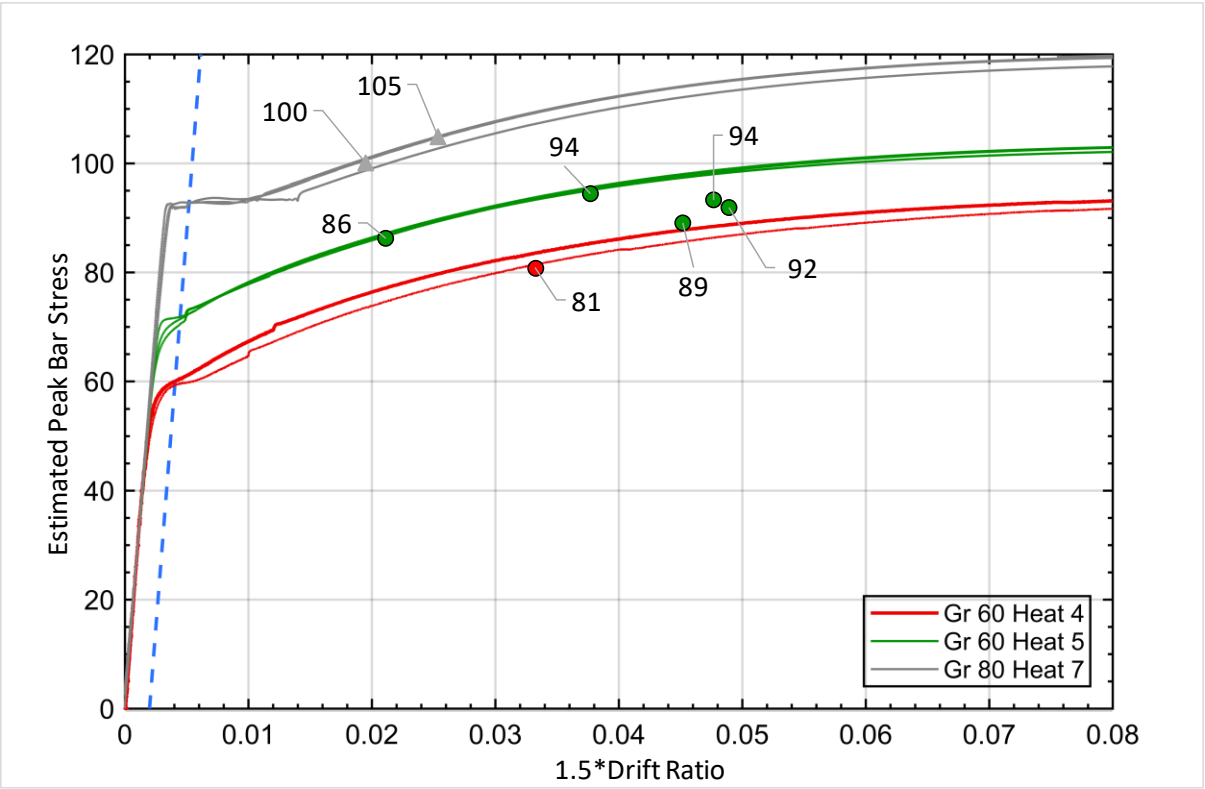

a. Unit Stress v. Strain from Bar Coupons, and Peak Bar Stress v. 1.5 times Drift Ratio – Test Beams

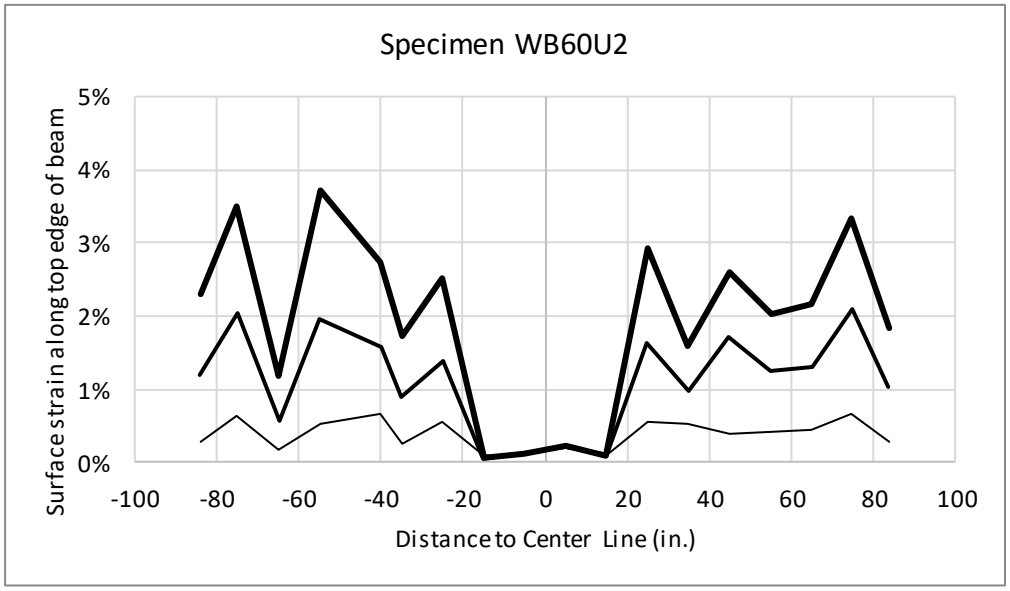

b. Variations in surface strain measured in 8 to 10-in. long gage lengths along the upper edge of test beam moment span at drift ratios of 1.5, 0.9, and 0.4%.

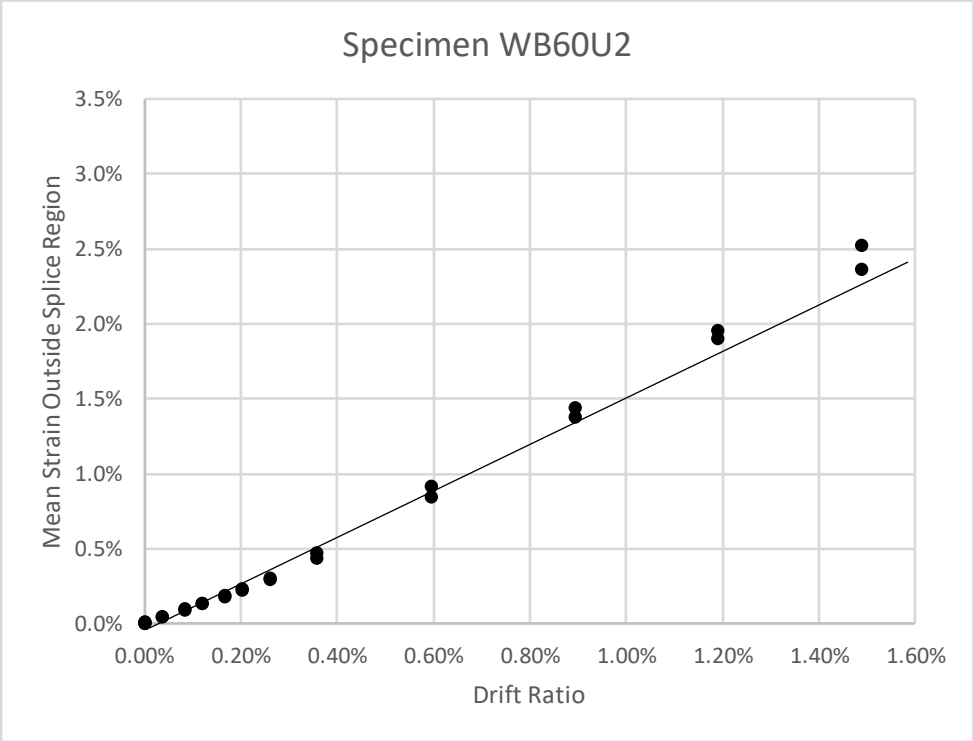

c. Mean Strain Measured along the upper edge of test beam from Support to Optical Target Placed 10 in. Inside 60-in. Splice End.

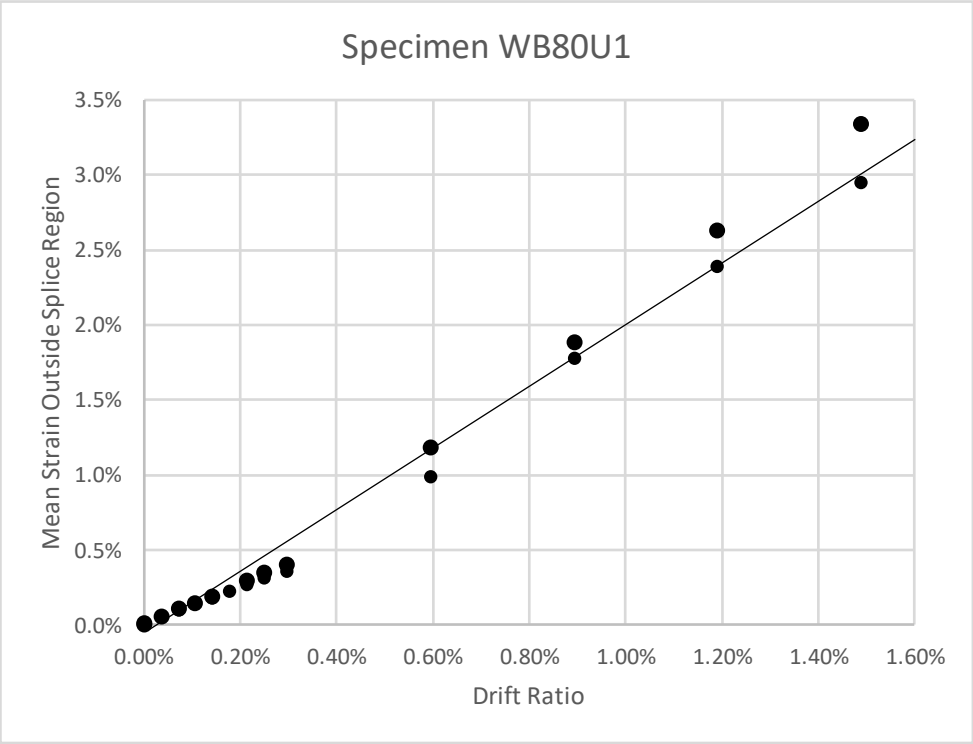

d. Mean Strain Measured along the upper edge of test beam from Support to Optical Target Placed 10 in. Inside 80-in. Splice End.

Figure 56 – Relationships Between Drift, Strain, and Bar Stress.

8.1.4 Comparing Experimental Results with Results from Existing Formulations

The test results are examined next in relation to existing knowledge on splice strength. Three relationships are considered, although more exist. Key parameters needed in this examination are listed in Table 11.

Table 11. Test Results and Parameters.

Series	Specimen ID	Moment Gradient	Transverse Reinf. Type	Span (ft)	h (in)	b (in)	f_y (ksi)	f'_c (ksi)	db_{tr}	s (in)	c_s (in)	c_L (in)	c_b (in)	Nominal f_y (ksi)	l_s (db)	Δu in	Drift Ratio (%)	f_s ksi
Richter (2012)	T-60-8-A	Constant	II	10	30	8	78	4.3	0.375	5	0.75	1.50	1.25	60	60	0.78	1.3%	81
	T-60-8-B	Constant	I	10	30	8	78	4.1	0.375	5	0.75	0.50	0.75	60	60	0.33	0.6%	78
	T-60-8-C	Constant	None	10	30	8	78	4.1	0	---	0.75	1.5	1.25	60	60	0.17	0.3%	59
Hardisty (2015)	T-60-8-D	Constant	II	10	30	8	63	5.9	0.375	8	0.75	1.50	1.25	60	60	0.58	1.0%	86
	T-60-8-E	Constant	I	10	30	8	63	5.2	0.375	8	0.75	1.50	1.25	60	60	0.62	1.0%	88
	T-60-8-F	Constant	II	10	30	8	63	6.3	0.375	11	0.75	1.50	1.25	60	60	0.56	0.9%	86
Pollalis (2020)	WB60U0	Constant	II	14	48	10	60	5.4	0.375	6	0.75	2.25	1.63	60	60	1.86	2.2%	81
	WB60U1	Constant	III	14	48	10	72	5.8	0.375	6	1.50	2.25	1.63	60	50	2.53	3.0%	89
	WB60U2	Constant	III	14	48	10	72	6.0	0.375	6	1.50	1.00	1	60	60	2.74	3.3%	92
	WB60U3	Constant	III	14	48	10	72	6.2	0.375	6	1.50	1.00	1	60	60	2.67	3.2%	94
	WB60U4	Constant	III	14	48	10	72	5.6	0.375	6	0.75	1.00	1	60	60	2.11	2.5%	94
	WB60U5	Constant	II	14	48	10	72	5.8	0.375	6	0.75	1.00	1	60	60	1.18	1.4%	86
	W60U	Varying	III	33	84	10	72	5.4	0.375	6	1.50	1.00	1	60	60	7.40	1.9%	85
	W60C	Varying	IV	33	84	10	72	5.6	0.5	6	0.75	1.00	1	60	40	7.92	2.0%	83
	WB80U1	Constant	III	14	48	10	93	5.3	0.5	12	0.75	1.00	1	80	80	1.42	1.7%	105
	WB80U2	Constant	III	14	48	10	93	5.2	0.5	12	1.50	1.00	1	80	80	1.09	1.3%	100
	W80U	Varying	III	33	84	10	93	6.1	0.5	12	1.50	1.00	1	80	90	7.92	2.0%	105
	W80C	Varying	IV	33	84	10	93	6.0	0.5	6	0.75	1.00	1	80	60	9.90	2.5%	118

Notes: h is cross sectional depth, b is cross sectional thickness, f_y is measured yield stress, f'_c is measured compressive strength of standard concrete cylinders, db_{tr} is bar diameter of transverse reinforcement, s is spacing of stirrups / ties, c_s is clear concrete cover measured to surface of stirrups / ties, c_L is clear spacing between longitudinal bars, c_b is minimum concrete cover measured center of longitudinal bar, l_s is provided splice length, Δu is displacement measured at failures, f_s is inferred peak bar stress. All longitudinal reinforcing bars had a diameter of 1 in.

The recommendation by Sozen and Moehle (1990)

Sozen and Moehle (1990) recommended the following expression to estimate bond strength for lap splices with lengths not exceeding 40 bar diameters:

$$\mu = \left[6 + \frac{A_{tr} \times f_y/ksi}{n \times d_b \times s}\right]\sqrt{f_c'\ psi} < 10\sqrt{f_c'\ psi}$$

Eq. 1

A_{tr} is area of transverse reinforcement crossing potential splitting plane
n is number of bars being developed
d_b is bar diameter
s is stirrup spacing
$f_y$is yield stress of stirrups (taken as the nominal yield stress in this evaluation)
μ is bond strength expressed as force in bar divided by surface area as was done in the tradition that followed from the early work of Abrams (1913) on bond.

One of the questions addressed in this investigation is about interpreting the terms A_{tr} and n for lap splices in walls. It can be argued that in a wall there are potential planes of splitting:

- parallel to the long direction of the cross section (and perpendicular to wall thickness), and
- transverse to the long direction of the cross section (and parallel to wall thickness).

For simplicity these directions are referred to as 'longitudinal' and 'transverse' as illustrated in Figure 57.

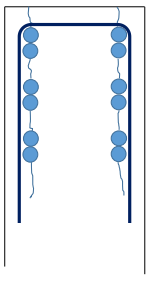	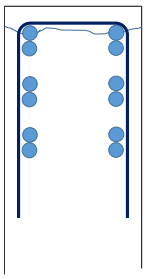
Longitudinal Splitting $n = 3$ A_{tr} = cross sectional area of tie x 1	Transverse Splitting $n = 2$ A_{tr} = cross sectional area of tie x 2

Figure 57 – Illustration of assumed directions of splitting and examples of choices for parameters n and A_{tr}.

For longitudinal splitting, focusing on one of the two splitting cracks flanking the wall at a time, the term n refers to spliced bars parallel to the length of the cross section. It is reasonable to assume that the bars near the end of the cross section are more critical than bars in the web. In the tests described here, spliced boundary reinforcement was concentrated within 6 to 10 bar diameters from the end of the cross section. For the purposes of the comparisons that follow, n was taken as 2 in test beams, and n was taken as 3 in test walls, implying all boundary

reinforcement caused and/or was affected by longitudinal splitting cracks. Consequently, the term A_{tr} was taken as the cross-sectional area of one tie (for a group of 2 or 3 spliced bars affecting one longitudinal splitting crack) for specimens without hoops and three times as much for specimens with hoops and cross-ties in wall boundaries (transverse reinforcement Type IV – used in test walls only). The failures illustrated in Figure 52 suggest all the bars on each side of the boundary element were affected by longitudinal splitting. In a wall with uniformly distributed longitudinal reinforcement it may be prudent to consider that all the bars expected to yield may cause and/or be affected by longitudinal splitting.

The case of transverse splitting is closer to the cases discussed in Volume I. The conditions leading to this type of splitting are closer to conditions represented in conventional tests of lap splices in beams in which the potential plane of splitting is parallel to the thickness of the section. In this case and for the test specimens considered in the comparisons below, n was taken as 2 and A_{tr} was taken as twice the cross-sectional area of the transverse reinforcement.

To use the formulation by Sozen and Moehle (1990) requires careful consideration of the ranges of the data for which it was developed. Sozen and Moehle focused on lap splice lengths not exceeding 40 bar diameters. The tests in the investigation reported here had longer lap lengths ranging from 40 to 90 bar diameters, with the majority of lap lengths being 60 bar diameters. For these splice lengths Eq. 1 is adjusted as follows:

$$\mu = \left[4 + \frac{A_{tr} \times f_y/ksi}{N \times d_b \times s}\right]\sqrt{f_c'\ psi} \qquad \text{Eq. 2}$$

For unconfined lap splices ($A_{tr} = 0$) this expression produces an estimate of bond strength of $4\sqrt{f_c'\ psi}$ instead of $6\sqrt{f_c'\ psi}$. This is consistent with a) the idea that unit bond strength decreases with lap splice length because bond is not uniformly distributed along the splice length, and with b) the data in Figure 58 produced by Richter (2012):

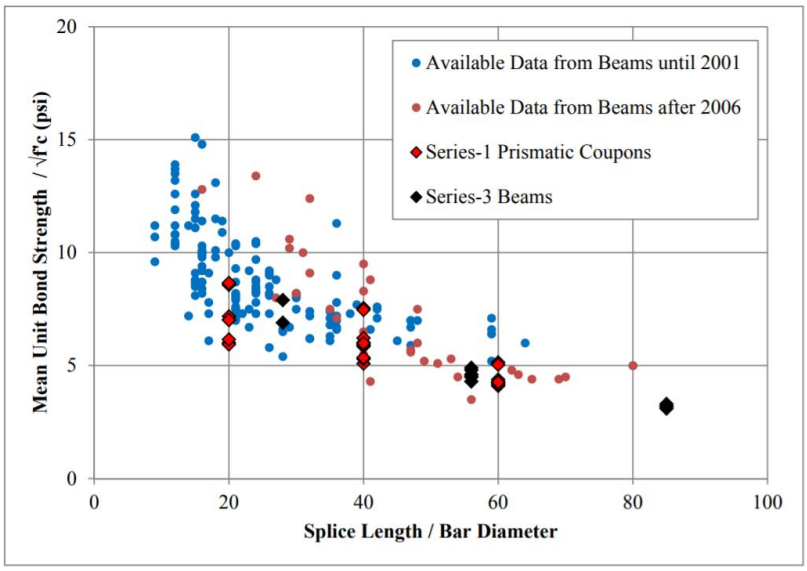

Figure 58 – Mean Bond Strength in Unconfined Lap Splices (after Richter 2012).

Multiplying the result from Equation 2 times surface area produces peak force. Peak force divided by bar cross-sectional area in turn produces peak stress. In Figure 59, measured peak stresses are compared with peak bar stresses calculated as described.

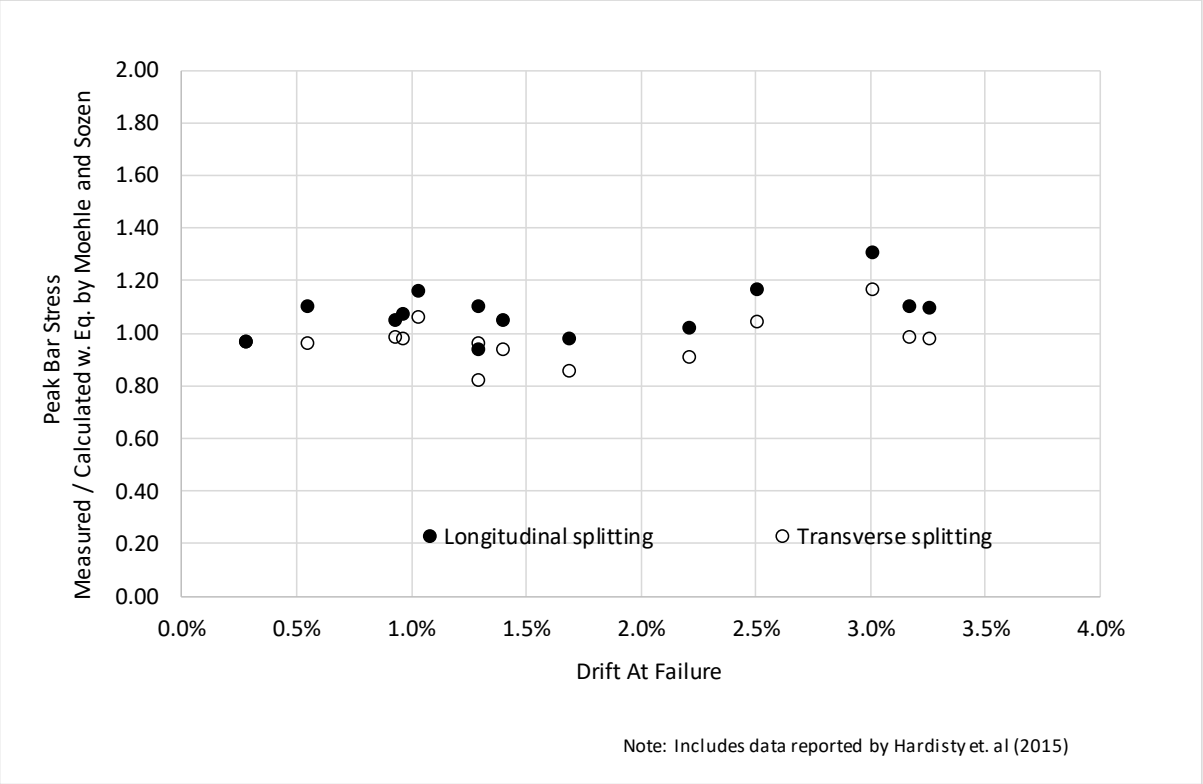

Figure 59[6] – Ratio of Measured to Calculated Peak Bar Stress - Formulation by Sozen and Moehle (1990).

Figure 59 shows that assuming longitudinal splitting controls (affecting all bars in the boundary element) yielded safer results. The examined equation was intended to produce safe results, not to reproduce test averages. The figure also shows that the quality of the estimates was not affected by the drift –or strain- reached in the tests in a perceptible way. This observation is relevant because it implies that –in the tests reported in Volume II- bond strength did not appear to be critically sensitive to strain. This observation is likely to help produce splices that lead to structures with toughness using results from previous tests in the literature that focused on strength instead of deformability.

The extent to which the results obtained in this investigation fall within the ranges of results reported before is examined in a different format in Figure 60. The figure reemphasizes the idea that yielding did not affect splice strength to a degree discernible from the scatter in the data from tests in which yielding did not occur. In the figure TRI is the term $\frac{A_{tr} \times f_y/ksi}{N \times d_b \times s}$ from Eq. 2.

[6] Includes data reported by Hardisty et al. Key parameters of their tests are listed in Table 11.

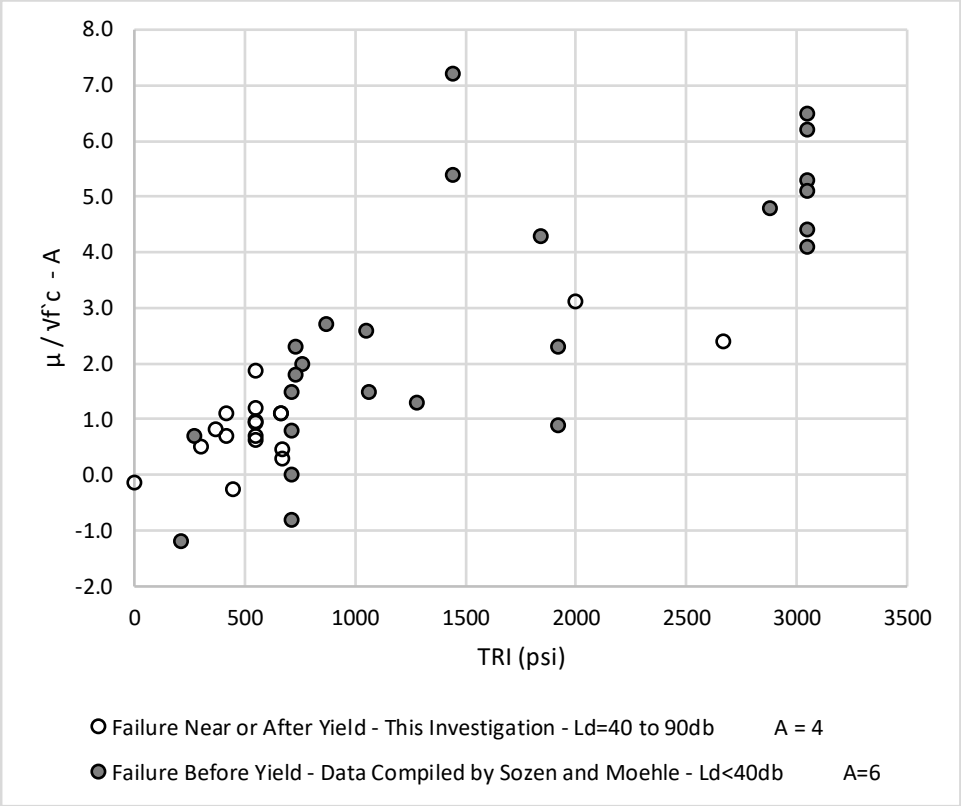

Figure 60 – Comparison of Test Results Compiled by Sozen and Moehle (1990) and Results from This Study.

The recommendation by Fleet et al. (Volume I)

Fleet et al. recommend peak bar stress –causing bond failure- is:

$$f_b = (f_c')^{0.25}\left(\frac{l_s}{d_b}\right)^{0.5}\left(\frac{c_{so}}{d_b}\right)^{0.25} + 30ksi\,\frac{N_s N_l A_t}{N_b A_b}$$

Eq. 3

where:

A_b = *area of one longitudinal reinforcing bar (in.^{2})*

A_t = *area of one stirrup leg (in.^{2})*

c_{so} = *side clear cover of spliced bars (in.)*

d_b = *longitudinal bar diameter (in.)*

f_b = *total bond strength (ksi)*

f_c' = *concrete compressive strength (psi)*

l_s = *splice or development length (in.)*

N_b = *number of longitudinal reinforcing bars*

N_l = *number of legs of transverse reinforcement crossing the splice plane*

N_s = *number of stirrups in the splice region*

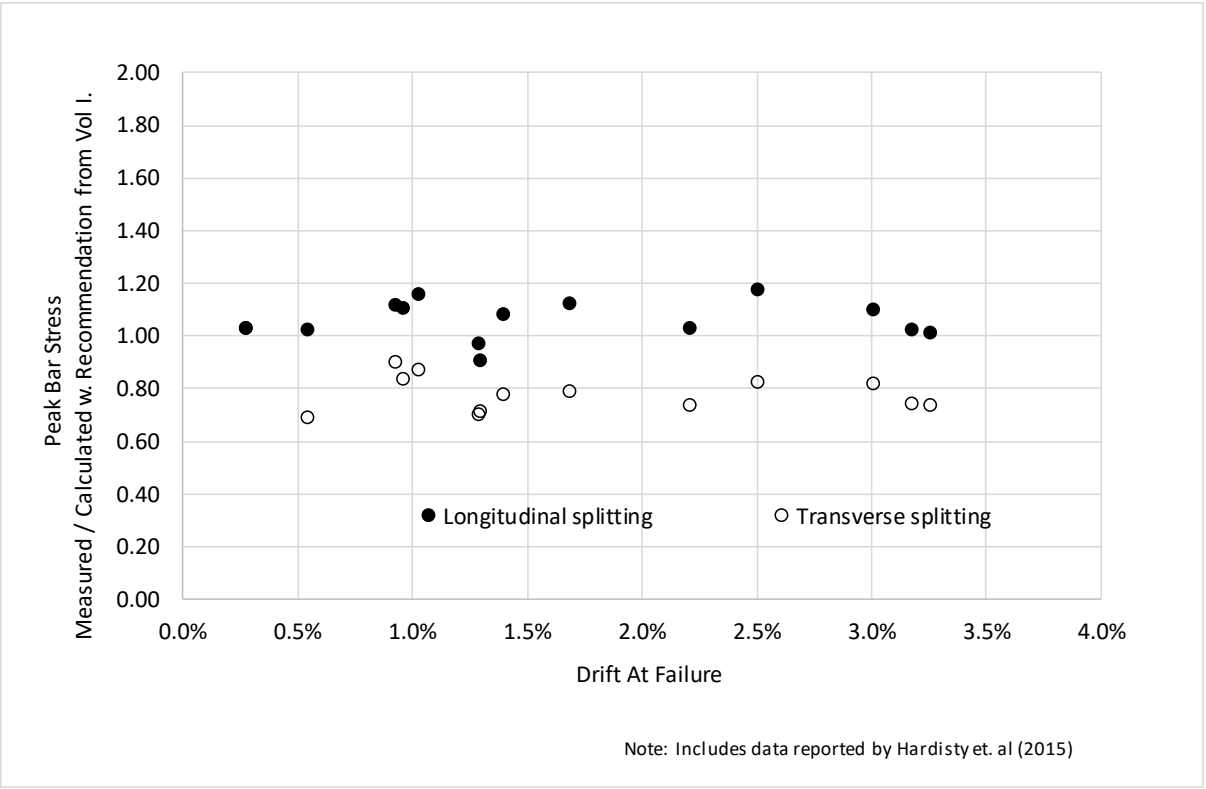

Figure 61[7] *– Ratio of Measured to Calculated Peak Bar Stress - Formulation by Fleet et al. (2019).*

The data are organized again in reference to the assumed planes of splitting depicted in Figure 57. In relation to that figure, the terms N_b, N_l, N_s are defined in Table 12 for the purpose of comparing measurement and calculation results.

Table 12. Definition of Parameters for Evaluation of Bond Strength.

ID	N_s	N_l		N_b
		Longitudinal Splitting	Transverse Splitting	
T-60-8-A*	12	1	2	2
T-60-8-B*	12	1	2	2
T-60-8-C*	0	0	2	2
T-60-8-D*	8	1	2	2
T-60-8-E*	8	1	2	2
T-60-8-F*	6	1	2	2
WB60U0	10	1	2	2
WB60U1	9	1	2	2
WB60U2	11	1	2	2
WB60U3	11	1	2	2
WB60U4	11	1	2	2
WB60U5	10	1	2	2
WB80U1	7	1	2	2
WB80U2	7	1	2	2

*Hardisty (2015)

Assuming longitudinal splitting governs produced results closer to the measurements. In this case, the examined equation was intended to produce results close to test averages (not safe

[7] Includes data reported by Hardisty et al. Key parameters of their tests are listed in Table 11.

estimates as in the expression by Sozen and Moehle). The figure shows again that the quality of the estimates was not affected by the drift –or strain– reached in the tests.

The recommendation included in ACI318-19

ACI318-19 does not implicitly contain expressions to estimate bar stress at splitting failure. And solving design equations for one of the variables they include always comes at a risk. Nevertheless, the design expression given by 318 for required lap splice length $l_{s\ REQUIRED}$ was used as follows to estimate peak bar stress:

$$f_b = f_y \times \frac{l_{s\ PROVIDED}}{l_{s\ REQUIRED}}$$

Eq. 4

$l_{s\ PROVIDED}$ is lap splice length used in test specimen. $l_{s\ REQUIRED}$ was obtained as:

$$l_{s\ REQUIRED} = 1.3 l_d$$

Eq. 5

where:

$$l_d = \frac{3}{40} \frac{f_y}{\sqrt{f'_c}} \frac{\psi_g}{\left(\frac{c_b + K_{tr}}{d_b}\right)} d_b$$

Eq. 6

f_y was taken as nominal yield tress for the purpose of evaluating $l_{s\ REQUIRED}$ (and cancels out in the calculation)
K_{tr} is transverse reinforcement index 40 A_{tr}/ ($n \times s$)
c_b is minimum concrete cover measured to bar center
ψ_g factor equal to 1.15 for Gr. 80 and 1.0 for Gr. 60

In reference to the values used to evaluate the formulation by Fleet (Vol. I), the value of A_{tr} was taken equal to the product $A_t \times N_l$, and n was taken equal to N_b. The resulting values of A_{tr} and n are consistent with the illustrations in Figure 57 and the values assumed for these same variables in the case of the formulation by Sozen and Moehle (1990) described above.
The values of peak bar stress obtained as explained are compared with measured peak stresses in Figure 62.

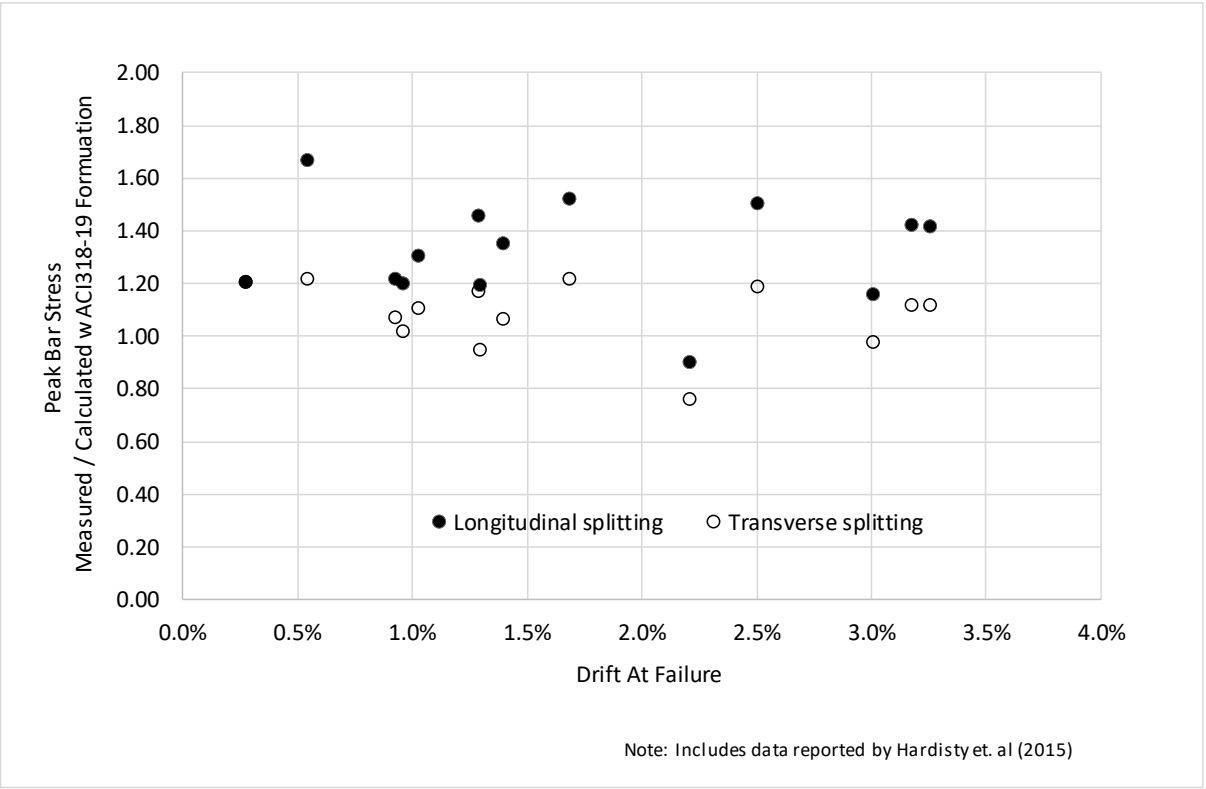

Figure 62[8] *– Ratio of Measured to Calculated Peak Bar Stress - Formulation by ACI 318-19 (ACI, 2019).*

Once more, relatively safer results (expected from a design expression) were obtained assuming longitudinal splitting controls and drift and/or strain did not seem to affect the quality of results in a clear fashion.

8.1.5 Organizing the Results in Terms of Drift Capacity

The observations made in previous sections suggest that the information obtained on drift at splice failure can be organized in terms of a parameter that can help quantify the strength of the splice. An alternative is illustrated in Figure 63 below. The alternative is appealing because it uses terms that would be familiar to a practicing engineer already using the current design code (ACI 318-19).

[8] Includes data reported by Hardisty et al. Key parameters of their tests are listed in Table 11.

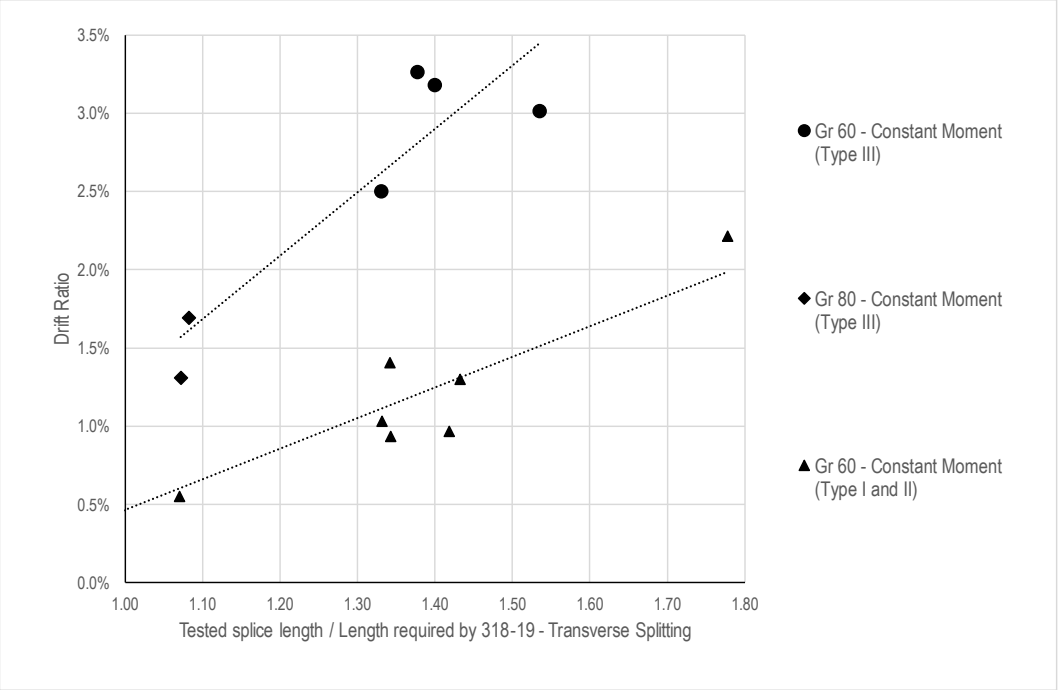

Figure 63 – Variation in Drift Ratio at Failure with Increases in Ratio of Length of Lap Splice to Length Required by ACI318-19 Formulation Used Assuming Transverse Splitting Controlled.

This figure was produced assuming that transverse splitting controls. To assume instead that longitudinal splitting controls produces safer estimates of splice strength (see previous section) but it does not help produce a clearly better or more intuitive correlation between drift capacity and the chosen horizontal axis representing the strength of the lap splice.

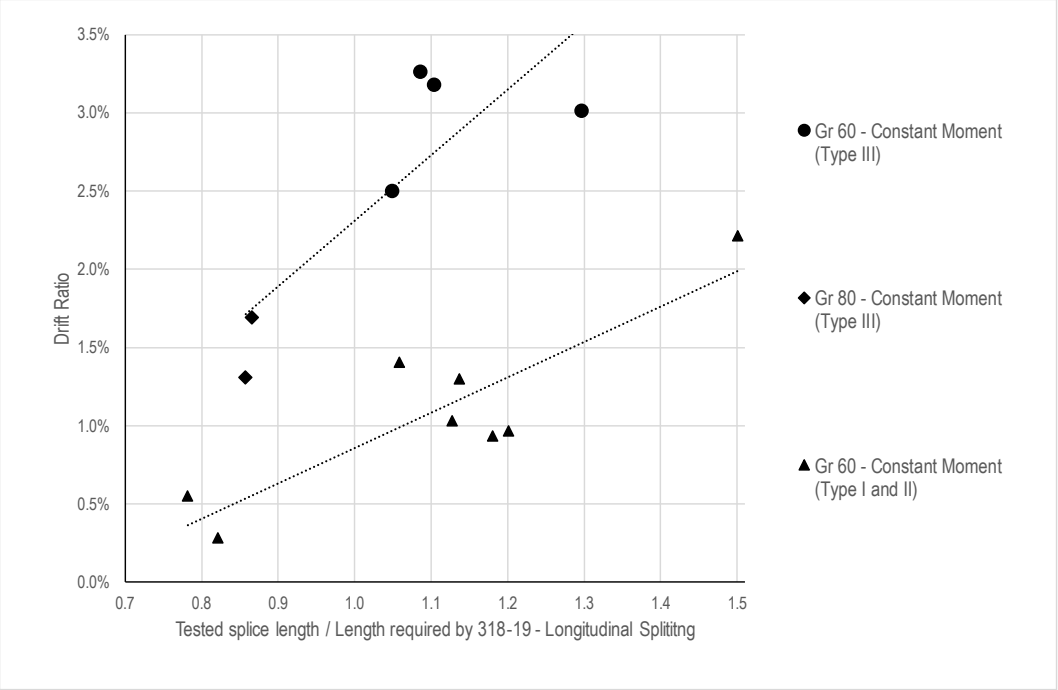

Figure 64 – Variation in Drift Ratio at Failure with Increases in Ratio of Length of Lap Splice to Length Required by ACI318-19 Formulation Used Assuming Longitudinal Splitting Controlled.

Figures 63 and 64 include data reported by Hardisty et al. Key parameters of their tests are listed in Table 11.

A key limitation of Figures 63 and 64 is that they were produced using data from test specimens in which splices were tested without a moment gradient. The next section addresses that limitation by examining the results obtained with test walls tested as cantilevers.

8.2 Test Walls

The beam tests described above helped identify detailing leading to better element deformability. Transverse reinforcement Type III (Figure 20) led to ratios of midspan deflection to half moment span ranging from 2.5 to 3.3% in beams with Grade-60 reinforcement. In contrast, Type II (Figure 20) produced 1.4 and 2.2%. Previous tests with Type II by Hardisty et al. produced drift ratios between 0.9 and 1.3%. In all these cases splice length was 60 bar diameters. It was concluded transverse reinforcement Type III was likely to produce better deformability. Test walls were fabricated using Type III details. Given their scale, each wall test required a large investment of time and resources. The better detailing was favored because it was rather apparent that the alternative was going to produce poor results. It did not seem worth testing a large specimen requiring a lot of effort to produce a result that was quite likely to be negative. So, the test walls were designed to try to provide ideas to solve what seems to be a problem with the deformation capacity of structural walls with lap splices near their bases meeting only minimum requirements. So, the tests reported here need to be interpreted considering they represent rather ideal conditions in which:

-bar cover was generous (equal to 1.5 x bar diameter), in 6 out of 12 tests,

-tolerances were tight (with bar spacing and cover kept within 1/8 in. of the specified value within the splice region),

-material properties and curing were controlled,

-transverse reinforcement anchorage exceeded the minimum required in 10 out of 12 tests (that had transverse reinforcement Types III and IV –Figure 24– instead of Type II),

-there were no problems with consolidation during casting.

Structural walls built in less favourable conditions are likely to have less drift capacity than the test walls described here.

8.2.1. Crack Maps

The first cracks were attributable to flexure and were first noticed at a lateral force of nearly 40 kips in all test walls. The estimated maximum tensile stress in the concrete associated with this lateral force was nearly $11.5\sqrt{f_c' \times psi}$. This value seems reasonable considering 1) it is difficult to spot a small crack at the joint between a wall and its foundation, 2) the values of modulus of rupture listed in Table 6 range from 8 to $10.6\sqrt{f_c' \times psi}$.

Observed crack patterns are illustrated in Figures 65 and 66. Initial splitting cracks were first observed at lateral forces ranging from 55 to 75 kip. These initial splitting cracks formed near the base of the wall. They were followed by splitting cracks near the upper end of the lap splice.

Buckling of longitudinal bars was first observed in cycles at drift ratios of 1.5%, 2%, 2%, and 2% for specimens W60U, W60C, W80U, W80C.

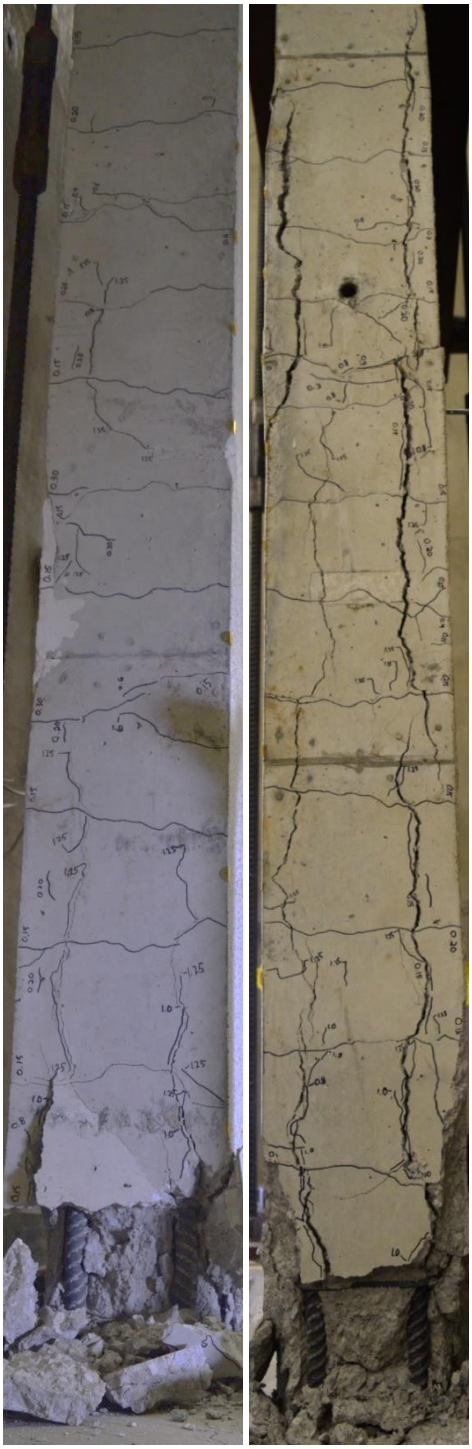

South North

W60U Crack Patterns

South North

W60C Crack Patterns

Figure 65 –Crack Patterns Observed at Wall Ends

North South North South

W80U Crack Maps W80C Crack Maps

Figure 65 (Continued) –Crack Patterns Observed at Wall Ends

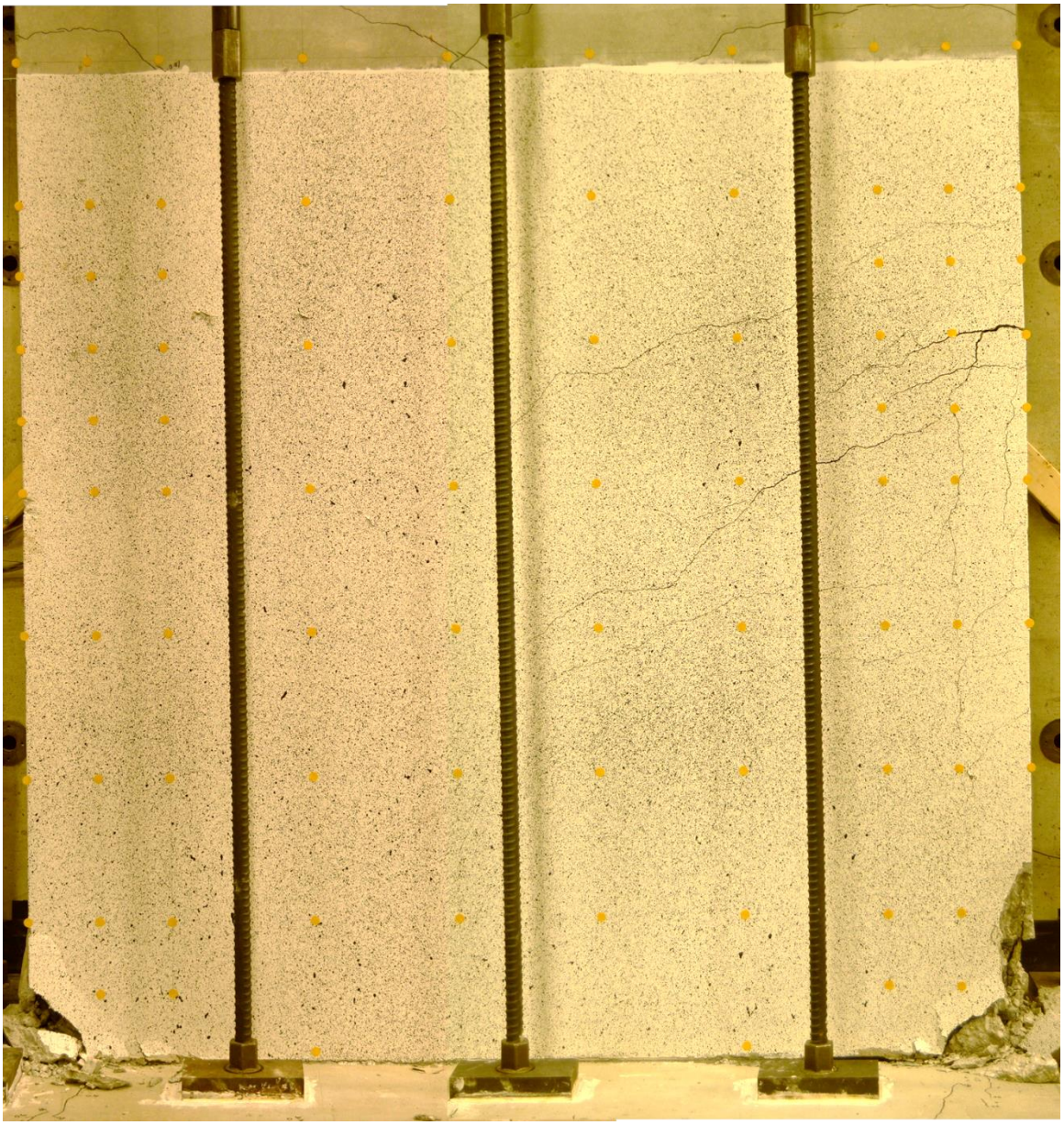

a. W60U Final Cycle – Side View

Figure 66 –Damage Observed

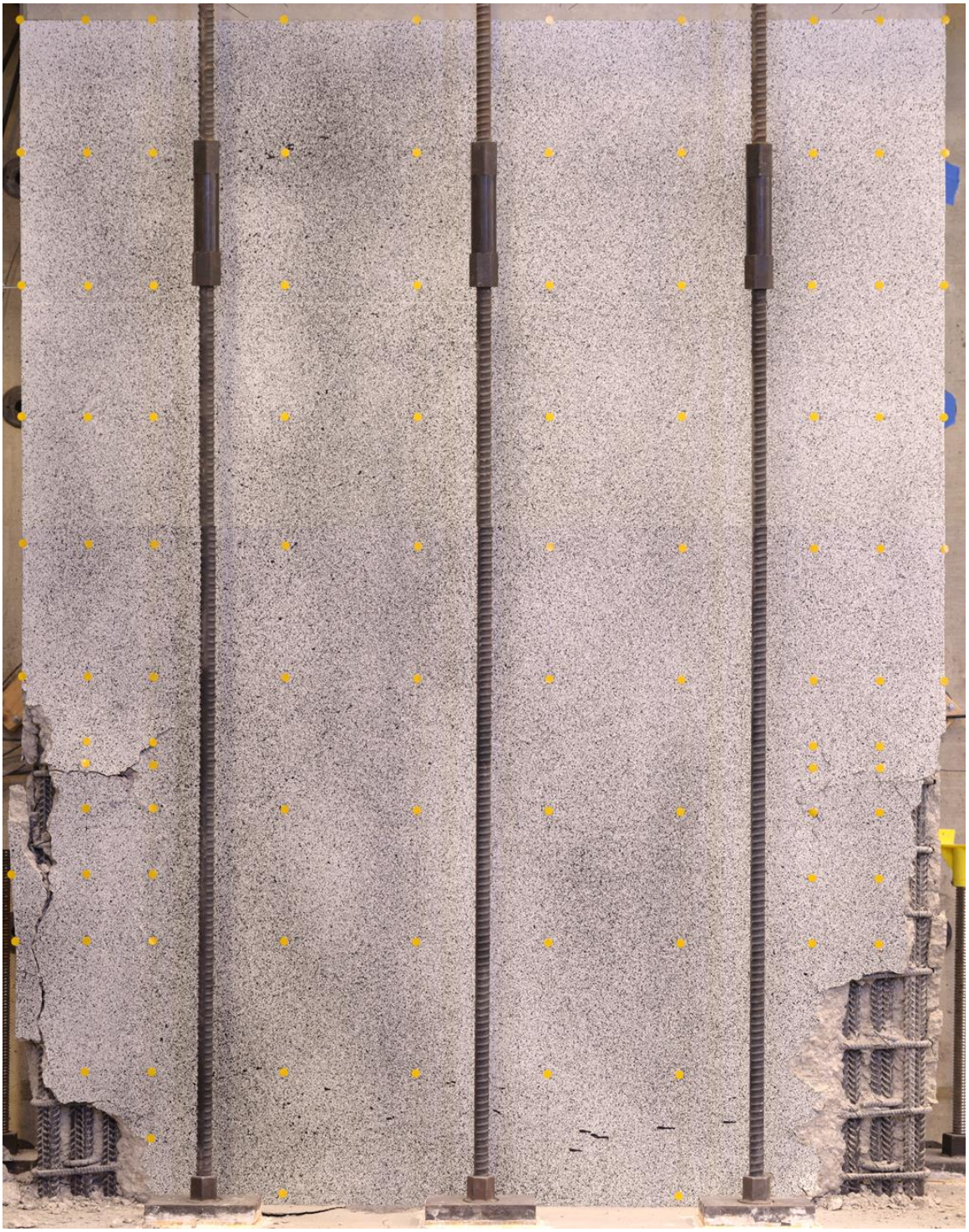

b. W60C End of test – Side View

Figure 66 (Continued) –Damage Observed.

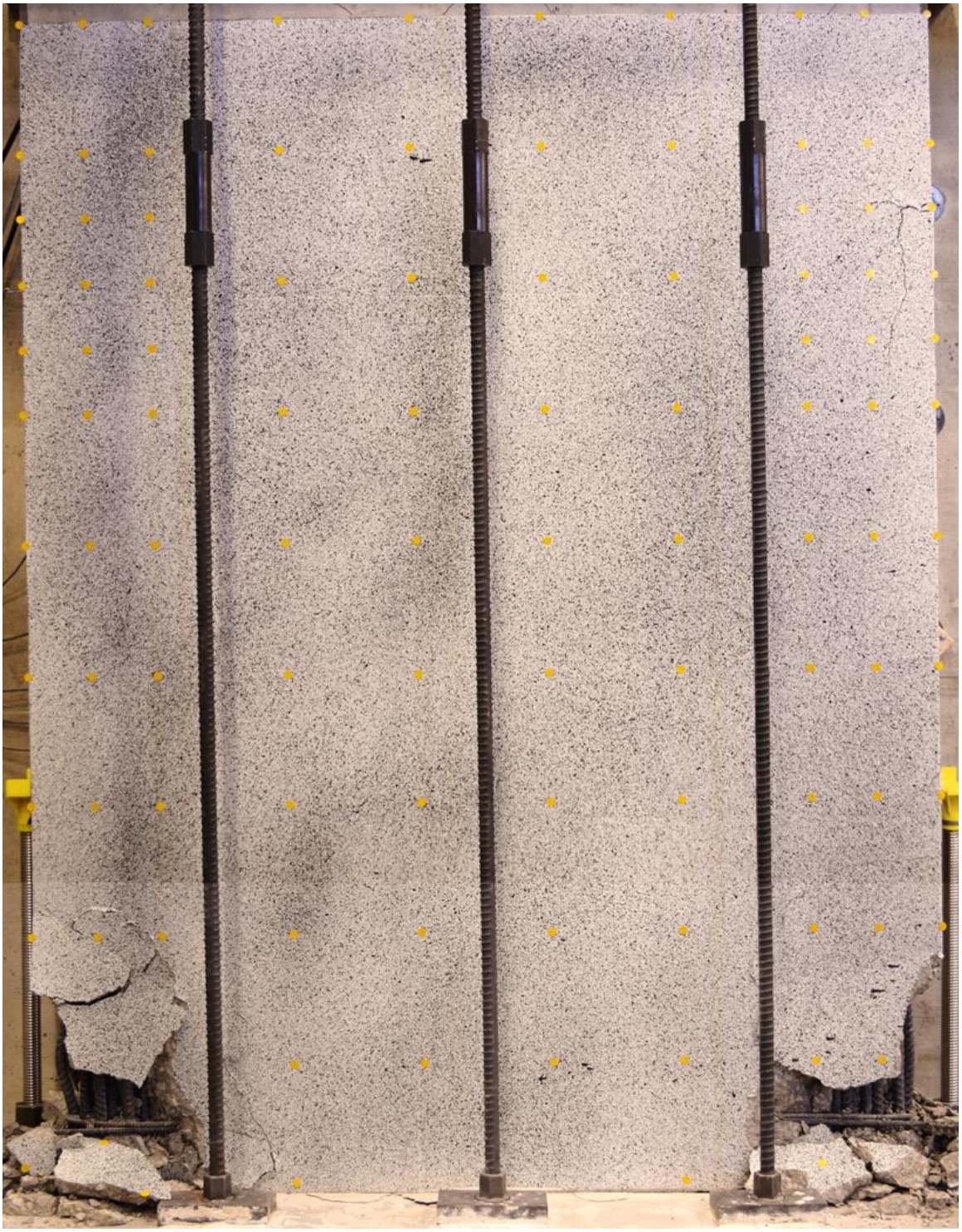

c. W80U Final Cycle – Side View

Figure 66 (Continued) –Damage Observed.

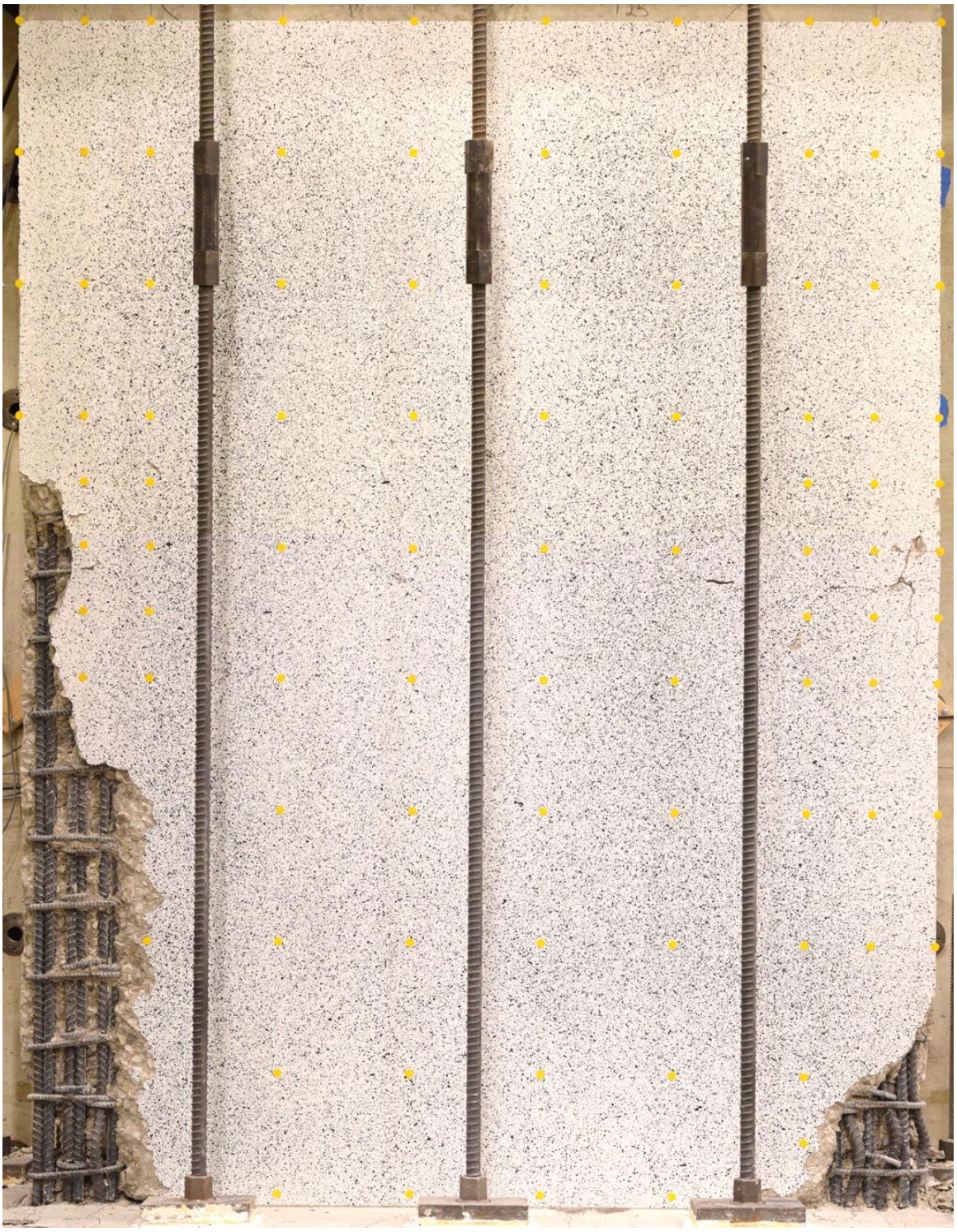

d. W80C End of test, spalling removed – Side View

Figure 66 (Continued) –Damage Observed.

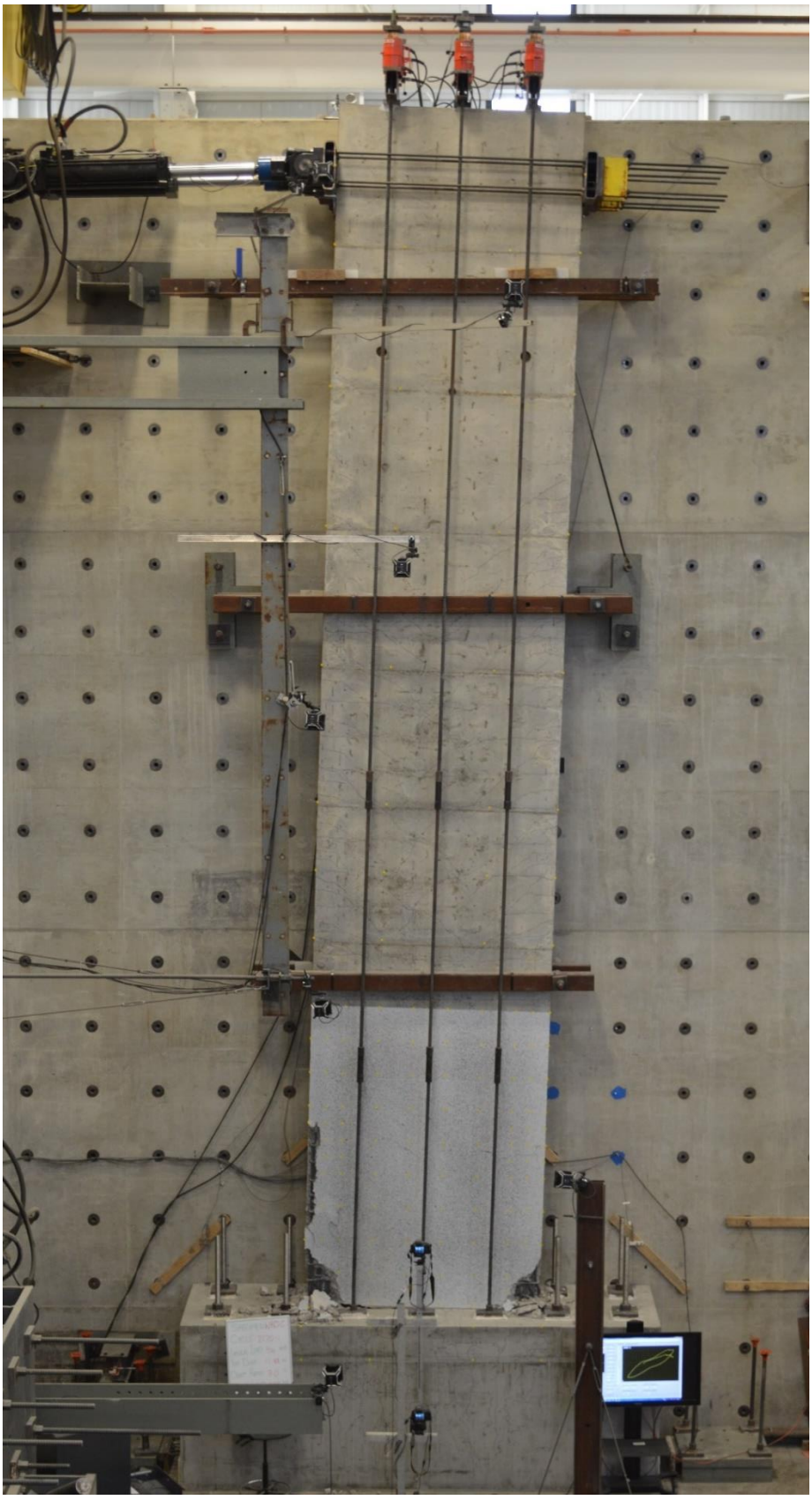

e. W80C Final Cycle (3% Drift North) – Overall View

Figure 66 (Continued) –Damage Observed.

f. W80C Splice Failure (South East Edge)

g. W80C Bar Fractures (South West Edge)

Figure 66 (Continued) –Damage Observed.

In all test walls failure was caused by the bursting of the lap splice. Failure was sudden and associated with a loud 'explosion' of the concrete around the lap splice except in W60C in which no loud sounds were heard and it took one additional load cycle after the first drop in lateral force was noticed to cause splice disintegration. Drift ratios at failure ranged from 1.9 to 2.5%.

When splice failure occurred, crushing had extended as far as 20% of the effective depth d along the wall length. Before splice failure, crushing concentrated within the lower 6-12 in. of height of the test walls. After splice failure, the concrete cover around entire splice length seemed to bulge out as loads were reversed. Tests were stopped because it was unclear whether buckling of longitudinal bars and crushing of the boundary along the entire lap length could occur making the entire test wall unstable.

In test wall W80C, two boundary-element bar fractures were discovered after the test was stopped and loose concrete was removed. It was unclear when these fractures occurred. But the first indication of failure (that caused a loud bang) occurred when 1) the first sudden drop in lateral load was measured at a drift ratio of 2.5% (in a cycle meant to reach 3%) and 2) a large splitting crack formed (Figure 66f). At the same time the force in the actuator closest to the observed splitting crack was observed to drop more than the force in the other actuator (of the two used), while the described bar fractures occurred on the opposite face of the boundary element (Figure 66g). For these reasons the failure was judged to have been triggered by the lap splice with bar fractures occurring in a later cycle.

8.2.2 Force-Deformation Curves

Recorded force-deformation relationships are plotted in Figures 67 to 70. The most salient features of these plots are:

1. Yielding occurred at a deflection of ~2.8 in. –for a drift ratio of nearly 0.7%– in specimens with Gr.-60 reinforcing bars.
2. Yielding occurred at a deflection of ~3.5 in. –for a drift ratio of nearly 0.9%– in specimens with Gr.-80 reinforcing bars.
3. The ratio of yield displacements (0.7/0.9) is close to the ratio of yield stresses measured for the reinforcing bars used (70/93).
4. The drop in lateral resistance that occurred at failure was catastrophic even though the loading system was operated in displacement control.

   In the 'static' tests done, the actuator itself prevents collapse when failure occurs. But in the response to strong ground motion, the potential energy released at the moment the splice fails is likely to become kinetic energy increasing the likelihood of overturning.
5. Before lap splice failure occurred, hysteresis loops were quite stable suggesting that the failure process was not gradual, or that at least its consequences were not perceptibly so.
6. The increased numbers of low-amplitude cycles included in the testing protocols of test walls W60C and W80C did not lead to readily evident effects on test results.
7. The similarities in drift ratios at failure suggests that the shortenings in lap splice lengths introduced in specimens W60C and W80C –relative to their counterparts (W60U and W80U)- were compensated by the confinement provided by the closed hoops placed in their boundaries. These shortenings represented 1/3 of the lengths of the splices in the specimens without hoops.
8. Specimen W60C reached a peak lateral force within 1% of the peak force reached by specimen W60U. In contrast specimen W80C reached a force nearly 10% larger than the peak force reached by W80U. Nevertheless, at a lateral displacement of 6 in (corresponding to a drift ratio of 1.5%) the difference in maximum forces in these two specimens was smaller than 3% indicating consistency in test results.

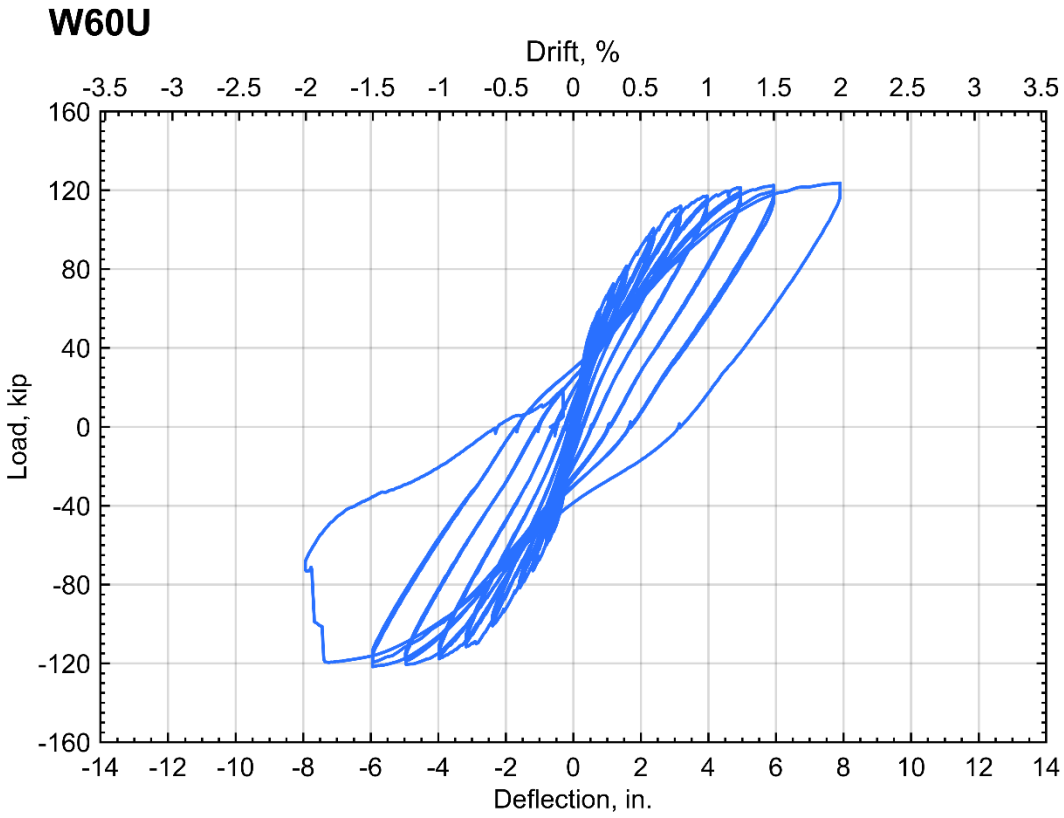

Figure 67 – Specimen W60U, Measured Load-Deflection Curve.

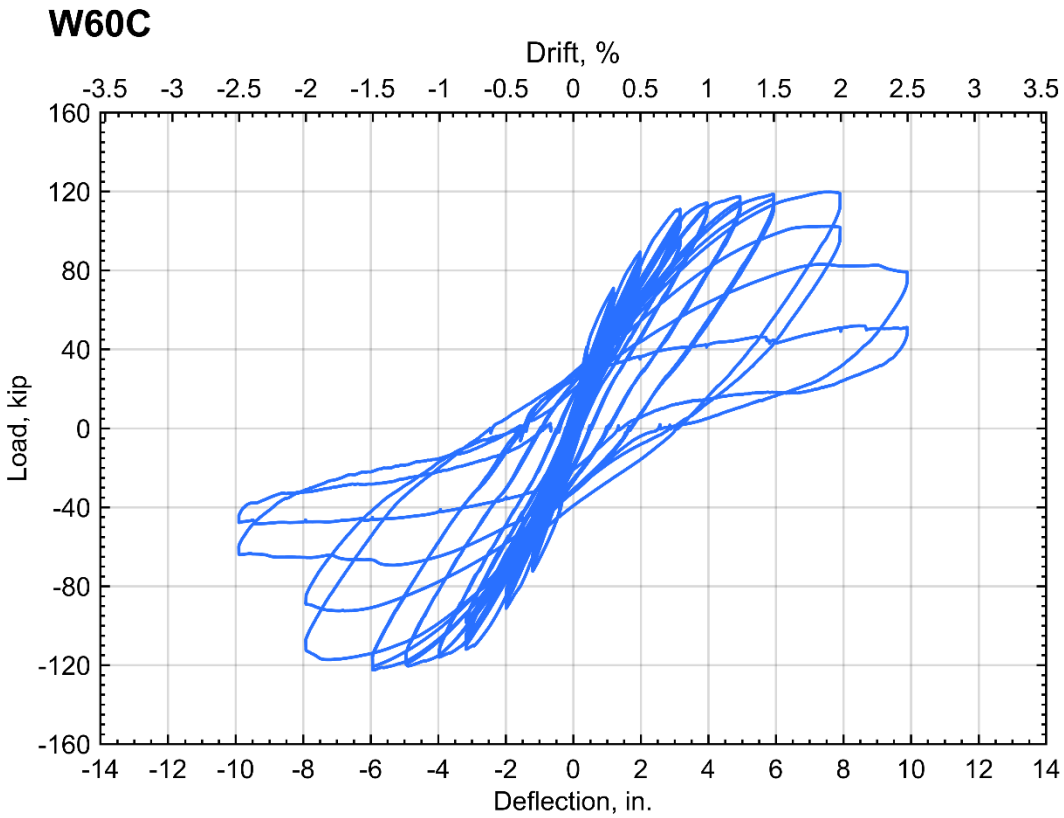

Figure 68 – Specimen W60C, Measured Load-Deflection Curve.

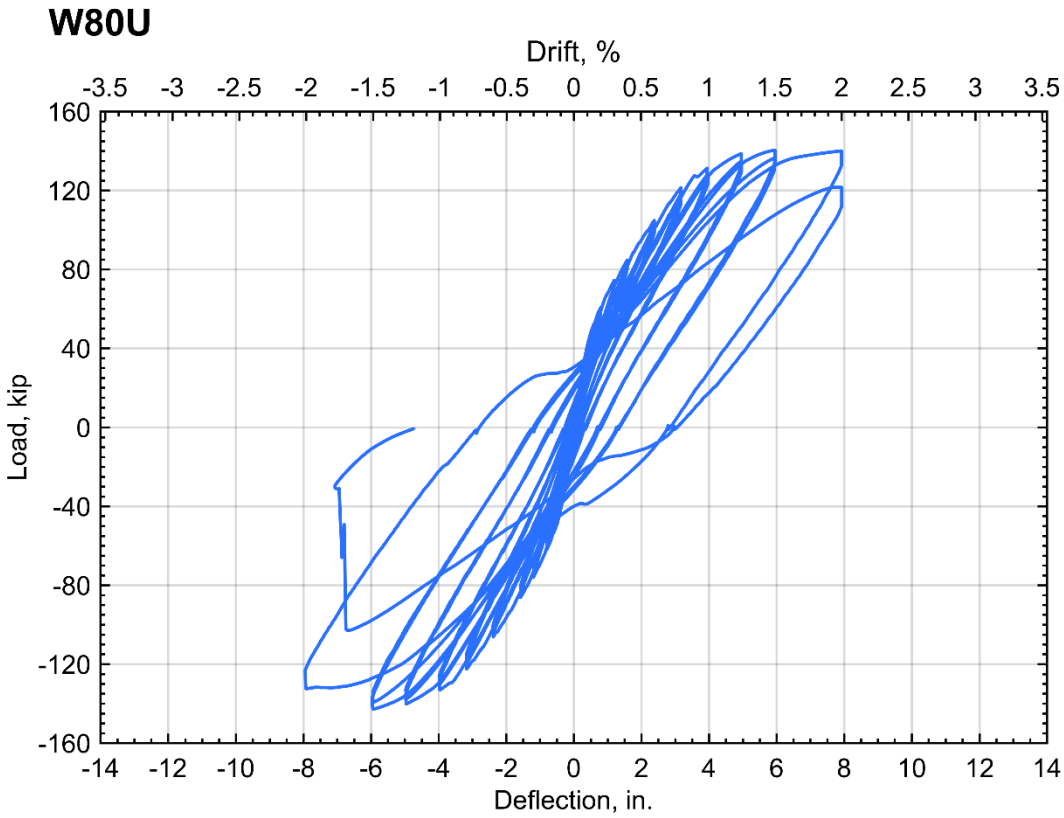

Figure 69 – Specimen W80U, Measured Load-Deflection Curve.

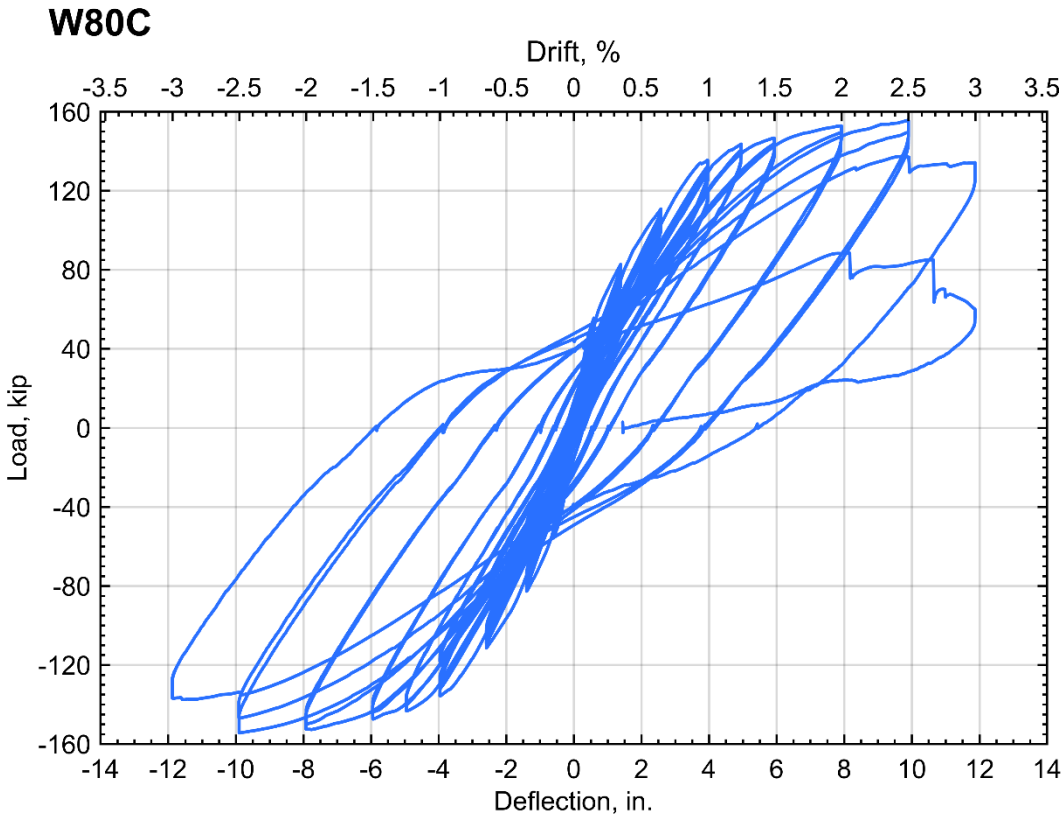

Figure 70 – Specimen W80C, Measured Load-Deflection Curve.

8.2.3 Stresses, Strains and Drift Ratios

Estimating maximum bar stress for the test walls is not as simple as it is for the test beams. The following assumptions are made to provide plausible estimates of peak bar stress:

The effective arm of the boundary reinforcement is $0.93d$, and the line of action of the resultant of compression forces is at $0.07d$ from the outermost fibre in compression (coinciding with the centroid of the longitudinal reinforcement in the boundary).

The contribution of axial force, self-weight, and equipment weight to moment resistance was $(400 + 34)kip\ (h/2 - 0.07d)$, with $h = 7ft$.

The contribution of web reinforcement to moment resistance was $70ksi \times 6 \times 0.2\ in^2 \times (50\ in. - 0.07d)$ for W60U and W60C, and $90ksi \times 6 \times 0.2\ in^2 \times (50\ in. - 0.07d)$ for W80U and W80C.

The values produced with these assumptions are not exact representations of peak bar stress. They are only plausible values that are sensitive to variations in the assumed locations (and magnitudes) of resultant forces. These locations were estimated studying the equilibrium of the cross section of the specimen in what is called 'sectional' or 'moment-curvature' analysis done using measured material properties.

Table 13. Key Results from Test Walls.

Specimen ID	Peak Force [kip]	Estimated Peak Reinforcement Stress [ksi]*	Estimated Peak Mean Bond Stress[psi]	Displacement at Failure [in]	Drift Ratio at Failure†	Ratio of Provided Splice Length to Length Obtained using ACI 318-19 Recommendations (Assuming Transverse Splitting, See Sec. 8.1.4)	Inferred Mean Bond Strength $\sqrt{f_c' \times psi}$
W60U	124	85	358	7.4	1.9%	1.30	4.9
W60C	123	83	524	7.9	2.0%	1.19	7.0
W80U	143	105	292	7.9	2.0%	1.30	3.8
W80C	156	118	495	9.9	2.5%	1.20	6.4

*In boundary reinforcement

†Midspan deflection divided by half constant-moment span - in Test Beams. Lateral displacement along line of action of lateral force divided by height to same level (33 ft) - in Test Walls.

Figure 71 shows the described approximations to peak bar stress plotted against drift ratio at failure together with measured stress-strain relationships.

Figure 72 shows the described approximations to peak bar stress plotted against 3/2 times drift ratio at failure. The reason drift is multiplied by 3/2 in the abscissae of the points representing test-walls is the recommendation by Y. Wang (2014) that maximum tensile surface strain in structural walls, on average, can be approximated as 1.5 to 2.5 times drift ratio. For a discussion of how surface strain was related to drift ratio in test beams refer to Section 8.1.3.

Figure 72 shows again why the lap splices in the specimens with Grade-80 bars were stronger, but the additional strength did not result in additional drift capacity. The figure also reiterates that drift capacity results from plastic deformation. A wall with splices that can merely yield is unlikely to have

adequate drift capacity. And for the same reason, bars with too much strain hardening may not be beneficial if they are lapped in critical regions of structural walls.

In examining Figure 72, consider that in an element with moment gradient the effect of the yield plateau on drift has been observed to be negligible (Wight, Sozen, 1975). An alternative interpretation of the data consistent with this observation is illustrated in Figure 72 through the use of dashed lines representing offset stress v. strain curves. In examining this figure, one should also consider that stress cycles result in deviations from the stress-strain curve obtained for monotonic loading (Aktan, 1973).

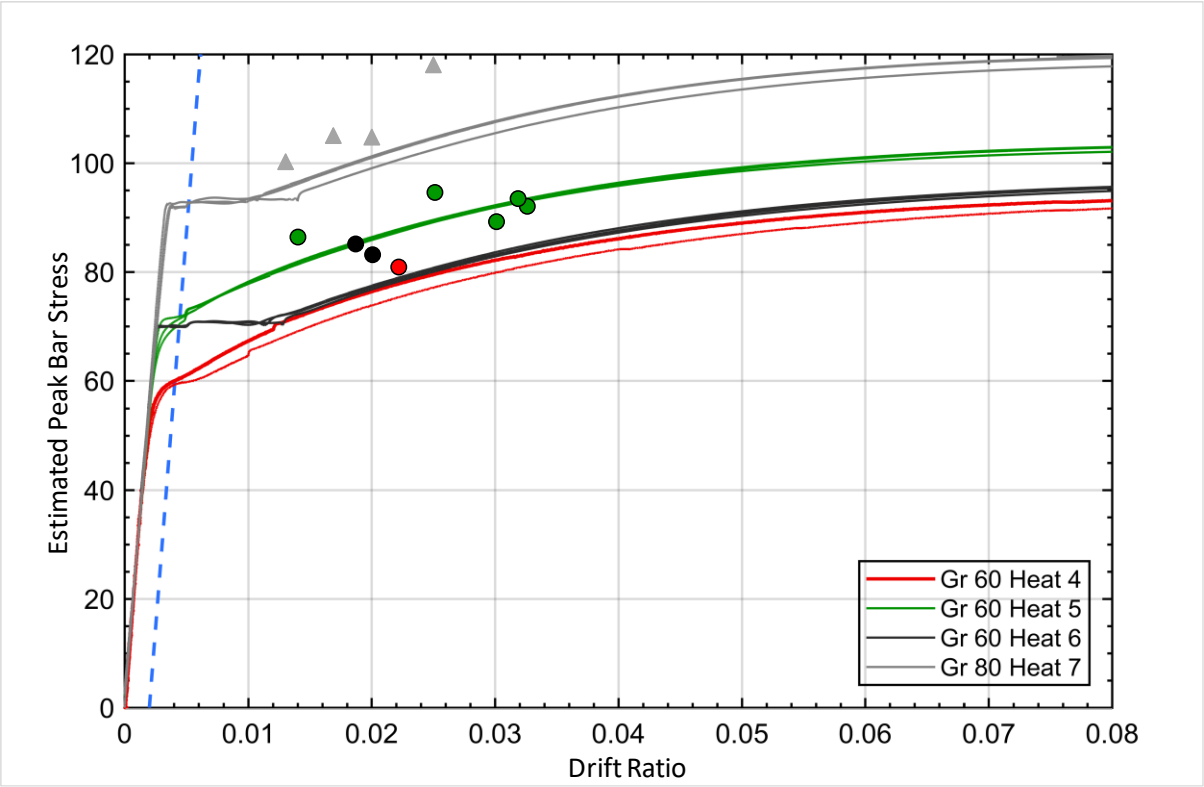

Figure 71 – Variation of Peak Bar Stress with Drift Ratio at Failure Superimposed on Monotonic Bar Stress-Strain Relationships Measured in Test Coupons – All Specimens.

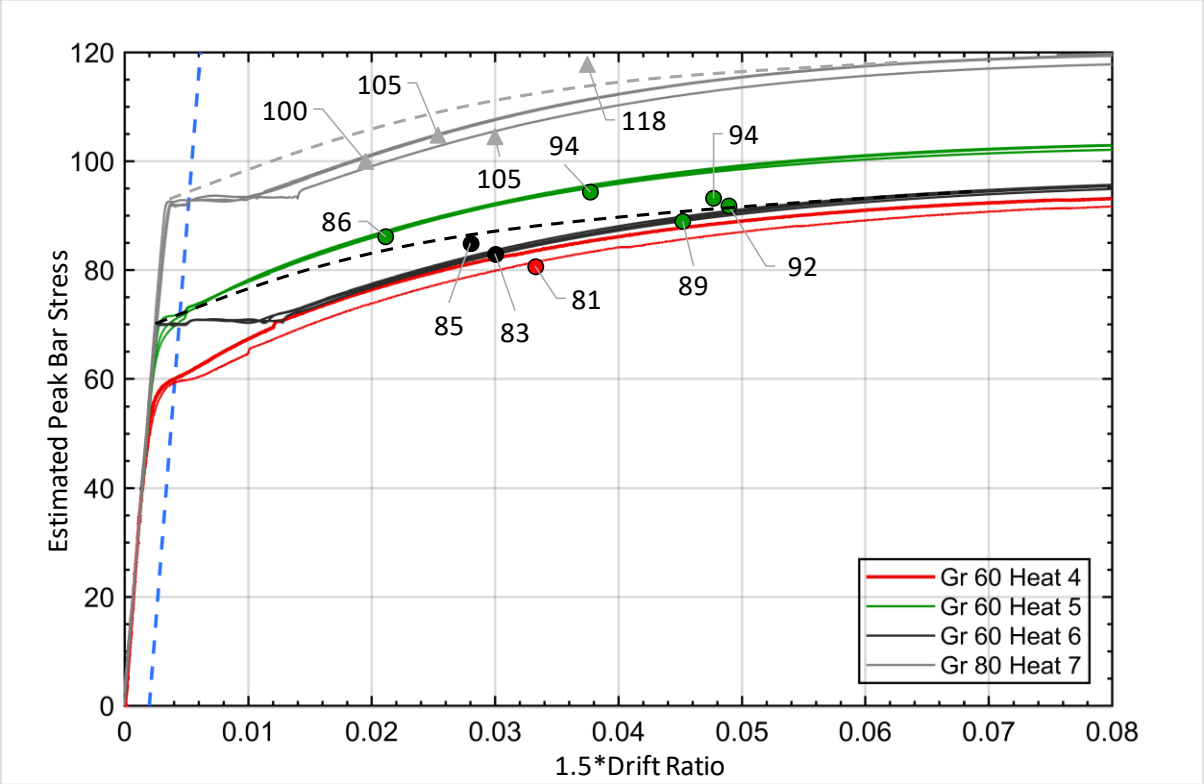

Figure 72 – Variation of Peak Bar Stress with 1.5 x Drift Ratio Superimposed on Monotonic Bar Stress-Strain Relationships Measured in Test Coupons – All Specimens.

To explore how strain and drift were related to one another in the test walls from this investigation and to test the approximations in Figure 72 implying that strain was close to 3/2 times drift in test walls as in test beams, consider Figures 73 and 74. These figures show how surface strains measured using Optitrack infrared cameras and optical targets installed along the edge of the wall in tension (on and close to the foundation). The relationship between strain and drift is likely to be affected by a) wall aspect ratio and, b) gage length. Gage length is particularly critical because the mentioned strains were measured on the surface of the concrete not on bars. Bars were not instrumented with strain gages a) to avoid disturbing their bond to concrete and b) to avoid the grinding required for installation that can affect the apparent yield stress and reduce the elongation capacity of the bar.

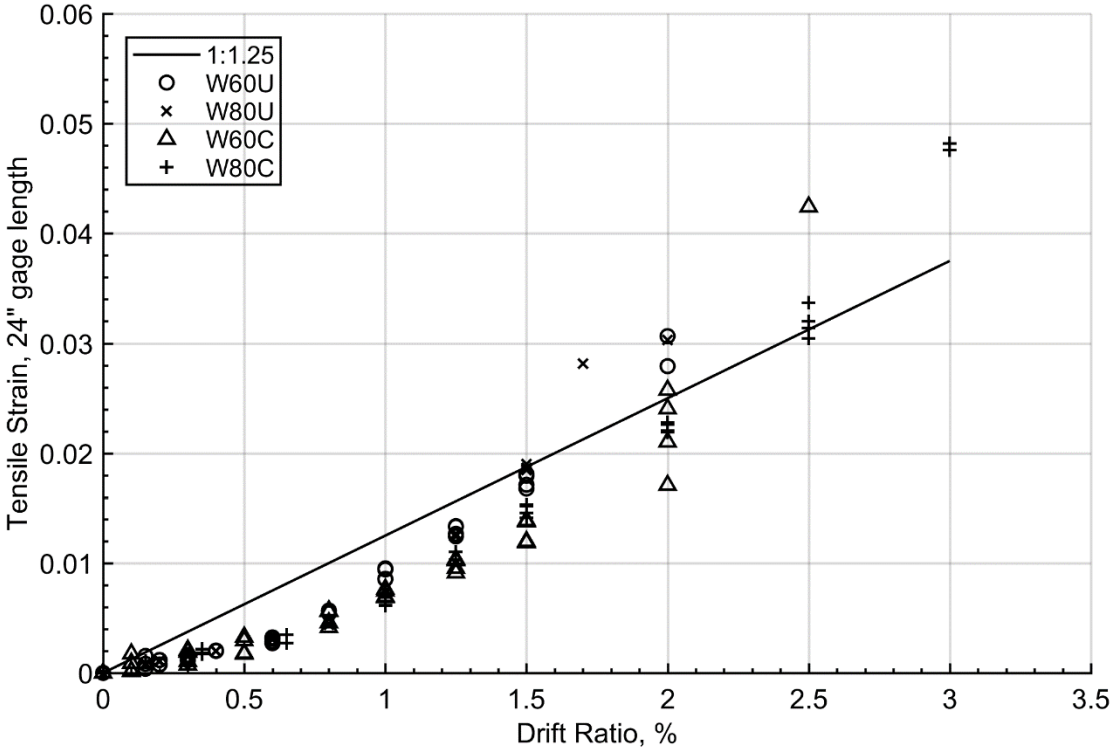

Figure 73 –Drift –Strain Relationship for Surface Strains Measured Along a Gage Length of 2 ft (i.e. 2/7=0.28 times wall length and 24 longitudinal bar diameters).

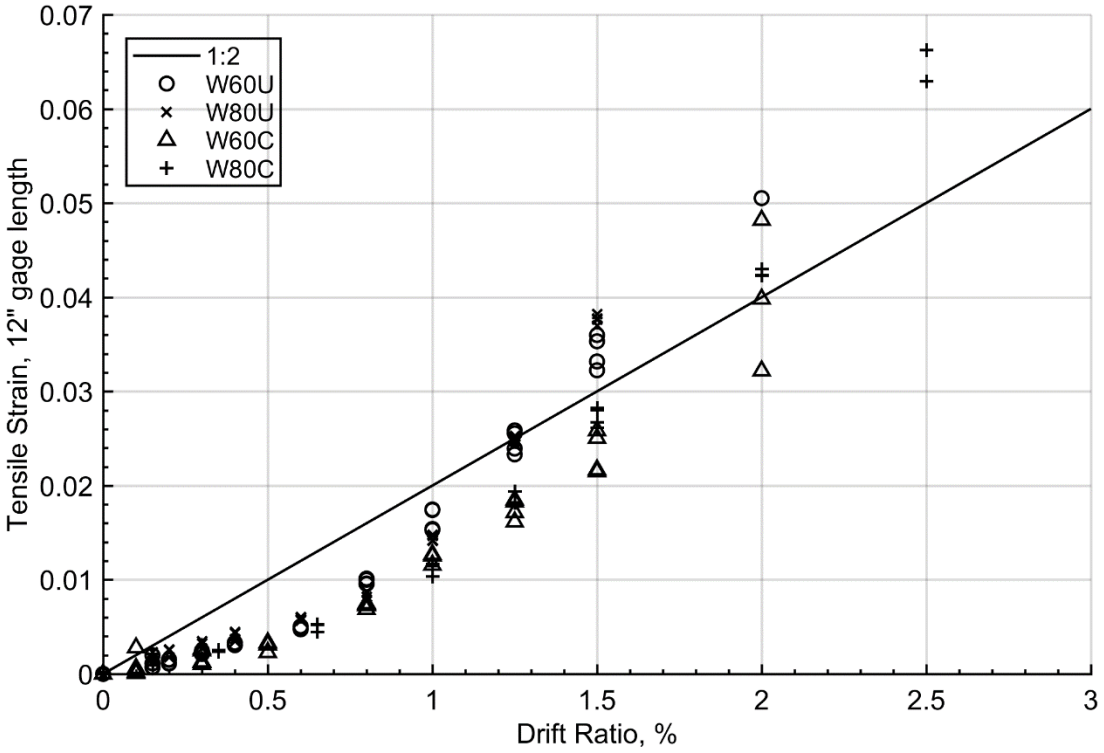

Figure 74 –Drift –Strain Relationship for Surface Strains Measured Along a Gage Length of 1 ft (i.e. 1/7=0.14 times wall length and 24 longitudinal bar diameters).

Figures 73 and 74 show how sensitive surface strain is to the chosen gage length. The measurements were obtained near the bases of walls and are affected by bar slip in the foundation. In addition, strains concentrated near the end of the splice because the lap splice tends to stiffen the wall. And bar strain is likely to differ from the reported strains especially if one considers how the location of cracks and bond stresses can affect it. For these reasons, the reported surface strains are only a proxy for bar strain.

Focusing on drift ratios close to 2% (where most failures occurred), Figure 73 -obtained for a gage length of 24 in. (0.28 times wall length and 24 bar diameters)- suggests surface strain was close to 5/4 times drift ratio. For larger drift ratios close to 2% again, Figure 74 -obtained for a gage length of 12 in. (0.14 times wall length and 12 bar diameters)- suggests surface strain was close to 2 times drift ratio. In contrast, Wang worked with gage lengths of 0.2 to 0.25 times wall length (7 to 12 bar diameters). Estimating strain as 1.5 times drift ratio as done in Figure 72 is therefore plausible but it is certainly not the only choice. Interpolating the reported surface strains in terms of gage length expressed as a fraction of wall length leads to a ratio of strain to drift ratio of 1.4 for a gage length of 0.25 times wall length and 1.7 for a gage length of 0.2 times wall length. But extrapolation in terms of gage length expressed as multiple of bar diameter[9] leads to larger ratios of strain to drift ratio. For design purposes it may be safer to assume strain in walls similar to the test walls can be as high as 2 to 2.5 times peak drift ratio as recommended by Wang (2014). Implications of variations in this factor are discussed in Section 8.2.5.

[9] Assuming such projection may be a better way to consider how bond may affect surface strain.

8.2.4 Comparing the Results with Results from Existing Formulations

The described estimates of peak bar stress are compared with estimates produced using the formulations described in Section 8.1.4. These comparisons are illustrated in Figures 75 to 77. In all cases, the discussed estimates of peak bar stress in test walls add to the scatter in the plots. They are identified by a circle drawn around the markers associated with the test-wall results.

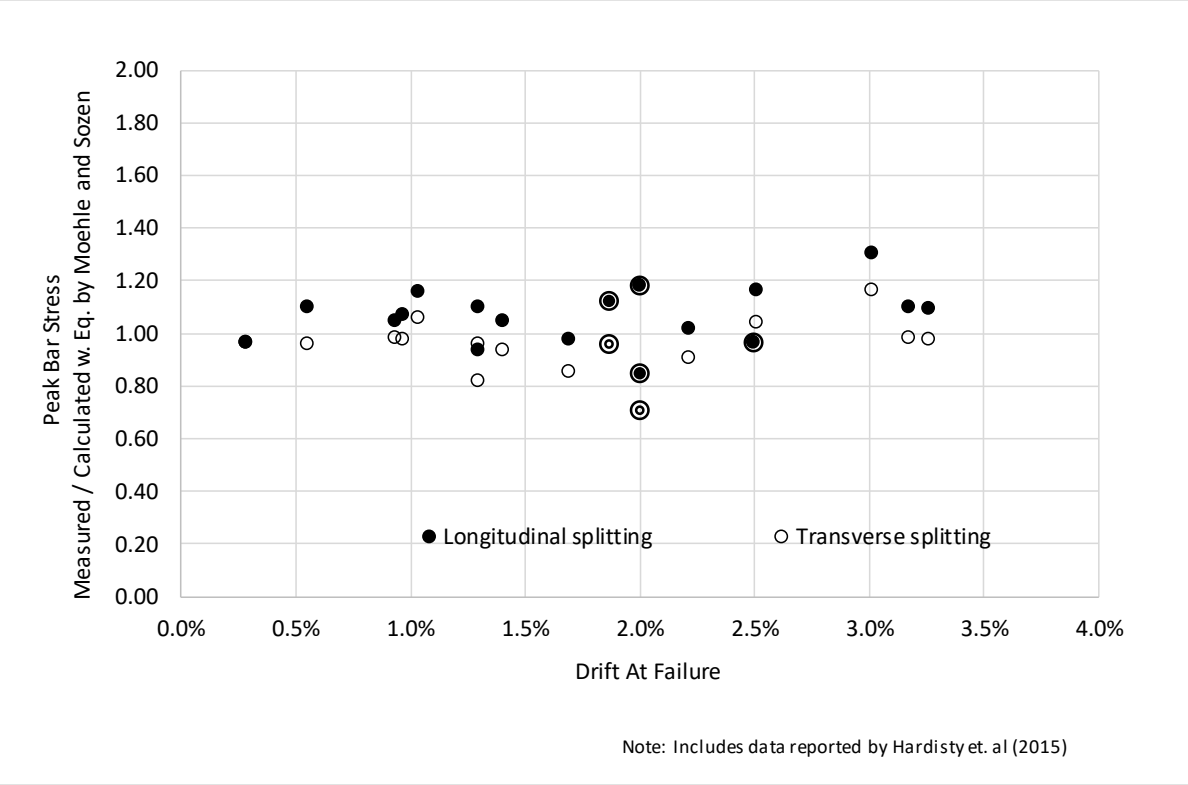

Formulation by Moehle and Sozen (1990)

Figure 75 –Variation of Ratio of Measured to Calculated Peak Bar Stress with Drift Ratio at Failure – Calculations Made Using Formulation by Moehle and Sozen (1990).

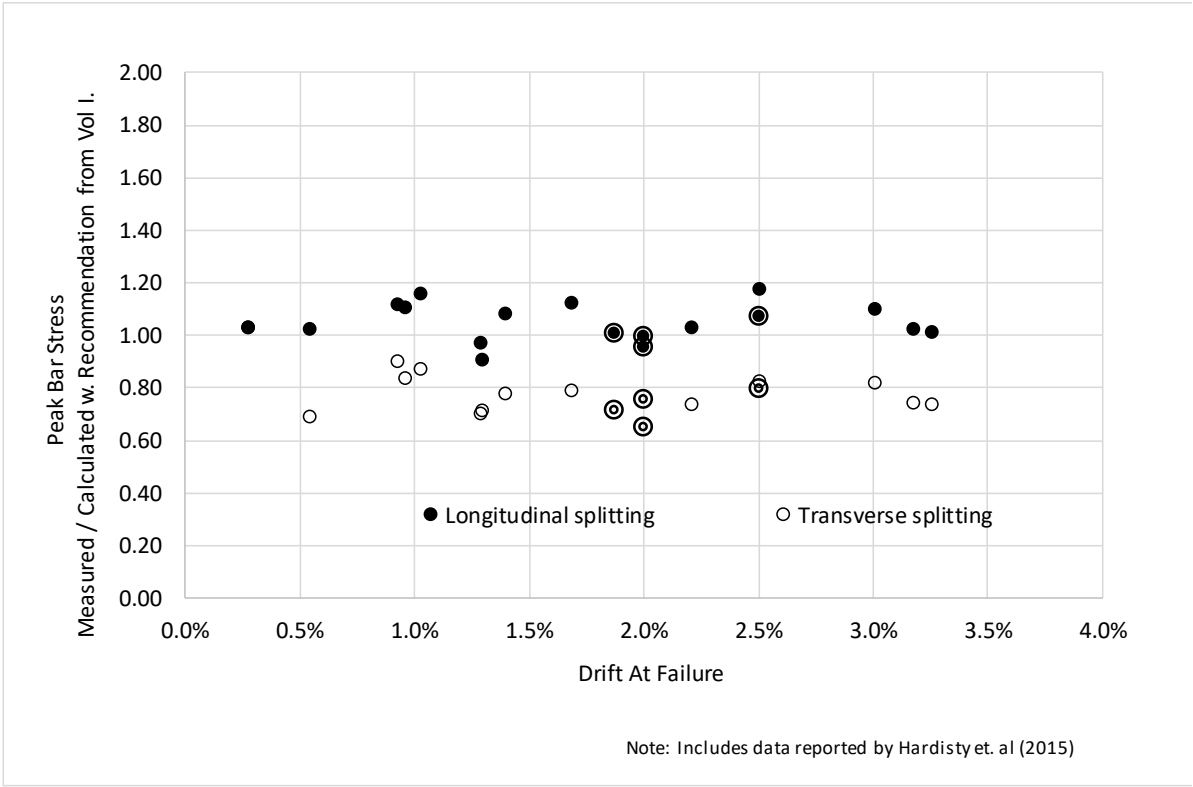

Formulation by Fleet et al. (Volume I)

Figure 76 –Variation of Ratio of Measured to Calculated Peak Bar Stress with Drift Ratio at Failure – Calculations Made Using Formulation by Fleet et al. (2019).

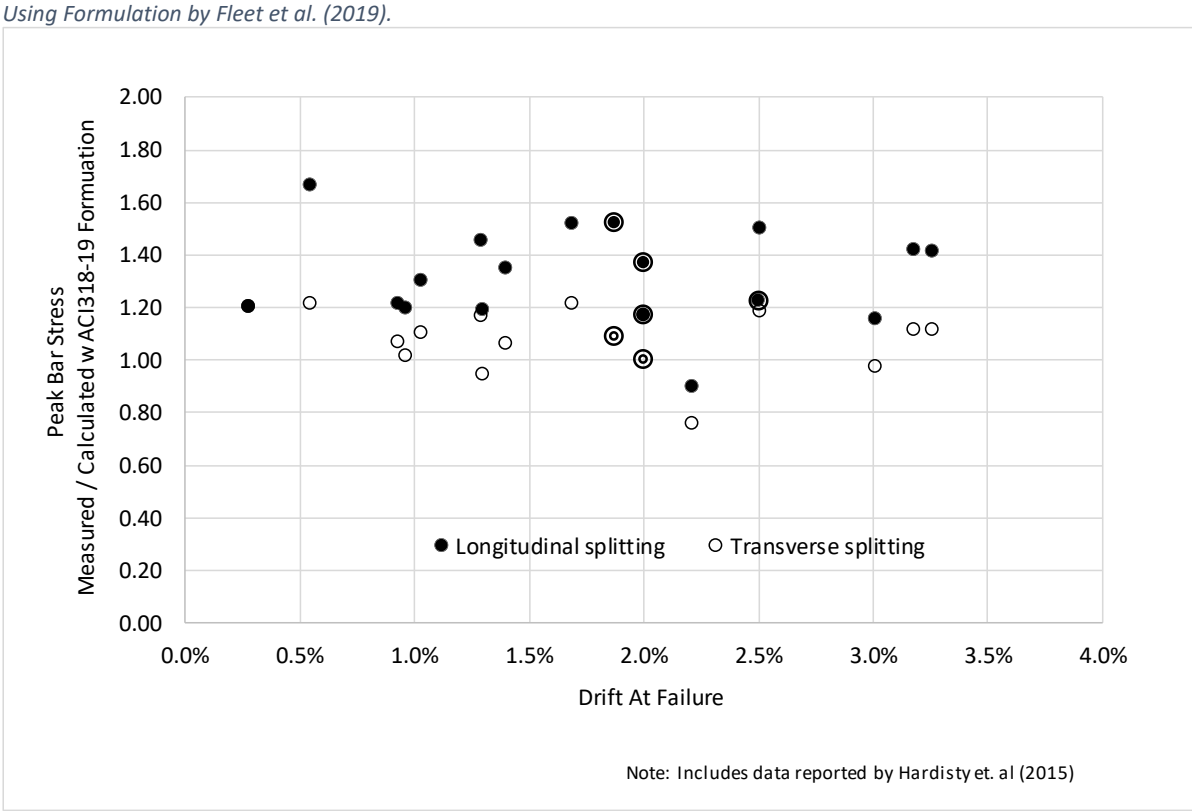

Formulation in ACI318-19

Figure 77 –Variation of Ratio of Measured to Calculated Peak Bar Stress with Drift Ratio at Failure – Calculations Made Extrapolating Recommendations by ACI318 (2019).

In terms of conservatism, scatter, and familiarity, the option to use the current design formulation (recommended by ACI318-19) assuming that transverse splitting controls appears to be a reasonable compromise:

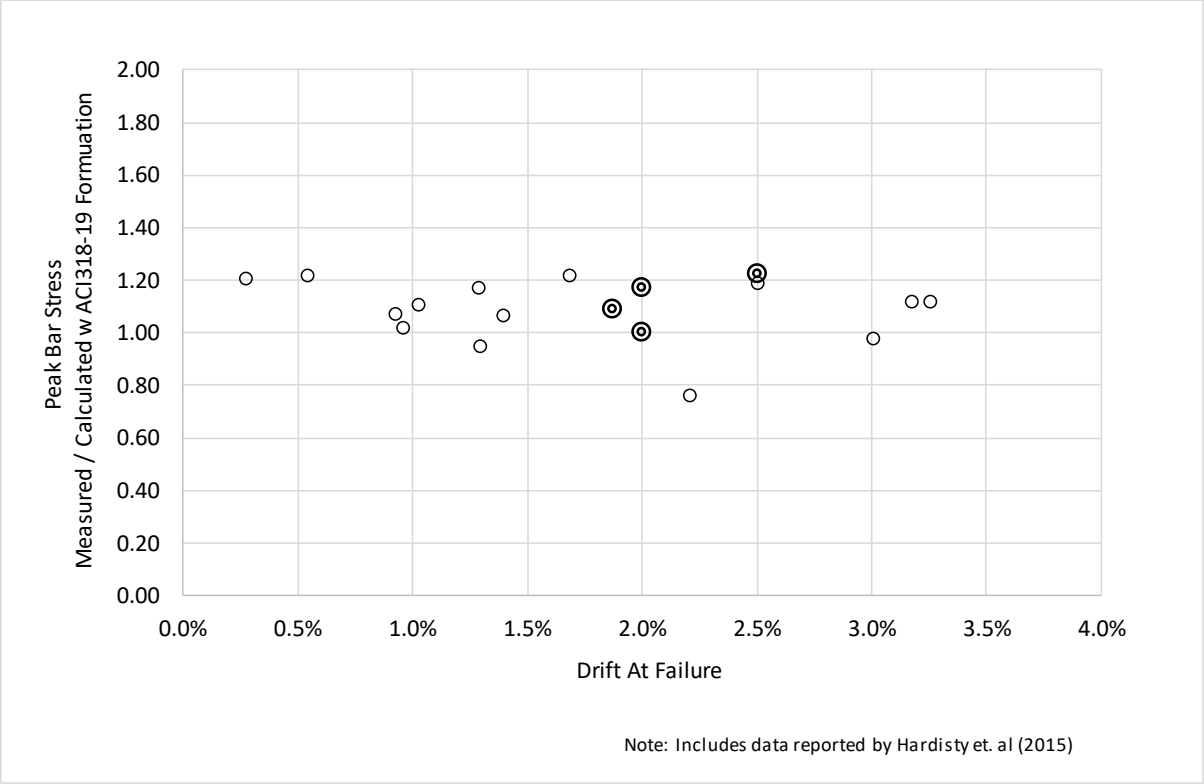

Figure 78 –Variation of Ratio of Measured to Calculated Peak Bar Stress with Drift Ratio at Failure – Calculations Made Extrapolating Recommendations by ACI318 (2019) – Results Obtained Assuming Transverse Splitting Controls.

8.2.5 Organizing the Results in Terms of Drift Capacity

Including the results from test walls in Figure 63 leads to Figure 79 below:

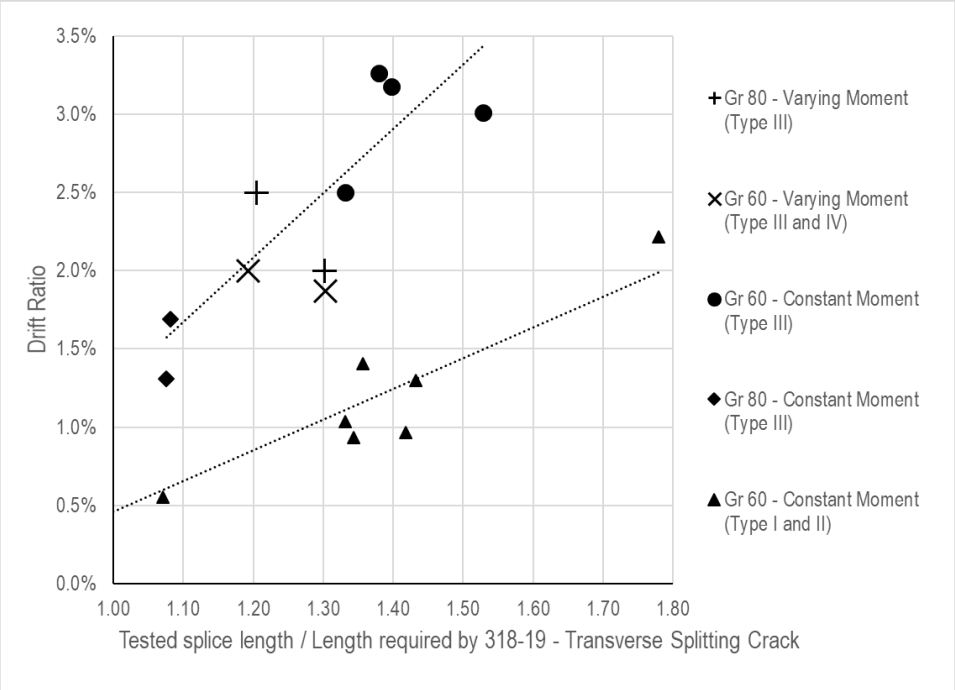

Figure 79 – Variation in Drift Ratio at Failure with Increases in Ratio of Length of Lap Splice to Length Required by ACI318-19 - Formulation Used Assuming Transverse Splitting Controlled.

Assuming longitudinal splitting controls results in Figure 80.

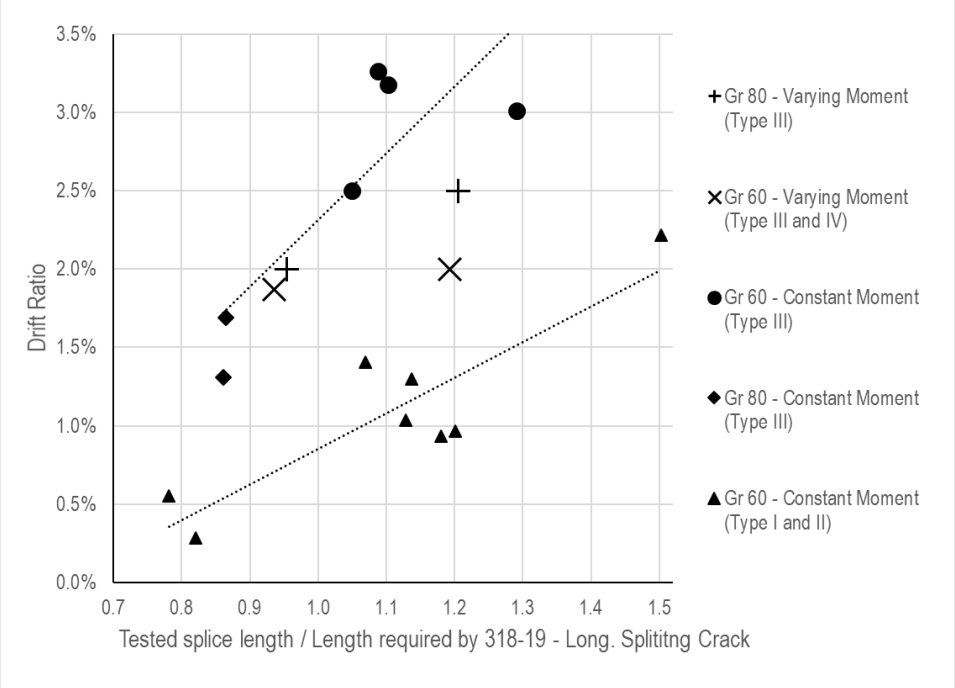

Figure 80 – Variations in Limiting Drift Ratio with Increases in Ratio of Length of Lap Splice to Length Required by ACI318-19.- Formulation Used Assuming Longitudinal Splitting Controlled

The ranges of key variables expected to affect the results in Figure 80 are:

1)	concrete strength f'_c	4100 to 6300 psi
2)	steel yield stress f_y	60 to 93 ksi
3)	steel strength / yield stress	1.28 to 1.57 for longitudinal reinforcing bars 1.26 to 1.47 for transverse reinforcing bars
4)	clear concrete cover	3/4 to 1.5 in. (measured to ties)
5)	clear bar spacing	0.5 to 2¼ bar diameters
6)	lap splice length	40 to 90 bar diameters
7)	Transverse reinforcement index	
	K_{tr} (ACI 318-19)	0 to 1.3 bar diameters
	TRI (Sozen and Moehle, 1990)	0 to 2.7
8)	wall aspect ratio	4.7
9)	half-length of constant moment region to cross-sectional depth (test beams)	1.8 to 2

In reference to Figure 79, multiplying required length by 1.5 for splices meeting only minimum requirements (transverse reinforcement Types I and II) leads to Figures 81a. Figure 81a (obtained assuming transverse splitting controls) suggests that - for the listed ranges- drift ratio was close to or more than:

$$DR = 2\% \times \left(\frac{l_{s\ PROVIDED}}{C \times l_{s\ REQUIRED}} - 0.5 \right) > 0$$

Where C =1.5 for transverse reinforcement Types I and II (ties and stirrups anchored by short hooks and clear cover not exceeding ¾ in) and C =1.0 otherwise. A note of caution is in order. This expression should be considered a synthesis of the test results rather than a reliable vehicle to estimate wall drift capacity. Walls with aspect ratios smaller than the aspect ratios of the described test walls are likely to reach smaller drifts. Other deviations from the test parameters and construction defects may also affect results. Consider also that a wall with $\frac{l_{s\ PROVIDED}}{l_{s\ REQUIRED}} > 1$ is unlikely to fail at a drift ratio smaller than the drift ratio at yield (often 0.5% or more for aspect ratios of at least 2). An alternative expression can be drawn for the assumption that longitudinal splitting occurs, but the plausible improvement in reliability seems limited in light of a) the scatter in the data b) the limited number of results available and c) the original intent in the formulation of the ACI equation.

Considering that peak surface strain in walls can be as much as 2 times drift ratio or more (Figure 73 and 74) while in beams it was consistently closer to 1.5 times drift ratio[10] implies that a given splice can produce 2/1.5=4/3 times more drift in a test beam than in a test wall. The ratio of 2 (of strain to drift ratio) was obtained in Figure 74 for a gage length of 12 in. Toward the end of the tests, crushing had affected much of this length (Sec. 8.2.1). It is reasonable to assume that at that stage, the apparent strain obtained with the 12-in. gage length approached bar strain. From that point of view, it would be safer to project the obtained observations by reducing the limiting drift ratios measured in test beams by the factor 1.5/2=3/4. That exercise produced Figure 81b. Considering other

[10] For 60-bar diameter splices

plausible relationships between strain and drift ratio discussed in Section 8.1.3 leads to the following factors to project the limiting drifts reached in test beams and Figure 81c:

Splice Length	Projection Factor
50 in.	$\frac{4}{3} \div 2 = \frac{2}{3}$
60 in.	$1.5 \div 2 = \frac{3}{4}$
80 in.	$2 \div 2 = 1$

These projection factors are based on the geometry of the beams tested. For the tests reported by Hardisty et al. (2015) a projection factor of 0.9 was used in Figure 81 c.

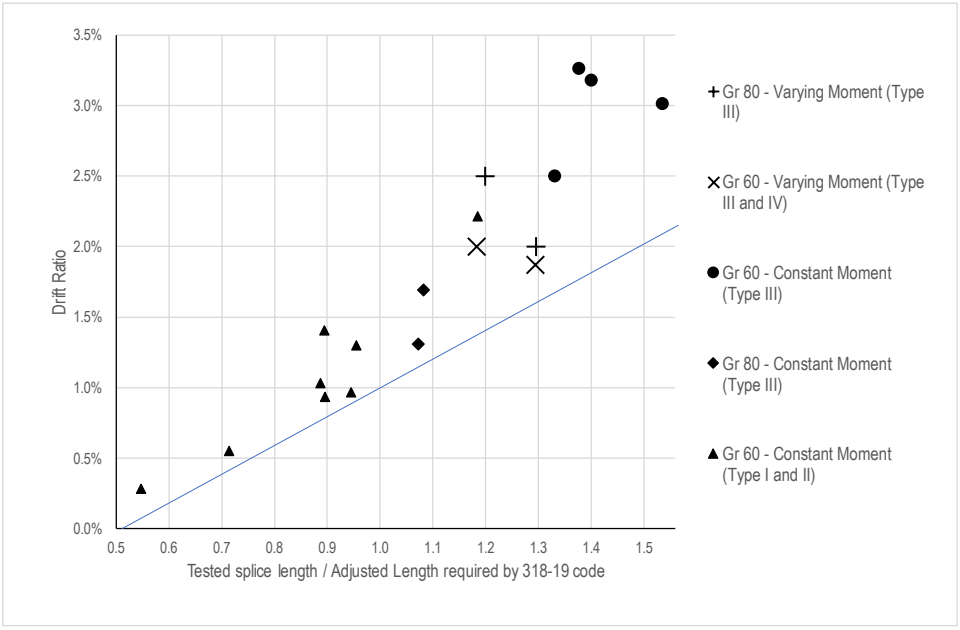

a) drift ratios measured at failure

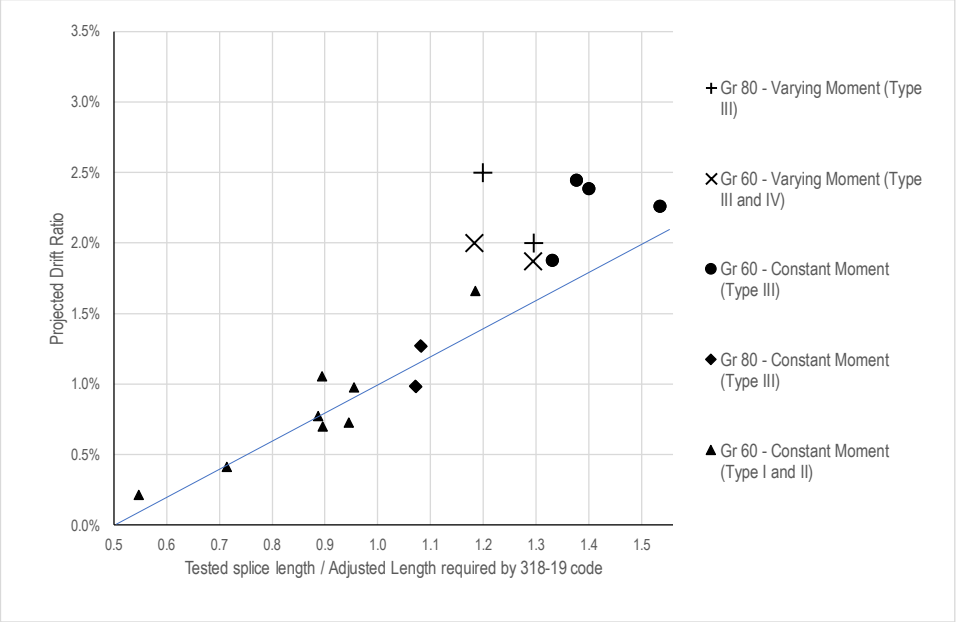

b) drift ratios measured in test beams at failure multiplied by 3/4

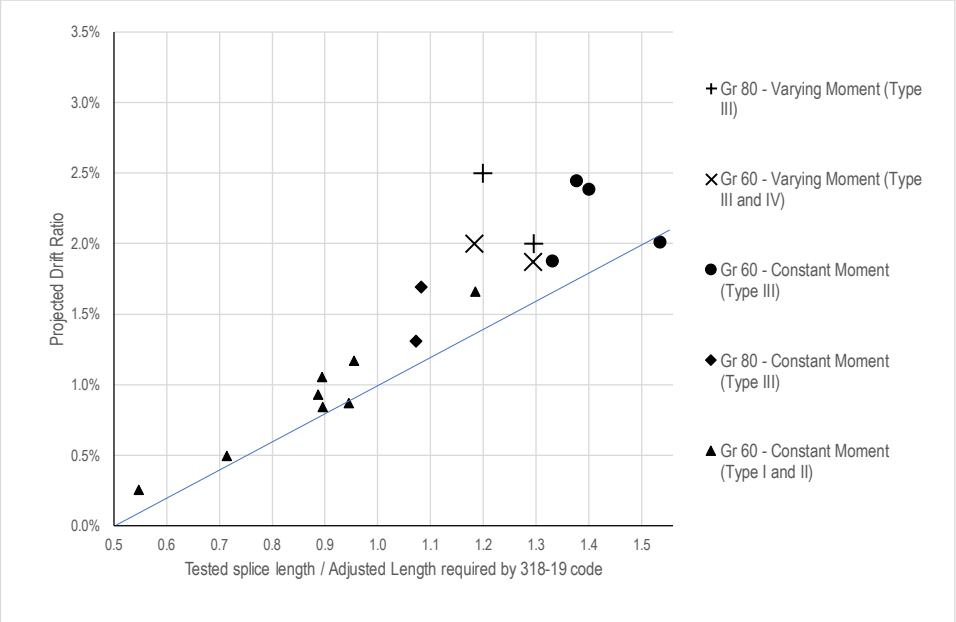

c) drift ratios measured in test beams at failure multiplied by projection factors adjusted in relation to splice length (2/3 for 50 in., 3/4 for 60 in., 1 for 80 in., 0.9 for beams tested by Richter and Hardisty, 2012,2015)

Figure 81 – Variations in Limiting Drift Ratio with Increases in Ratio of Length of Lap Splice to Length Required by ACI318-19.- Formulation Used Assuming Transverse Splitting Controlled – Required Length Increased by 1.5x for Transverse Reinforcement Types I and II.

Figures 81 b and c show the expression presented is a reasonable synthesis of what occurred in the described tests expressed in terms used in current practice in the U.S.

9. Variation in Stiffness with Increases in Number of Cycles

The increased numbers of cycles in Loading Protocol B used to test specimens W60C and W80C helped produce more demanding testing conditions that may represent the effects of initial demands attributable to phenomena other than earthquakes (wind for instance). They also helped produce information on how initial low amplitude cycles may affect response at larger amplitude cycles. Figure 82 shows how peak-to-peak stiffness (defined as the slope of a line drawn from one peak in each hysteresis force-deflection loop to the opposite peak in the same loop) varied with drift and with number of cycles. Stiffness was normalized relative to the stiffness of an idealized cantilever ($3EI \div H^3$) with modulus of elasticity $E = 4900ksi$, cross sectional moment of inertia I equal to the moment of inertia of the gross cross section, and height $H = 33ft$. At each drift target there are two or three symbols for each test wall. The 'highest' symbol represents the stiffness reached in the first cycle applied at the given drift. The second (lower or lowest) symbol represents stiffness in the second cycle at the same drift. In cases in which more than two cycles were applied at a given drift target, the third (and lowest) cycle represents the stiffness measured in the last cycle at that drift. Two observations are more salient from this figure(s):

-The reduction in stiffness that occurred at a given drift and in up to 500 cycles with amplitudes not exceeding 1.25% was smaller than 10%.

-The initial stiffness was measured to vary between 75% and 85% of the value obtained for an ideal cantilever ($3EI \div H^3$). The difference between the measured and the ideal value can be attributed to the fact that the initial cycles neared (W60C) or exceeded (Other Walls) the load required for cracking to occur and to flexibility of the base, shear deformations, and shrinkage cracks.

-At a drift ratio of 0.5% stiffness was nearly 35 to 40% of $3EI \div H^3$. At 1%, it was 25 to 30% of $3EI \div H^3$. Interestingly, in the cycles of decreasing amplitude that followed cycles at 1 and 1.25% in Protocol B, stiffness had an apparent increase to nearly 40% (at 0.1%) both in W60C and W80C. It is difficult to explain this apparent increase in stiffness in terms of extent of cracking and its effects on the cross section, but it has been observed before (Takeda et al., 1970).

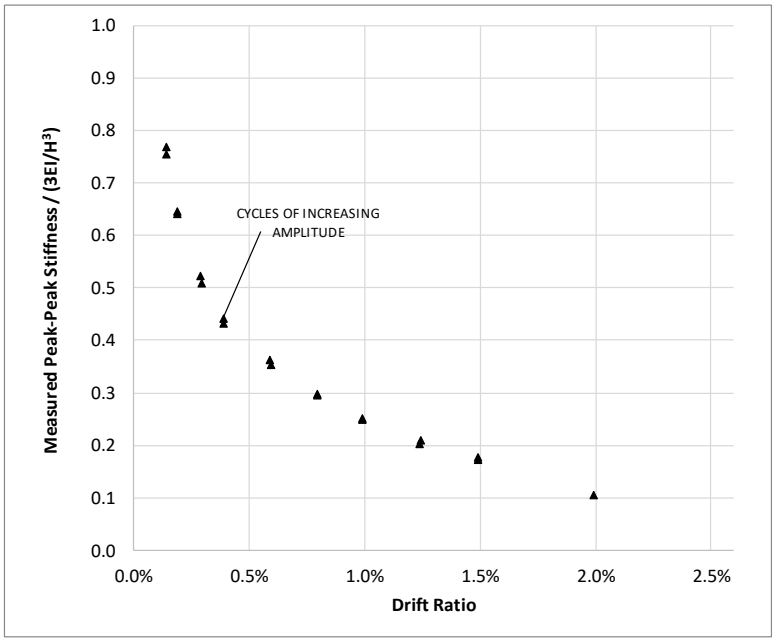

a) Test Wall W60U

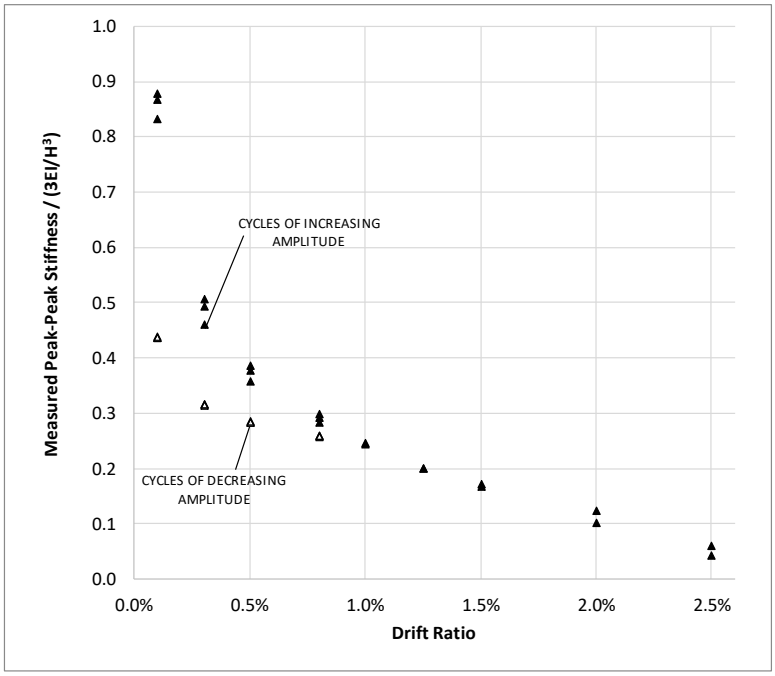

b) Test Wall W60C

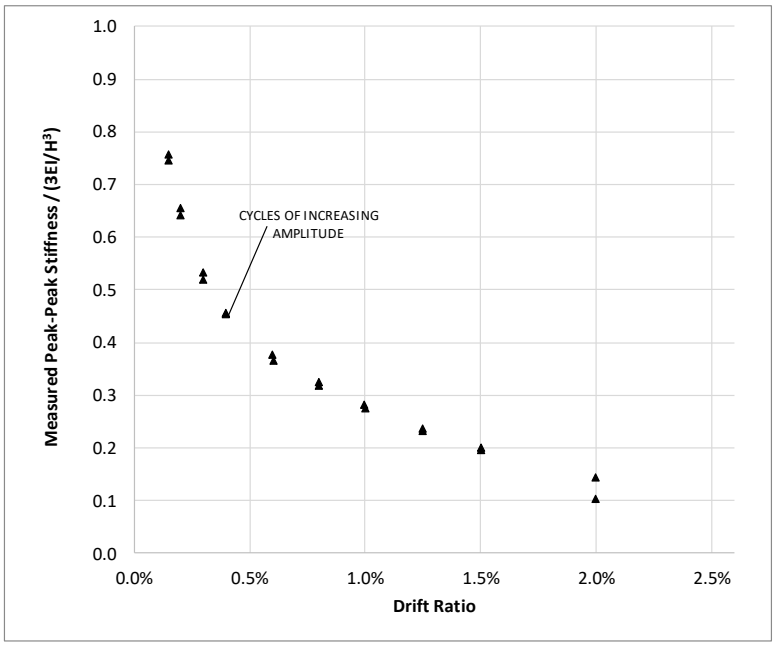

c) Test Wall W80U

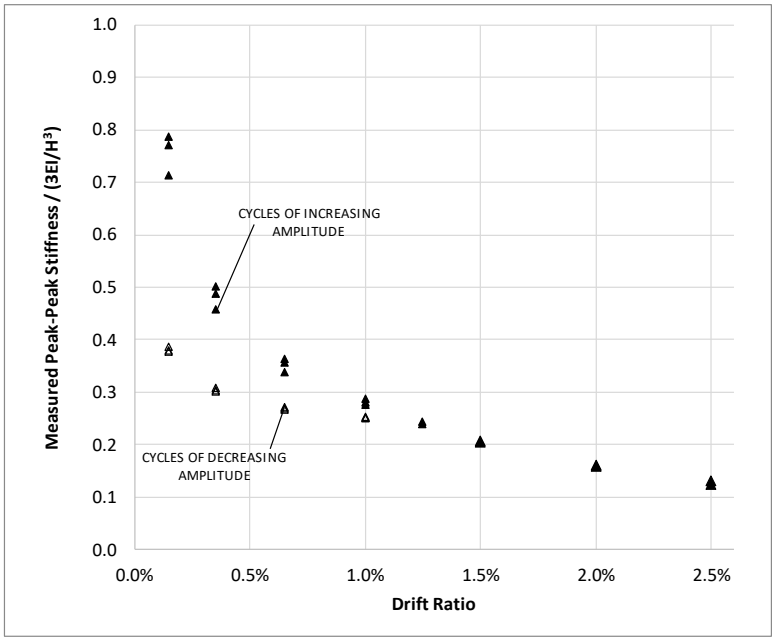

d) Test Wall W80C

Figure 82 – Variations in Stiffness

Comparing specimens W60U vs W60C, and W80U vs W80C (Figure 83), it is apparent that the initial cycles (with amplitudes not exceeding 1.25%) had no clear effect on the peak-to-peak stiffness reached in cycles with larger amplitudes.

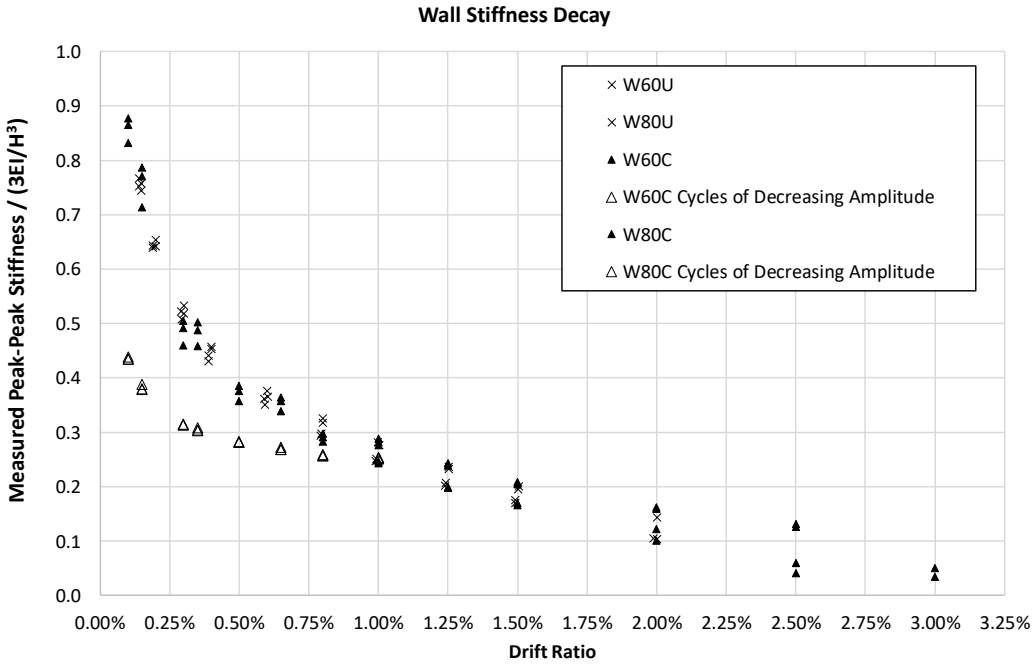

Figure 83 – Comparison of Variations in Stiffness

10. Inferences

For the observations obtained, developing a relationship between lap splice properties and drift at splice failure is feasible. But given

1) the limited number of observations available and
2) that it is unlikely that, in practice, a good representation of the stress-strain relationship will be known ahead of time –especially for cyclic demands from wind or earthquake-

the following reasonable lower bounds to drift capacity are provided instead of an elaborate relationship between drift and splice properties that is likely to have many a limitation.

For structural walls with lap splices comparable to those tested, the observations collected suggest that drift capacity can be as low as 0.5% for splices with minimum cover (0.75 in.), minimum transverse reinforcement terminating in hooks at the lap splice, and lap splice lengths selected 'just' to reach yielding in the spliced bars. That is, splice failure can occur as yield is reached or soon after. For cover twice as thick and transverse reinforcement that is continuous around the lap splice (Type III and Type IV transverse reinforcement details as shown in in Figure 24), drift capacity can increase to at least 1%. For lap splices 1.3 times longer than required to reach yield, drift ratio at splice failure increased to approximately 0.75% (for minimum cover and transverse reinforcement terminating in hooks at lap splices) and 1.5% or more (for additional cover and continuous transverse reinforcement).

Given the magnitude of these projections, given that the properties of the tested walls represented ideal conditions, and given the consequences of splice failure in a structural wall that may be the only element providing lateral stability in a building, it seems reasonable to:

1. Prohibit the use of lap splices in the longitudinal reinforcement near critical sections of structural walls for seismic applications, regardless of wall classification.

For applications not related to earthquake demands:

2. Ban the use of lap splices not confined by closed hoops in critical sections of slender walls in which yielding at their bases is expected.
3. Require the use of closed hoops confining lap splices in structural walls with longitudinal bars expected to yield under design lateral demands. The projections reported here were obtained for hoops associated with transverse reinforcement ratios (defined for gross cross-sectional dimensions) of ⅔%.

11. Conclusions

Within these ranges:

concrete strength f'_c	4100 to 6300 psi
steel yield stress f_y	60 to 93 ksi
steel strength / yield stress	1.28 to 1.57 for longitudinal reinforcing bars 1.26 to 1.47 for transverse reinforcing bars
clear concrete cover	3/4 to 1.5 in. (measured to ties)
clear bar spacing	0.5 to 2¼ bar diameters
lap splice length	40 to 90 bar diameters
Transverse reinforcement index	
K_{tr} (ACI 318-19)	0 to 1.3 bar diameters
TRI (Sozen and Moehle, 1990)	0 to 2.7
wall aspect ratio	4.7
half-length of constant moment region to cross-sectional depth (test beams)	1.8 to 2

Lap Splice failure caused an abrupt and nearly complete loss of lateral load-carrying capacity in all tests. Bond failures took place after yielding of the longitudinal reinforcement and in the range of strains associated with strain hardening. Nevertheless, the inferred strengths of lap splices were consistent with the results obtained with formulations to estimate splice strength based on results from test without yielding. Inferred splice strength did not appear to be sensitive to strain.

The test results and their projections suggest that structural walls with lap splices in longitudinal reinforcement near critical sections may fail at drift ratios as ranging from 0.5% to 0.75%, or near the drift ratio at yield for splices with:

a) minimum bar cover of 0.75 x bar diameter

b) transverse reinforcement terminating in hooks at lap splices and

c) lap-splice length ranging from 1 to 1.3 times the length required to reach bar yielding.

For cover twice as large and ties that are continuous around the lap splice (as in Figure 24), drift capacity was projected to increase to 1% to 1.5% for lap-splice lengths ranging from 1 to 1.3 times the length required to reach bar yielding.

The values of drift capacity presented suggest that lap splices not confined by closed hoops and not exceeding current detailing minima should not be used in the longitudinal reinforcement of walls required to exhibit any toughness through yielding of the spliced bars.

Increased number of loading cycles in the linear range of response of the tested walls did not cause an apparent reduction in the ability of the walls to deform laterally.

12. Data, Photographs, and Video

All test data, photos and videos are available at datacernterhub.org

13. Acknowledgements

This study was made possible by the generous support and funding provided by the Charles Pankow Foundation under the direction of Anne Ellis and Marc Perniconi. The Concrete Reinforcement Steel Institute worked tirelessly with its members to provide all the reinforcement needed at a time when Grade-80 reinforcing bars were not common in the USA. Special thanks are due to Pete Fosnough and Mike Mota for their efforts in procuring the steel through donations from Harris Rebar, Nucor, and Gerdeau. The project advisory team (Ron Klemencic, Dominic Kelly, and Jack Moehle) provided invaluable advice. And the study would not have been possible without the persistent help of Harry Tidrick, Kevin Brower, Prateek Shah, Charles Kerby, Felipe Osandon, Jonathan Monical, and Kinsey Skillen. The efforts of Aishwarya Puranam to help get the first wall test underway deserve special mention.

13. References

Aaleti, S., Brueggen, B. L., Johnson, B., French, C. E., and Sritharan, S., (2013). “Cyclic response of reinforced concrete walls with different anchorage details: Experimental investigation.” Journal of Structural Engineering, 139(7).

Abrams, Duff A., (1913)."Tests of Bond Between Concrete and Steel," University of Illinois Eng. Exp. Station, Bulletin No. 71, Vol. XI, No. 15, Dec. 8, 1913.

ACI (American Concrete Institute), (2001). “Development and splice lengths of uncoated bars.” ACI 408, Farmington Hills, MI.

ACI (American Concrete Institute), (2012). “Report on bond of steel reinforcing bars under cyclic loads.” Joint ACI-ASCE Committee 408, Farmington Hills, MI.

ACI (American Concrete Institute), (2019). “Building Code Requirements for Structural Concrete and Commentary.” Farmington Hills, MI.

Aktan, A. & Karlsson, B.I. & Sozen, Mete. (1973). “Stress-Strain Relationships of Reinforcing Bars Subjected to Large Strain Reversals.” Illinois University, Civ Eng Stud, SRS 397.

Almeida, J. P., Prodan, O., Rosso, A., and Beyer, K., (2017). “Tests on Thin Reinforced Concrete Walls Subjected to In-Plane and Out-of-Plane Cyclic Loading.” Earthquake Spectra, 33(1).

Almeida, J.P., Prodan, O., Tarquini, D., Beyer, K., (2017). ‘Influence of Lap Splices on the Deformation Capacity of RC Walls. I: Database Assembly, Recent Experimental Data, and Findings for Model Development, J.” Journal of Structural Engineering, 143(12).

Bimschas, M., (2010). “Displacement Based Seismic Assessment of Existing Bridges in Regions of Moderate Seismicity.” Ph.D. Thesis, ETH Zurich, Zürich, Switzerland.

Birely, A.C., (2012). “Seismic Performance of Slender Reinforced Concrete Structural Walls,” Ph.D. Thesis, University of Washington.

Canbay, E., and Frosch, R. J., (2005). “Bond strength of lap-spliced bars.” ACI Structural Journal, 102(4).

Elnady, E. M. M., (2008). “Seismic Rehabilitation of RC Structural Walls.” Ph.D. Thesis, McMaster University, Hamilton, ON, Canada.

Ferguson, P. M., and Briceno, E. A., (1969). “Tensile Lap Splices. Part I: Retaining Wall Type, Varying Moment Zone.” Research Rep. No. 113-2, Texas Highway Dept., Austin, TX.

Ferguson, P. M., and Krishnaswamy, C. N., (1971). “Tensile Lap Splices. Part II: Design Recommendations for Retaining Wall, Splices and Large Bar Splices.” The Texas Highway Department in cooperation with the U.S. Department of Transportation, Rep. 113-2 Cont., Federal Highway Administration, Bureau of Public Roads, Washington, DC.

Fleet, E., Glucksman, R., Frosch, R., (2019). “Development and Splice Lengths for High-Strength Reinforcement Volume I: General Bar Development,” Report, CPF Research Grant No. 02-17.

Hannewald, P., (2013). “Seismic Behavior of Poorly Detailed RC Bridge Piers.” Ph.D. Thesis, École Polytechnique Fédérale de Lausanne, Lausanne, Switzerland.

Layssi, H., and Mitchell, D., (2012). “Experiments on Seismic Retrofit and Repair of Reinforced Concrete Shear Walls.” Proceedings, 6th Int. Conf. FRP Composites in Civil Engineering—CICE, Rome.

Hardisty, J.N., Villalobos, E., Richter, B., Pujol, S., (2015). “Seismic Response of Walls with Unconfined Lap Splices,” Concrete International, 37(1).

Johnson, B. M., (2007). “Longitudinal Reinforcement Anchorage Detailing Effects on RC Structural Wall Behavior.” M.S. Thesis, Univ. of Minnesota, Minneapolis.

Kilic, S. A., and Sozen, M. A., (2003). “Evaluation of Effect of August 17, 1999, Marmara earthquake on two tall reinforced concrete chimneys.” ACI Struct. J., 100(3), 357–364.

Kim, S., and Shiohara, H., (2012). “Dynamic response analysis of a tall RC chimney damaged during 2007 Niigata-ken Chuetsu-Oki earthquake.” 15th World Conf. on Earthquake Engineering, Lisbon, Portugal.

Kluge, R. W., and Tuma, E. C., (1945). Lapped Bar Splices in Concrete Beams, Journal of the American Concrete Institute, 42(9).

Kunze, W.E., Sbarounis, J.A., Amrhein, J.A., (1965). "Behaviour of Prestressed Concrete Structures during the Alaskan Earthquake". Journal of the Prestressed Concrete Institute, V.10, No.2.

Lowes, L. N., Lehman, D. E., Birely, A. C., Kuchma, D. A., Marley, K. P., and Hart, C. R., (2012). “Earthquake Response of Slender Planar Concrete Walls with Modern Detailing.” Engineering Structures, 43.

Paterson, J., and Mitchell, D., (2003). “Seismic Retrofit of Shear Walls with Headed Bars and Carbon Fiber Wrap,” Journal of Structural Engineering, 129(5).

Orangun, C.O., Jirsa, J.O. and Breen, J.E., (1977). "A Reevaluation of Test Data on Development Length and Splices," Journal of the American Concrete Institute, 74(11).

Puranam, A., (2018). “Strength and Serviceability of Concrete Elements Reinforced with High-Strength Steel,” Ph.D. Thesis, Purdue University, West Lafayette, IN.

Richter, B.P., (2012). “A New Perspective on the Tensile Strength of Lap Splices in Reinforced Concrete Members,” M.S. thesis, Purdue University, West Lafayette, IN.

Song. C., (2013). “The Collapse of the Alto Rio Building during the 27 February 2010, Maule, Chile Earthquake,” MS Thesis, Purdue University, West Lafayette, IN.

Song, C., Pujol, S., Lepage, A., (2012). “The Collapse of the Alto Rio Building during the 27 February 2010 Maule, Chile, Earthquake,” Earthquake Spectra, 28(S1).

Sozen, M. A., and Moehle, J. P., (1990). “Development and Lap-Splice Lengths for Deformed Reinforcing Bars in Concrete,” Report, Portland Cement Association, Skokie, IL, and Concrete Reinforcing Steel Institute, Schaumburg, IL.

Tarquini, D., Almeida, J. P., and Beyer, K., (2015). “Database on 16 Reinforced Concrete Walls with Lap Splices and 8 Reference Units with Continuous Reinforcement,” www.zenodo.org.

T. Takeda, M. A. Sozen, and N. N. Nielsen, (1970). "Reinforced Concrete Response to Simulated Earthquake," Journal of Structural Division, 96(12).

Villalobos, E. J. F., (2014). “Seismic Response of Structural Walls with Geometric and Reinforcement Discontinuities.” Ph.D. Thesis, Purdue University, West Lafayette, IN.

Villalobos, E., Escolano-Margarit, D., Ramìrez-Màrquez, A. L., and Pujol, S., (2017). “Seismic Response of Reinforced Concrete Walls with Lap Splices.” Bulletin of Earthquake Engineering, 15(5).

Wang, Y. (2014), “Effects of Web Reinforcement Discontinuities on the Seismic Response of Structural Walls” Ph.D. Thesis, Purdue University, West Lafayette, IN.

Wight, J.K. and Sozen, M.A., (1975). “Strength Decay of RC Columns under Shear Reversals,” Journal of the Structural Division, Proceedings of the ASCE, 101(ST5).

Appendix

Wall Loading Protocol Target Drift Ratios

Table A1: Loading Protocol A, used for W60U and W80U, Based on recommendations by FEMA 461.

Target Drift Ratio	Displacement at point of lateral load application (in.)	Number of cycles
0.15%	0.59	2
0.20%	0.79	2
0.30%	1.19	2
0.40%	1.58	2
0.60%	2.38	2
0.80%	3.17	2
1.00%	3.96	2
1.25%	4.95	2
1.50%	5.94	2
2.00%	7.92	2
2.50%	9.90	2
3.00%	11.88	2
3.50%	13.86	2

Table A2: Loading Protocol B, used for W60C.

	Drift/δ_y	Target Drift Ratio	Displacement at point of lateral load application (in.)	Number of cycles
Wind Loading	0.15	0.10%	0.40	500
	0.4	0.30%	1.19	500
	0.75	0.50%	1.98	75
	1.2	0.80%	3.17	5
	1.5	1.00%	3.96	2
	1.2	0.80%	3.17	5
	0.75	0.50%	1.98	75
	0.4	0.30%	1.19	500
	0.15	0.10%	0.40	500
FEMA 461		1.25%	4.95	2
		1.50%	5.94	2
		2.00%	7.92	2
		2.50%	9.90	2

Table A3: Loading Protocol B, used for W80C.

	Drift/δ_y	Target Drift Ratio	Displacement at point of lateral load application (in.)	Number of cycles
Wind Loading	0.15	0.15%	0.59	500
	0.4	0.35%	1.39	500
	0.75	0.65%	2.57	75
	1.2	1.00%	3.96	5
	1.5	1.25%	4.95	2
	1.2	1.00%	3.96	5
	0.75	0.65%	2.57	75
	0.4	0.35%	1.39	500
	0.15	0.15%	0.59	500
FEMA 461		1.50%	5.94	2
		2.00%	7.92	2
		2.50%	9.90	2
		3.00%	11.88	2

Mix Proportions Reported on Day of Cast

Table A4: Test specimen Concrete mix proportions

Specimen ID	Casting Date	Total Volume (yds)	Sand-23 (lb)	# 8 Stone	Buzzi Cement (lb)	Water (lb)	Water in Sand (gal)	Water in Stone (gal)	Added Water (gal)	Measured Slump (in)	W/C
WB60U0	3/22/2017	7	12220	11740	3140	928	66	10	0	5.125	0.50
WB60U1	11/2/2017	5.5	9180	9580	2450	677	52	15	0	4	0.50
WB60U2	12/22/2017	5.5	8440	9880	2520	1064	25	6	0	2.625	0.52
WB60U3	1/17/2018	5.5	8520	9880	2555	980	30	3	5.0	3.5	0.51
WB60U4	2/16/2018	5.5	8540	9880	2520	948	35	6	0.0	3.0	0.51
WB60U5	3/29/2018	5.5	8520	9860	2535	890	35	6	0.0	3.0	0.49
WB80U1	5/3/2018	5.5	8539	9925	2530	1061	35	3	0.0	3.3	0.54
WB80U2	5/31/2018	5.5	8500	9860	2530	930	30	6	0.0	3.0	0.49
W60U	7/20/2018	9.5	14680	17140	4340	1780	59	10	0.0	2.5	0.54
W80U	1/15/2019	9.5	14880	17120	4365	1464	81	15	0.0	3.0	0.52
W60C	5/28/2019	9.5	14680	17140	4340	1780	59	10	0.0	3.8	0.54
W80C	10/7/2019	9.5	14700	17040	4145	1824	60	5	0.0	3.3	0.57

Table A5: Wall Foundation Concrete Mix Proportions

Specimen ID	Casting Date	Total Volume (yds)	Sand-23 (lb)	# 8 Limestone	3/8" Pea Gravel	Buzzi Cement (lb)	Class F Ash	Water (lb)	Water in Sand (gal)	Water in Stone (gal)	Total Water	Added Water (gal)	Measured Spread (in)	W/C
W60U F1	10/1/2018	6	8460	5680	3000	3475	790	1216	44	3	3	0.0	26	0.38
W60U F2	10/1/2018	6	8460	5680	3080	3465	830	1218	44	3	3	0.0	26	0.38
W80U F1	3/7/2019	6	8360	5700	3000	3450	870	1350	32	3	3	0.0	25	0.39
W80U F2	3/7/2019	6	8380	5680	3023	3450	870	1348	32	3	3	0.0	26	0.39
W60U F1	7/25/2019	6	8340	5660	3040	3475	875	1376	31	2	1	0.0	25	0.38
W60U F2	7/25/2019	6	8363	5700	3008	3495	870	1389	31	2	1	0.0	28	0.38
W80C F1	11/19/2019	6	8620	5680	3020	3460	865	1307	40	3	1	0.0	25	0.39
W80C F2	11/19/2019	6	8600	5720	3000	3465	865	1300	40	3	1	0.0	26	0.39

As Built Dimensions

Table A6: Beam Splice Lengths

Specimen ID	Lap Splice Lengths, inches			
	UO	UI	LO	LI
WB60U0	59.94	60.06	60.00	60.06
WB60U1	50.13	50.06	50.06	50.06
WB60U2	60.06	60.06	59.94	60.06
WB60U3	60.00	59.94	60.06	60.06
WB60U4	60.06	60.06	60.00	59.94
WB60U5	60.00	60.00	59.94	59.94
WB80U1	80.13	79.94	80.06	80.06
WB80U2	80.00	80.00	79.88	80.00

UO	Upper Outermost splice length
UI	Upper Innermost splice length
LO	Lower Outermost splice length
LI	Lower Innermost splice length

Table A7: Wall Splice Lengths

Specimen ID		Lap Splice Lengths, inches									
		BEUO	BEUM	BEUI	BELO	BELM	BELI	WUO	WUI	WLO	WLI
W60U	S	60.06	60.06	60.06	59.94	59.94	60.00	30.00	30.06	30.06	30.06
	N	60.06	60.13	60.00	60.00	59.88	59.94	30.06	30.06	29.94	30.00
W60C	S	40.00	40.06	40.00	40.00	40.06	40.00	30.00	30.06	30.00	30.06
	N	40.13	40.13	40.13	40.13	40.06	40.06	30.00	30.00	30.00	30.00
W80U	S	90.00	90.06	90.00	90.00	90.06	90.06	44.94	44.94	45.13	44.88
	N	90.00	90.13	90.06	89.94	90.06	90.06	45.00	44.94	44.88	44.88
W80C	S	59.94	60.06	59.94	60.06	60.00	60.00	40.00	40.06	40.06	40.00
	N	60.06	60.00	59.94	60.00	60.00	60.00	39.94	40.06	40.06	40.06

BEUO	BE splice length, upper outermost
BEUM	BE splice length, upper middle
BEUI	BE splice length, upper innermost
BELO	BE splice length, lower outermost
BELM	BE splice length, lower middle
BELI	BE splice length, lower innermost

WUO	Web splice length, Upper outermost
WUI	Web splice length, Upper innermost
WLO	Web splice length, Lower outermost
WLI	Web splice length, Lower innermost

Table A8: Total Wall Heights

Specimen ID	Total Height, in.
W60U	479.9
W60C	479.2
W80U	479.8
W80C	479.2

Table A9: Beam Specimen measured As-Built dimensions

Specimen ID	Measurement Location	h	w_{top}	c_{ou}	c_{ol}	c_{stu}	c_{stl}	c_{Lu}	c_{Ll}	w_{bot}	c_{bu}	c_{bl}	c_{sbu}	c_{sbl}
WB60U0	- 16 ft	48.00	10.06	1.25	1.38	-	-	3.25	3.25	10.06	1.13	-	-	-
	- 7 ft	47.81	10.06	1.31	1.38	-	-	3.38	3.38	10.06	1.00	-	-	-
	Splice end -	47.94	10.06	1.38	1.44	-	-	2.25	2.25	10.06	1.13	-	-	-
	0 ft	48.00	10.06	1.38	1.44	-	-	2.25	2.25	10.13	1.13	-	-	-
	Splice end +	48.00	10.06	1.38	1.25	-	-	2.25	2.25	10.13	1.19	-	-	-
	7 ft	48.00	10.13	2.25	2.13	-	-	3.25	3.25	10.00	1.38	-	-	-
	16 ft	48.00	10.06	2.13	2.25	-	-	3.25	3.25	10.19	1.13	-	-	-
WB60U1	- 16 ft	48.00	10.13	3.25	3.00	-	-	3.25	3.25	10.13	2.25	-	-	-
	- 7 ft	47.75	10.06	3.00	3.00	-	-	3.25	3.25	10.13	2.63	-	-	-
	Splice end -	47.88	10.13	1.94	1.94	-	-	2.25	2.25	10.13	2.88	-	-	-
	0 ft	47.88	10.06	2.00	1.94	-	-	2.25	2.25	10.13	2.88	-	-	-
	Splice end +	48.00	10.06	2.00	2.00	-	-	2.25	2.25	10.06	2.88	-	-	-
	7 ft	48.00	10.13	2.25	2.25	-	-	3.25	3.25	10.06	2.25	-	-	-
	16 ft	48.00	10.25	1.88	1.88	-	-	3.25	3.25	10.13	2.50	-	-	-
WB60U2	- 16 ft	47.88	10.06	2.63	2.75	2.13	1.88	2.00	2.00	10.06	2.38	2.38	2.25	1.75
	- 7 ft	47.75	10.00	2.75	2.75	2.13	1.75	2.00	2.00	10.06	2.38	2.38	2.13	1.88
	Splice end -	47.88	10.00	1.75	1.88	2.13	1.75	1.00	1.00	10.06	2.63	2.63	2.38	1.50
	0 ft	47.88	10.13	1.75	1.88	2.13	2.00	1.00	1.00	10.13	2.75	2.63	2.38	1.75
	Splice end +	47.88	10.00	1.88	1.75	2.00	2.00	1.00	1.06	10.00	2.63	2.63	2.25	1.88
	7 ft	48.00	10.13	1.88	1.75	2.00	2.00	2.00	2.00	10.06	2.38	2.50	2.13	1.88
	16 ft	47.88	10.19	2.00	1.88	2.25	1.75	2.00	1.94	10.06	2.38	2.75	2.25	1.75

	- 16 ft	47.88	10.00	3.25	3.13	2.13	1.88	1.00	1.13	10.06	1.88	1.75	2.13	1.88
	- 7 ft	47.88	10.00	2.75	2.88	2.13	1.88	1.00	1.00	10.13	2.25	2.25	2.25	1.88
	Splice end -	47.88	10.06	1.75	1.88	2.25	1.94	1.06	1.00	10.06	2.50	2.38	2.13	2.00
WB60U3	0 ft	47.81	10.13	1.75	1.75	2.25	2.00	1.00	1.00	10.13	2.50	2.25	2.25	1.88
	Splice end +	47.94	10.06	1.75	1.75	2.00	2.00	1.00	1.00	10.06	2.75	2.38	2.13	1.94
	7 ft	48.00	10.06	1.75	1.75	2.25	1.94	3.00	2.94	10.06	2.63	2.50	2.25	1.88
	16 ft	47.75	10.06	2.25	2.25	2.25	1.88	3.00	3.00	10.00	2.13	2.00	2.25	1.88
	- 16 ft	47.75	10.00	2.50	2.25	1.25	1.25	2.00	2.00	10.06	1.50	1.25	1.50	1.25
	- 7 ft	47.88	10.00	2.38	2.25	1.25	1.25	2.00	2.06	10.06	1.75	1.63	1.38	1.25
	Splice end -	47.88	10.06	1.25	1.25	1.50	1.25	1.00	1.00	10.00	1.75	1.88	1.50	1.38
WB60U4	0 ft	47.88	10.00	1.38	1.25	1.38	1.25	1.00	1.00	10.06	1.75	1.75	1.50	1.25
	Splice end +	47.88	10.06	1.38	1.25	1.25	1.38	1.00	1.00	10.00	1.63	1.75	1.38	1.25
	7 ft	47.88	10.06	1.50	1.50	1.38	1.25	2.00	2.00	10.06	1.50	1.50	1.38	1.25
	16 ft	47.88	10.06	1.25	1.25	1.38	1.25	2.00	1.94	10.06	1.75	1.50	1.50	1.38
	- 16 ft	48.00	10.06	2.13	2.13	1.13	1.25	2.00	2.06	10.00	1.50	1.38	1.38	1.25
	- 7 ft	47.88	10.13	2.13	2.13	1.13	1.25	2.06	2.00	10.06	1.50	1.63	1.25	1.25
	Splice end -	47.94	10.06	1.25	1.25	1.13	1.19	1.00	1.00	10.13	1.63	1.63	1.31	1.19
WB60U5	0 ft	48.00	10.00	1.25	1.19	1.13	1.13	1.00	1.00	10.13	1.75	1.63	1.25	1.13
	Splice end +	48.00	10.06	1.25	1.19	1.13	1.13	1.00	1.06	10.06	1.63	1.75	1.19	1.19
	7 ft	48.00	10.13	1.25	1.19	1.25	1.25	2.00	2.00	10.06	1.63	1.75	1.25	1.25
	16 ft	48.06	10.60	1.25	1.19	1.38	1.25	2.06	2.06	10.00	1.88	1.75	1.25	1.31
	- 16 ft	47.94	10.00	2.38	2.25	1.25	1.38	2.00	2.06	10.06	1.75	1.75	1.25	1.38
	- 7 ft	47.88	10.06	2.38	2.50	1.38	1.31	2.06	2.00	10.00	1.75	1.75	1.50	1.31
	Splice end -	48.00	10.06	1.50	1.50	1.50	1.38	1.00	1.00	10.13	1.75	1.75	1.88	1.38
WB80U1	0 ft	48.00	10.06	1.50	1.50	1.50	1.38	1.00	1.00	10.13	1.75	1.63	1.75	1.31
	Splice end +	47.94	10.06	1.56	1.56	1.56	1.38	1.00	1.00	10.06	1.69	1.50	1.69	1.31
	7 ft	47.94	10.06	1.75	1.75	1.50	1.50	2.13	2.00	10.00	1.63	1.63	1.50	1.38
	16 ft	47.88	10.00	2.00	2.00	1.50	1.25	2.06	2.00	10.06	1.88	1.63	1.50	1.38

	- 16 ft	48.00	10.00	3.00	2.94	2.25	1.88	2.00	1.94	10.00	2.63	2.75	2.00	2.00
	- 7 ft	47.88	10.06	3.00	3.00	2.25	2.00	2.06	2.00	10.00	2.63	2.63	2.06	2.00
	Splice end -	47.94	10.06	2.00	2.06	2.00	1.94	1.06	1.00	10.13	2.75	2.75	2.06	1.94
WB80U2	0 ft	48.00	10.06	2.00	2.06	2.00	1.94	1.00	1.00	10.13	2.75	2.88	2.00	2.00
	Splice end +	47.94	10.06	2.06	2.06	2.00	1.94	1.00	0.94	10.06	2.88	3.00	2.00	2.00
	7 ft	47.94	10.06	2.06	2.00	2.19	1.88	1.94	2.00	10.06	3.00	3.00	2.00	2.00
	16 ft	48.00	10.06	2.06	2.06	2.38	1.88	2.00	2.00	10.13	3.00	3.00	2.13	1.94

d depth, in.

w_{top} width, top, in.

c_{ou} outer cover to the face of the upper longitudinal bar, in.

c_{ol} outer cover to the face of the lower longitudinal bar, in.

c_{stu} side cover to the face of the upper longitudinal bar, in.

c_{stl} side cover to the face of the lower longitudinal bar, in.

c_{Lu} clear spacing, upper longitudinal bars, in.

c_{Ll} clear spacing, lower longitudinal bars, in.

w_{bot} beam width, bottom, in.

c_{bu} bottom cover, upper bar, in.

c_{bl} bottom cover, lower bar, in.

c_{sbu} side cover, upper bar, in.

c_{sbl} side cover, lower bar, in.

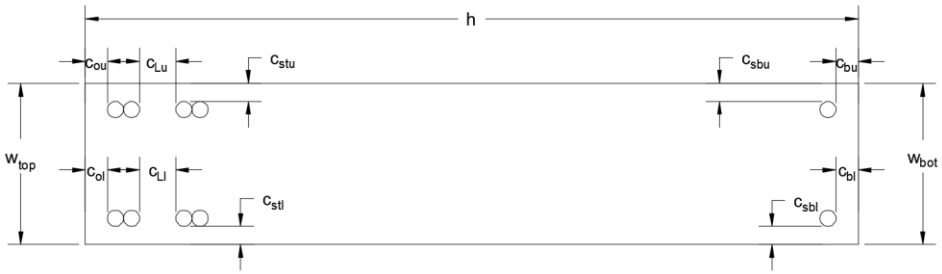

Table A10: Wall Specimen measured As-Built dimensions

Specimen ID	Measurement Location	h	BE Location	w	c_{ou}	c_{ol}	c_{su}	c_{sl}	c_{Luo}	c_{Lui}	c_{Llo}	c_{Lli}
W60U	30 ft	83.94	South	10.00	3.06	3.13	2.13	1.94	2.00	2.00	2.00	2.00
	25 ft	84.00		10.00	3.06	3.06	2.13	2.00	2.00	2.00	2.00	2.06
	20 ft	84.06		9.94	3.06	3.00	2.06	2.00	2.00	2.00	2.00	2.00
	15 ft	84.13		9.94	3.13	3.06	2.00	1.94	2.06	2.00	2.00	2.00
	10 ft	84.00		10.00	3.06	3.06	2.00	1.94	2.06	1.94	2.00	2.00
	Splice end +	84.00		10.00	2.00	2.00	2.06	1.94	1.06	1.00	1.00	1.06
	0 (Base of Wall)	84.06		9.94	2.00	2.00	2.06	2.00	1.00	1.00	1.00	1.00
	-5 ft (Stub)	48.06		10.00								
	30 ft		North	10.00	3.00	3.00	2.06	1.94	2.00	2.06	2.00	2.00
	25 ft			10.06	3.00	3.06	2.13	1.94	2.06	2.00	2.00	2.00
	20 ft			10.00	2.88	3.06	2.06	1.94	2.00	2.00	1.88	2.06
	15 ft			10.00	2.94	3.19	2.13	1.94	2.06	2.00	1.88	2.00
	10 ft			10.06	3.00	3.06	2.13	1.94	2.13	2.00	2.00	1.94
	Splice end +			10.00	2.00	2.00	2.06	1.94	1.00	1.00	1.06	1.00
	0 (Base of Wall)			10.00	2.00	2.00	2.06	1.94	1.06	1.00	1.00	1.06
	-5 ft (Stub)			10.00								
W60C	30 ft	83.94	South	9.94	2.38	2.13	1.38	1.25	2.00	2.00	2.00	2.06
	25 ft	83.94		10.00	2.38	2.25	1.38	1.38	2.00	2.00	1.94	2.06
	20 ft	83.94		10.00	2.38	2.13	1.50	1.25	2.06	2.00	2.06	2.00
	15 ft	84.00		9.94	2.38	2.00	1.50	1.38	2.06	1.94	2.13	2.00
	10 ft	83.88		10.00	2.25	2.19	1.38	1.38	2.00	2.06	2.06	1.94
	Splice end +	83.88		10.00	1.25	1.25	1.31	1.38	1.00	1.06	1.00	1.06
	0 (Base of Wall)	83.94		9.94	1.25	1.25	1.25	1.38	1.00	1.00	1.00	1.00
	-5 ft (Stub)	48.06		10.00								
	30 ft		North	10.00	2.13	2.25	1.31	1.38	2.00	2.00	2.00	2.13

	25 ft			10.00	2.25	2.38	1.31	1.25	2.06	2.00	2.00	2.06
	20 ft			10.00	2.31	2.38	1.31	1.31	2.06	2.00	2.13	2.06
	15 ft			10.00	2.38	2.38	1.38	1.25	2.00	2.00	2.06	2.06
	10 ft			10.06	2.25	2.25	1.50	1.31	2.00	2.00	2.06	2.00
	Splice end +			10.00	1.25	1.25	1.31	1.25	1.06	1.00	1.00	1.00
	0 (Base of Wall)			10.00	1.25	1.25	1.38	1.25	1.00	1.06	1.06	1.06
	-5 ft (Stub)			10.00								
W80U	30 ft	83.94	South	10.00	3.00	3.00	2.13	2.00	2.00	2.00	1.88	2.00
	25 ft	84.00		10.00	3.00	2.88	2.13	2.06	1.94	2.00	1.94	2.00
	20 ft	83.94		10.00	2.94	2.94	2.13	2.06	2.00	2.00	1.88	2.00
	15 ft	83.94		10.00	2.94	2.94	2.06	2.00	2.00	1.94	2.06	2.00
	10 ft	83.88		10.00	3.00	2.88	2.13	2.00	1.94	2.00	2.00	2.00
	Splice end +	84.00		10.00	2.13	2.00	2.13	2.06	1.00	1.00	1.00	1.00
	0 (Base of Wall)	83.88		10.00	2.06	2.00	2.06	2.00	1.06	1.00	1.06	1.00
	-5 ft (Stub)	48.00		10.13								
	30 ft		North	10.06	2.88	2.88	2.13	2.00	2.13	2.00	2.00	2.06
	25 ft			10.00	3.00	2.94	2.13	2.00	2.00	2.00	2.00	2.00
	20 ft			9.94	2.88	2.88	2.13	2.00	2.06	2.06	2.00	2.06
	15 ft			9.94	3.00	2.81	2.06	2.00	2.00	2.00	2.00	2.00
	10 ft			10.13	2.94	2.94	2.19	2.00	2.00	2.00	2.00	2.06
	Splice end +			10.06	2.06	2.00	2.13	2.06	1.00	1.00	1.00	1.00
	0 (Base of Wall)			10.00	2.06	2.00	2.13	1.94	1.00	1.06	1.00	1.00
	-5 ft (Stub)			10.13								
W80C	30 ft	83.88	South	9.94	2.25	2.25	1.31	1.31	2.13	2.06	2.13	1.94
	25 ft	83.88		10.00	2.25	2.38	1.56	1.25	2.00	1.94	2.13	2.00
	20 ft	83.88		10.06	2.50	2.25	1.56	1.38	2.06	1.94	2.13	2.00
	15 ft	83.94		10.00	2.56	2.25	1.44	1.31	2.00	2.13	2.00	2.06
	10 ft	83.88		10.00	2.38	2.31	1.38	1.38	2.00	2.00	2.19	1.94
	Splice end +	83.88		10.00	1.31	1.31	1.31	1.31	1.00	1.00	1.06	1.06

	0 (Base of Wall)	83.94		9.94	1.25	1.25	1.25	1.31	1.00	1.00	1.00	1.00
	-5 ft (Stub)	48.06		10.06								
	30 ft			10.00	2.50	2.25	1.44	1.31	2.00	2.00	2.00	2.06
	25 ft			9.94	2.50	2.25	1.44	1.38	2.00	2.06	2.00	2.00
	20 ft			10.00	2.25	2.31	1.44	1.38	1.94	2.06	1.94	1.94
	15 ft			10.00	2.25	2.44	1.38	1.31	2.13	2.00	1.94	1.94
	10 ft		North	10.13	2.25	2.56	1.38	1.31	2.13	2.13	1.88	1.94
	Splice end +			10.06	1.31	1.31	1.38	1.25	1.06	1.13	1.06	1.06
	0 (Base of Wall)			10.00	1.31	1.25	1.25	1.25	1.00	1.06	1.00	1.00
	-5 ft (Stub)			10.06								

h	depth, in.
w	width, in.
c_{ou}	outer cover to upper longitudinal bar face, in.
c_{ol}	outer cover to lower longitudinal bar face, in.
c_{su}	side cover to upper longitudinal bar face, in.
c_{sl}	side cover to lower longitudinal bar face, in.
c_{Luo}	clear spacing, upper outer longitudinal bars, in.
c_{Lui}	clear spacing, upper inner longitudinal bars, in.
c_{Llo}	clear spacing, lower outer longitudinal bars, in.
c_{Lli}	clear spacing, lower inner longitudinal bars, in.